

1 WATKINSON & HALL. Fault systems of the eastern Indonesian triple junction: evaluation of
 2 Quaternary activity and implications for seismic hazards. *In: CUMMINS, P. R., & MEILANO, I. (eds.)*
 3 *Geohazards in Indonesia: Earth Science for Disaster Risk Reduction*. Geological Society of London
 4 Special Publication.

5 **Fault systems of the eastern Indonesian triple junction: evaluation of Quaternary**
 6 **activity and implications for seismic hazards.**

7 IAN M. WATKINSON* & ROBERT HALL

8 *SE Asia Research Group, Department of Earth Sciences,*

9 *Royal Holloway University of London, Egham, Surrey TW20 0EX, United Kingdom*

10 *Corresponding author (e-mail: ian.watkinson@rhul.ac.uk)

11

Text words	16,024
References number (words)	160 (4,730)
Tables number	3
Figures number	24

12 **Abbreviated title:** Quaternary fault activity in eastern Indonesia

13 **Abstract**

14 Eastern Indonesia is the site of intense deformation related to convergence between Australia, Eurasia,
 15 the Pacific and the Philippine Sea Plate. Analysis of tectonic geomorphology, drainage patterns,
 16 exhumed faults and historical seismicity highlights faults that have been active during the Quaternary
 17 (Pleistocene to present day), even if instrumental records suggest some are presently inactive. Of
 18 twenty-seven largely onshore fault systems studied, eleven show evidence of a maximal tectonic rate,
 19 a further five show evidence of rapid tectonic activity. Three faults indicating slow to minimal
 20 tectonic rate nonetheless show indications of Quaternary activity, and may simply have long
 21 interseismic periods. Although most studied fault systems are highly segmented, many are linked by
 22 narrow (<3 km) step-overs to form one or more long, quasi-continuous segments that are capable of
 23 producing $M > 7.5$ earthquakes. Sinistral shear across the soft-linked Yapen and Tarera-Aiduna faults
 24 and their continuation into the transpressive Seram fold-thrust belt represents perhaps the most active
 25 belt of deformation and hence greatest seismic hazard in the region. However, the Palu-Koro Fault,
 26 being long, straight and capable of generating supershear ruptures, is considered to represent the
 27 greatest seismic risk of all the faults evaluated in this region in view of important strike-slip strands
 28 that appear to traverse the thick Quaternary basin fill below Palu city.

29

30

31

32

33 During the last decade several devastating earthquakes occurred on faults around the world that were
34 either poorly understood or not recognised at all. The M_w 6.6 Bam earthquake (Iran) of 26th December
35 2003 ruptured a section of the Bam Fault that had poor surface expression and had not caused a
36 destructive earthquake for 2000 years (Eshghi & Zare 2003; Fu *et al.* 2004). The M_w 8.0 Wenchuan
37 earthquake (China) of 12th May 2008 resulted from complex rupture of part of the Lonmen Shan
38 tectonic belt (Burchfiel *et al.* 2008), an area that was previously considered not at risk from large
39 earthquakes (Chen & Hsu 2013). The M_w 7.1 Haiti earthquake of 12th January 2010 occurred on the
40 well known Enriquillo Fault, part of the fault system marking the northern boundary of the Caribbean
41 plate, but which had previously been mapped as having low seismic hazard based on recent seismicity
42 (Stein *et al.* 2012). The Canterbury earthquake sequence (New Zealand) ruptured the Greendale Fault,
43 which was previously unrecognised because it was buried beneath alluvial sediments (Quigley *et al.*
44 2012). The Canterbury sequence culminated in the M_w 6.3 Christchurch earthquake of 22nd February
45 2011. These events emphasise the need for accurate identification of faults that have been active
46 during the Quaternary and have the potential for modern tectonic activity.

47 Eastern Indonesia is a region of complex and rapid neotectonics. Convergence between Australia,
48 Eurasia, the Pacific and Philippine Sea plates (e.g. Hamilton 1979; DeMets *et al.* 1994; Hall 1996,
49 2012; Bock *et al.* 2003; Charlton 2010) results in both contraction and extension resulting from
50 subduction hinge rollback, lithospheric delamination and slab break off (e.g. Harris 1992; Spakman &
51 Hall 2010; Hall 2012).

52 Great uncertainty surrounds the position, tectonic role and modern activity of eastern Indonesia's
53 many Quaternary faults (e.g. Hamilton 1979; Okal 1999; Bailly *et al.* 2009; Charlton 2010). New fault
54 systems continue to be identified using both modern geophysical/remote sensing and conventional
55 field techniques (e.g. Stevens *et al.* 2002; Spencer 2011; Watkinson *et al.* 2011; Pownall *et al.* 2013)
56 and it is likely many others remain unknown, with important implications for seismic hazard analysis.

57 Despite intense seismicity in eastern Indonesia, there have been few catastrophic earthquake disasters
58 in the last one hundred years, compared to other rapidly deforming areas such as China, Iran, Japan
59 and Pakistan (e.g. Holzer & Savage 2013; National Geophysical Data Center / World Data Service).
60 Significant events include the 25th June 1976 M_w 7.1 Papua earthquake, which killed 3,000-6,000
61 people; the 12th December 1992 M_w 7.8 Flores earthquake, which killed 2,500 people and destroyed
62 31,800 houses; the 17th February 1996 M_w 8.2 Biak earthquake, which caused a 7 m tsunami and
63 killed at least 100 people (Okal 1999); the 16th November 2008 M_w 7.4 Minahasa earthquake, which
64 killed 6 and displaced 10,000; and the 16th June 2010 M_w 7.0 Yapen earthquake, which killed 17 and
65 destroyed 2,556 houses (National Geophysical Data Center / World Data Service; USGS Earthquake
66 Hazards Program). With increasing urban development and replacement of traditional wooden
67 dwellings with concrete construction, it is likely that damaging earthquakes will become more
68 frequent in the future (e.g. Wyss 2005).

69 This contribution aims to catalogue Quaternary fault systems onshore eastern Indonesia from
70 Sulawesi to Papua, to provide evidence for Quaternary tectonic activity, and to provide a
71 reconnaissance evaluation of the faults' seismic hazard.

72 **Method**

73 *Definitions and extent of study*

74 This study is concerned with evaluating Quaternary (Pleistocene and Holocene, 2.59 Ma to 0 Ma)
75 fault activity. Quaternary activity lies within the realm of neotectonics, the study of broadly post-
76 Miocene, ‘young’ and still-active tectonic events, whose effects are compatible with modern
77 seismotectonics (Pavrides 1989). It is distinct from palaeoseismology – the study of deformation
78 related to specific past earthquakes (e.g. Michetti *et al.* 2005). Thus faults that show evidence of
79 Quaternary activity may or may not also show evidence of palaeoseismicity, depending on whether
80 they have recently ruptured the surface, rates of sedimentation and erosion, and whether they are truly
81 ‘active’ in the sense that they have failed during the Holocene. Equally, Quaternary faults may or may
82 not be present in records of instrumental or historic seismicity, dependent on whether they have
83 recently become inactive, have a long interseismic period, or have yielded historic earthquakes in
84 locations where written documentation was not made. Quaternary fault activity is therefore distinct
85 from, but influential to the field of active tectonics, which includes future fault activity that may
86 impact human society (Wallace 1986).

87 Quaternary fault activity in this study is evaluated by the following criteria: 1) instrumental/historic
88 seismicity and geodetic observations; 2) deformation of Quaternary sediments, often indicated by
89 topographic lineaments that can be linked to an underlying fault; 3) systematic offset of modern
90 streams across a topographic lineament; 4) evidence of structurally-controlled drainage network
91 modification where signs of an earlier arrangement are preserved; 5) geomorphic indices recording
92 relative youthfulness of fault-controlled mountain fronts; 6) evidence of landslips localised to faults.

93 The study extent is a 2,200 km x 800 km swath of the Indonesian archipelago, centred on the triple
94 junction between Australia, Eurasia, the Pacific and Philippine Sea plates. It includes much of eastern
95 Indonesia from Sulawesi eastwards, except islands of the southern Banda arc. Because of the focus on
96 geomorphic expression the study mainly deals with onshore faults, except where multibeam
97 bathymetry is available.

98 *Datasets*

99 Interpretations of Quaternary fault activity are based on a variety of remote sensing data, field
100 observations by both authors and their students over several years (e.g. Roques 1999; Watkinson
101 2011; Pownall *et al.* 2013; Hennig *et al.* 2014) and published geodetic/geophysical data. Digital
102 elevation models (DEMs) based on Shuttle Radar Topography Mission (SRTM) 3 arc second/90 m
103 resolution and ASTER 30 m resolution data were processed using ERMapper software. These data
104 were also used to extract topographic contours and drainage networks using ArcGIS. Landsat TM and
105 ETM+ scenes composed of 30 m resolution bands 432, 451, 531 and 742 (red-green-blue
106 combinations) were used and where appropriate sharpened with ETM+ band 8 panchromatic 15 m
107 resolution data. Where available, high resolution visible spectrum imagery from Google Earth and
108 Bing Maps (compiled from a variety of sources) and the ESRI World Imagery compilation, which
109 includes 2.5 m SPOT and <1 m DigitalGlobe imagery, was also interpreted.

110 Multibeam bathymetric data (kindly provided by TGS, who provide global geoscientific data products
111 and services) from parts of the offshore Sorong Fault Zone and Cenderawasih Bay were interpreted in
112 the same way as the DEMs. Multibeam was acquired using a Kongsberg Simrad EM120 Multibeam
113 Echo Sounder using 191 beams at equidistant spacing. Positioning control used a C-Nav Starfire
114 DGPS. During processing, positioning, tidal and calibration corrections were applied, random noise
115 and artefacts were removed, and a terrain model using a 25 m bin size was gridded and exported to
116 ESRI format. Multibeam data were further processed in ERMapper to remove voids.

117 All data were integrated in ArcGIS together with georeferenced maps from the literature. CMT focal
 118 mechanisms are from the International Seismological Centre catalogue, plotted using Mirone
 119 software. We consider only earthquakes with a focal depth ≤ 35 km to avoid contamination from
 120 deeper structures that have little surface expression.

121 *Geomorphic indices*

122 Geomorphic indices are a valuable tool to rapidly evaluate the relative tectonic rate of surface faults
 123 on a reconnaissance scale (Keller 1986). We utilise mountain front sinuosity (S_{mf}) and valley-floor
 124 width to valley-height index (V_f) following the method of Bull & McFadden (1977) and Bull (1978).
 125 Key parameters are summarised in Table 1. An excellent description of the method and its
 126 uncertainties is given in Bull (2007). While conventionally applied to normal faults, geomorphic
 127 indices can be used in any setting where there is vertical motion, including regions of transpression
 128 and transtension. However, they are of little value in regions of pure strike-slip, and are not applied to
 129 pure strike-slip segments in this study.

130 Mountain front sinuosity is the ratio: $S_{mf} = L_{mf} / L_s$, where L_s is the straight line length of the mountain
 131 front, and L_{mf} is the true, or sinuous length along the mountain front following topographic contours
 132 at the contact between alluvial fans and the solid geology of the range front (Table 1). This method
 133 assumes that a fault-bounded range front will become more sinuous over time in the absence of
 134 tectonic activity (e.g. Bull & McFadden 1977; Rockwell *et al.* 1984). The method is well established
 135 for Quaternary fault evaluation in regions of extension (e.g. Ramírez-Herrera 1998), contraction and
 136 strike-slip (e.g. Dehbozorgi *et al.* 2010), transtension (e.g. Silva *et al.* 2003; Yildirim 2014), combined
 137 extension and contraction (Wells *et al.* 1988) and differential uplift (e.g. Sohoni *et al.* 1999). Critical
 138 uncertainties include interpreter definition of the sinuous mountain front, partly dependent on the
 139 quality of the input satellite data, and recognition of discrete mountain front segments. Climate also
 140 has an impact on S_{mf} independent of tectonic rate, in a humid environment like eastern Indonesia it is
 141 expected that erosion and hence S_{mf} will be higher than in an arid region for a given tectonic rate.

142 The valley-floor width to valley height index, V_f , measures the ratio between valley floor width and
 143 valley depth: $V_f = 2V_{fw} / ((E_{ld} - E_{sc}) - (E_{rd} - E_{sc}))$, where V_{fw} is the valley floor width, E_{ld} and E_{rd} are
 144 the topographic elevations of the left and right valley watersheds and E_{sc} is the elevation of the valley
 145 floor (Table 1). The method assumes that recently excavated river channels (i.e. those into which a
 146 river has incised due to recent uplift) are V-shaped, and become more U-shaped over time (e.g. Bull
 147 & McFadden 1977; Rockwell *et al.* 1984). Like S_{mf} , V_f has been applied in a wide range of tectonic
 148 settings (e.g. Wells *et al.* 1988; Ramírez-Herrera 1998; Yildirim 2014). V_f is sensitive to a number of
 149 variables apart from tectonic rate, so we standardised as much as possible: measuring V_f in all cases 1
 150 km upstream from the mountain front; measuring valley width as the width of the river channel
 151 visible on the highest resolution satellite imagery available, or the width of the valley to the point
 152 where the floor rises 10 m above the minimum elevation in individual transects; measuring only
 153 streams that reach the mountain front without joining a higher order stream; and measuring only
 154 streams oriented $\geq 70^\circ$ from the mountain front. Noise in the V_f signal was reduced by averaging 3-10
 155 separate V_f measurements along each fault segment.

156 High quality topographic maps are not available for eastern Indonesia, so both S_{mf} and V_f were
 157 measured in ArcGIS software using a combination of 30 m ASTER GDEM satellite data and the
 158 ESRI World Imagery compilation. This allowed the finest possible resolution of L_s and V_{fw} , which are
 159 critical but potentially subjective parameters. High quality satellite imagery may be better for such
 160 measurement than conventional maps (Bull 2007).

161 Schemes for the classification of relative tectonic activity based on a combination of geomorphic
162 indices have been proposed (e.g. Bull & McFadden 1977; Bull 1978, 2007). Here we apply a
163 modified scheme from McCalpin (2009). It uses S_{mf} and V_f to classify relative tectonic activity as
164 follows: $S_{mf} < 1.1$, mean $V_f < 0.15$, maximal activity; S_{mf} from 1.1-1.3, mean V_f 0.15, rapid activity;
165 S_{mf} from 1.6-2.3, mean V_f 1.5, slow activity; $S_{mf} \geq 2.5$, mean V_f 1.7-2.5, minimal activity; S_{mf} from
166 2.6-4.0, mean V_f 7.4, inactive. This classification allows comparison between faults with different
167 relative tectonic rates and corresponding geomorphic expression. Because the indices record undated
168 Quaternary fault activity expressed by geomorphology, the classes also correspond to a Quaternary
169 tectonic rate and not necessarily to a modern tectonic rate comparable to geodetic measurements. It
170 should also be remembered that the schemes were developed using faults in arid areas of the western
171 USA where tectonic landforms are preserved longer than they are in humid areas (e.g. Bull 1978),
172 meaning faults in the tropics will generally be classified as tectonically ‘slower’ than equivalent faults
173 at higher latitudes.

174 We analysed both S_{mf} and V_f for a total of 111 segments from 24 fault systems across the study area
175 (Fig. 2 a-r, Table 2) and found a good correlation between S_{mf} and V_f (Fig. 3), supporting the
176 reliability of each method. A previous study of geomorphic indices along a segment of the Palu-Koro
177 Fault (Vecchiotti 2008) obtained similar results to those presented here. However, we use these
178 indices only as a simple quantitative means to support other evidence for Quaternary fault activity,
179 and do not classify faults on the basis of these data alone.

180 **Sulawesi**

181 Sulawesi lies at the triple junction between the Australian, Eurasian and Philippine Sea plates (e.g.
182 Hamilton 1979; Silver *et al.* 1983a, b; Hall 1996). North of Sulawesi, the Celebes Sea is being
183 subducted beneath Sulawesi (e.g. Hamilton 1979; Silver *et al.* 1983a). Convergence across the
184 subduction margin increases from 20 ± 4 mm/yr in the east to 54 ± 10 mm/yr in the west, associated
185 with clockwise rotation of about $4^\circ/\text{Ma}$ about a pole close to Manado (Walpersdorf *et al.* 1998;
186 Rangin *et al.* 1999; Stevens *et al.* 1999; Beaudouin *et al.* 2003). Immediately east of Sulawesi’s north
187 ‘arm’, convergence between the Philippine Sea Plate and Sundaland is partly accommodated by the
188 Molucca Sea double subduction and the overlying Sangihe and Halmahera thrusts (e.g. Rangin *et al.*
189 1999; Hall 2002; Beaudouin *et al.* 2003).

190 Despite its setting within a collisional orogen, Sulawesi is subject to widespread and young extension.
191 Tomini Bay encloses a deep, enigmatic basin containing up to 10 km of late Cenozoic sediment
192 (Jablonski *et al.* 2007; Pholbud *et al.* 2011). Medium to high-K Pliocene to modern volcanism in the
193 Togian Islands within the bay results from Pliocene to Recent extension (Cottam *et al.* 2011), and
194 onshore metamorphic core complexes are in the process of being exhumed by processes related to
195 crustal thinning (Kavalieris *et al.* 1992; van Leeuwen *et al.* 2007; Spencer 2011).

196 Active strike-slip (e.g. Bellier *et al.* 2001), with left-lateral slip rates of up to 39 mm/yr (Socquet *et al.*
197 2006), characterise much of Sulawesi’s onshore Quaternary deformation. Often considered to result
198 from NW-directed collision between the Sula platform and Sulawesi (e.g. Silver *et al.* 1983b;
199 Simandjuntak 1986), modern reconstructions emphasise the process of subduction hinge rollback
200 related to the substantial amounts of oceanic crust that have been and continue to be subducted around
201 Sulawesi (e.g. Spakman & Hall 2010; Hall 2012). The occurrence of Late Miocene to apparently
202 modern N-S-directed continental extension (e.g. Spencer 2011) in a broad region adjacent to the
203 south-directed Celebes Sea subduction means that a rollback mechanism must be considered.

204 *Palu-Koro Fault*

205 The Palu-Koro Fault (Fig. 4) is the most prominent active fault of Sulawesi, and is of particular
206 importance because it is straddled by Palu city (pop. 340,000). The Palu-Koro Fault appears to pass
207 from the SW corner of the Celebes Sea to a diffuse termination onshore at the northern end of Bone
208 Bay, a distance of 500 km, of which 220 km is onshore.

209 The fault's tectonic role is disputed: sinistral shear along a joint Palu-Koro-Matano Fault system has
210 been thought to accommodate clockwise rotation and northward movement of a rigid eastern Sulawesi
211 block driven by collision of the Banggai-Sula block in the east (e.g. Hamilton 1979; Silver *et al.*
212 1983b; Beaudouin *et al.* 2003). However, it is significant that the Palu-Koro Fault and the North
213 Sulawesi Trench respectively form the western and northern limits of a region of late Cenozoic
214 extreme continental extension that includes deep sedimentary basins (e.g. Jablonski *et al.* 2007;
215 Pholbud *et al.* 2011), exhumation of the mid-lower crust in metamorphic core complex – like settings
216 (e.g. van Leeuwen *et al.* 2007; Watkinson 2011), exhumed low-angle normal faults (Spencer 2011)
217 and decompression-related mantle melts (Cottam *et al.* 2011). These features can be associated with
218 the overriding plate above a retreating subduction hinge, particularly in the early stages of continent-
219 continent collision (Royden 1993). The orientation and kinematics of the Palu-Koro Fault are
220 compatible with an interpretation that it is passively bounding a region of lithospheric extension
221 driven by northward rollback in the Celebes Sea, although it is unclear whether there is a hard linkage
222 between the fault and the trench.

223 That the fault is an active zone of high strain is not disputed. Geodetic measurements suggest a 39
224 mm/yr sinistral slip rate together with 11-14 mm/yr of extension (Socquet *et al.* 2006), consistent with
225 a 35 ± 8 mm/yr strike-slip rate determined from displaced alluvial fans of $11,000 \pm 2300$ years age
226 (Bellier *et al.* 2001).

227 There is palaeoseismic evidence for three M_w 6.8-8.0 earthquakes during the last 2000 years,
228 suggesting a recurrence interval of about 700 years (Beaudouin 1998; Bellier *et al.* 1998). However,
229 even allowing for 10 m slip per M_w 6.8-8.0 event, the resultant 30 m total displacement in 2000 years
230 is less than the 54-86 m predicted from Holocene slip rates (Bellier *et al.* 2001). While those authors
231 propose that the deficit is accommodated by aseismic creep, it is equally possible that large,
232 undetected earthquakes occurred on unobserved fault strands, and the total recurrence interval for all
233 Palu-Koro Fault strands is significantly less than 700 years. Socquet *et al.* (2006) propose 4 parallel
234 strands across a zone about 50 km wide, locked at depths between 0 and 5 km.

235 Records of historical seismicity in Sulawesi are poor. Damaging earthquakes occurred along the Palu-
236 Koro Fault in 1905, 1907, 1909, 1927, 1934, 1968 ($M_s \sim 6.7$), 1985 and 1993 ($M_s \sim 5.7$) (Katili 1970;
237 Hamilton 1979; Beaudouin 1998) but little detail is known. Large earthquakes close to the fault zone
238 occurred in 1996 (M_w 7.7) and 1998 (M_w 6.6 and 6.0), the former caused a 2-4 m high tsunami in the
239 Toli Toli region (Pelinovsky *et al.* 1997). However, these earthquakes originated offshore, did not lay
240 clearly on the active Palu-Koro Fault, and none had a focal mechanism that indicated left-lateral slip
241 along the Palu-Koro trend.

242 The Palu-Koro Fault has the clearest geomorphological expression of any of Eastern Indonesia's
243 faults. It occupies a steep sided narrow valley along much of its path through central Sulawesi, before
244 branching into the Palu valley, up to 15 km wide (Fig. 5a). Two prominent scarps bound the valley,
245 and form the base of mountains which rise to over 2.3 km elevation. The western scarp is highly
246 linear, particularly the remarkable central segments around 15 km south of Palu city. Mountain front

247 sinuosity values are consistently low at 1.08 to 1.09, indicating maximal tectonic activity, increasing
248 to 1.28 to 1.56 at the northern and southern ends of the valley, indicating rapid to moderate tectonic
249 activity (Fig. 5a). Valley floor curvature is generally correspondingly tight, with an average V_f of 0.24
250 along the western scarp.

251 Features such as prominent triangular facets, hanging valleys and steep-sided, deeply incised streams
252 are also focused along the central western basin-bounding segment (Fig. 5b). These landforms support
253 dominantly rapid normal faulting along the basin margin faults. Wine glass canyons in particular
254 indicate that the tectonic subsidence/uplift rate is faster than erosion. Lateral offset of alluvial fans and
255 rivers across the mountain front have been observed, notably in the northern and southern segments of
256 the fault system (e.g. Hamilton 1979; Bellier *et al.* 2006).

257 A 5° releasing bend/step-over is required to link the southern segments of the Palu-Koro Fault, where
258 it emerges from its narrow valley at Pakuli, with the northern segments NW of Palu city. In analogue
259 models and other non-linear strike-slip faults, such releasing geometries are often associated with well
260 defined oblique-normal sidewall faults and a cross-basin fault system with more subtle surface
261 expression that accommodates most of the strike-slip strain (e.g. Mann *et al.* 1995, 2007; Wu *et al.*
262 2009) (Fig. 6a inset).

263 Analysis of Palu River channels since 2003 from satellite imagery and the pattern of older filled
264 oxbow lakes on the valley floor indicates that long reaches of the river rarely deviate from a linear
265 path directly along strike from the strike-slip fault where it enters the Palu valley in the south (Fig.
266 6a,b). Many meanders have a square aspect with linear longitudinal segments parallel to the projected
267 fault (Fig. 6c). In the south of the valley a linear braided reach is similarly parallel to the projected
268 fault, and individual braid channels are anomalously linear (Fig. 6d). Palu-Koro Fault strands cutting
269 an alluvial fan and offsetting its incised drainage directly along strike to the south confirm that the
270 river is structurally controlled. It is more reasonable to project this southern fault strand directly north
271 across the basin than it is to consider strike-slip strain transferring immediately to the western sidewall
272 fault between Pakuli and Bolongga, particularly as geomorphic indices in that region indicate a
273 relatively low tectonic rate (Fig. 5a).

274 Thus we propose that much of the Palu-Koro Fault strike-slip strain through the Palu valley is not
275 accommodated on the prominent sidewall faults, but on a cross-basin fault system that is obscured by
276 fluvial deposits during interseismic periods (as it is now) (Figs. 5a & 6a). The sidewall faults are
277 largely an extensional partition, explaining the lateral slip deficit across them, noted by Bellier *et al.*
278 (2001). Confinement of the Palu river meander belts within the strike-slip cross-basin fault system
279 may be a due to development of a subtle graben, or to changes in permeability, cementation or
280 compaction in the Quaternary valley fill resulting from penetration by strike-slip strands.

281 The valley's eastern sidewall fault is generally much more segmented and strongly eroded than in the
282 west with gentle slopes and irregular mountain fronts (Fig. 6a). South of the intersection with the
283 Sapu valley fault system, S_{mf} values are 1.19-1.59 and V_f averages of 0.55 indicate rapid to moderate
284 tectonic activity. North of the Sapu valley intersection, S_{mf} is 2.30 and average V_f is 0.80, indicating
285 slow tectonic activity.

286 Further south along the Palu-Koro Fault the Gimpu basin exists at a small releasing step-over, and the
287 Leboni basin occupies a releasing bend near the faults southern termination (Fig. 4). The Palu-Koro
288 Fault bounding these flat-topped Quaternary basins has S_{mf} values of 1.11 and 1.12 respectively, and
289 similarly low V_f , 0.56 and 0.89, indicating rapid to moderate tectonic activity.

290 *Sapu valley fault system*

291 A complex NW-SE trending fault system 75 km long cuts across crystalline basement between Palu
292 valley and the Tokorondo Mountains in the east (Fig. 4). The fault system is dominated by a double
293 bend – a releasing bend forming the intermontane Sapu valley (~600 m elevation), and a restraining
294 bend associated with uplift at the head of the valley (Fig. 5a). Both bends are consistent with an
295 overall left-lateral shear sense for the fault system. Anecdotal reports from residents of the valley
296 (various, pers. comm. 2009) suggest that earthquakes are frequent and well known, though there is
297 little instrumental seismicity and no record of historical earthquakes.

298 Sapu valley is an irregular rhomboidal basin bounded by normal faults trending NNW-SSE and E-W
299 (Fig. 7a). Many of the faults are arcuate, convex into the basin. Their range front slopes are generally
300 gentle, but S_{mf} values of 1.09 to 1.45 and average V_f is 0.40 suggest rapid to moderate tectonic
301 activity (Fig. 7b). A conspicuous feature of the basin floor is the strong confinement of river channels
302 to narrow linear meander belts (Fig. 7b), as discussed above for the Palu River. Both modern and
303 abandoned channels have linear meander belt margins and square longitudinal sections parallel to the
304 projected trace of the fault system through the valley, implying fault penetration through the
305 Quaternary basin fill (Fig. 7c, d). In the same way as for the Palu valley, this evidence supports a
306 cross-basin fault system that accommodates most of the strike-slip strain, while the prominent
307 sidewall faults are dominantly extensional structures. The cross-basin fault system is buried by fluvial
308 sediments, but coseismic subsidence, or changes in permeability, cementation or compaction caused
309 by periodic surface rupture through the Quaternary basin fill continue to influence meander patterns.

310 At the head of the valley the entire fault system curves to a more NNW-SSE trend – a restraining
311 geometry under sinistral shear. A broad oversized valley in the west is presently at 700 m elevation
312 (Fig. 7a), i.e. 100 m above the modern Sapu valley floor. Exhumed brittle SW-dipping reverse-
313 sinistral faults in mica schists along the uplifted valley support long-lived uplift at this restraining
314 bend (Fig. 7e, f). At the foot of the westernmost oblique-reverse fault, S_{mf} is 1.08, suggesting maximal
315 tectonic activity (Fig. 5a).

316 Drainage networks extracted from SRTM data show that there is presently a drainage divide
317 separating the Salo Wuno and Salo Sapu catchments basins in the position of the thrust-related uplift
318 and oversized valley (Fig. 5a). Water presently exits Sapu valley via a narrow, steep-sided gorge (Fig.
319 7a). The extreme steepness and geomorphic immaturity of that gorge suggests that it has recently
320 captured the Sapu valley drainage, perhaps in response to tectonic uplift of its former well established
321 route to the NW via Salo Wuno. It is likely that for some time after uplift in the NW, Sapu valley was
322 internally drained and may have contained an intermontane lake similar to Lake Lindu to the south
323 (Fig. 4), explaining the flat base of Sapu valley.

324 In summary, four lines of evidence suggest the Sapu valley fault system has been active during the
325 Quaternary: a) control of modern river meander belts by a cross-basin fault system that traverses the
326 Quaternary basin fill; b) youthful geomorphic expression of the Salo Sapu gorge where it has
327 apparently recently captured the Salo Sapu in response to tectonic uplift in the NW; c) rapid to
328 moderate tectonic activity along the transtensional segment sidewall faults, indicated by geomorphic
329 indices; d) maximal tectonic activity along the transpressional segment's reverse faults implicated in
330 uplifting the oversized palaeo-valley in the east, indicated by geomorphic indices.

331 *Matano Fault*

332 The Matano Fault passes from southern central Sulawesi through the island's SE arm to Tolo Bay
333 (Fig. 4). It is typically shown to mark the southern edge of the Sula Block, linking to the Palu-Koro
334 Fault to the west and the North Sulawesi Trench to the north (e.g. Hamilton 1979; Rangin *et al.* 1999).
335 A hard linkage between either the Lawanopo or Matano and Palu-Koro faults is a requirement of
336 many rigid-block models for Sulawesi (e.g. Bellier *et al.* 2006; Socquet *et al.* 2006). However, Silver
337 *et al.* (1983b) noted that the nature of the connection was not known. Modern satellite imagery shows
338 a highly segmented and discontinuous westernmost Matano Fault curving towards the Palu-Koro
339 Fault, but the two structures remain largely isolated either side of the Gunung Balease massif (Fig. 4).

340 In the east, the Matano Fault passes into the northern Banda Sea. Some workers link it to the Tolo
341 Thrust (sometimes referred to as the Hamilton Thrust or the East Sulawesi Trench) (Fig. 1), an ESE-
342 verging thrust zone NE of Buton. Silver *et al.* (1983b) suggest that the Matano and Palu-Koro faults
343 act as a trench-trench transform between the north Sulawesi subduction and the Tolo Thrust. This
344 thrust has been considered to accommodate convergence between the Makassar block and the Banda
345 Sea block (e.g. Socquet *et al.* 2006). However, recent work suggests that the Tolo thrust is a gravity-
346 driven feature at the foot of a series of slumps (Rudyawan *et al.* 2011), rather than a tectonic block-
347 bounding structure (e.g. Silver *et al.* 1983b; Rangin *et al.* 1999).

348 Geological offsets (e.g. Ahmad 1975) and stream offsets (e.g. Hamilton 1979) across the Matano
349 Fault confirm that it is a left-lateral structure and that it has been active during the Quaternary (Bellier
350 *et al.* 2006). Laterally offset streams are routinely used to assess the shear sense and Quaternary
351 activity of strike-slip faults, usually in arid environments (e.g. Sieh & Jahns 1984), but also in humid,
352 forested environments (e.g. Lacassin *et al.* 1998; Wang *et al.* 2014). Nonetheless, such observations
353 must be interpreted cautiously, as stream offset may result from stream diversion along a fault and
354 capture by another downstream reach, as well as by genuine tectonic displacement of a single stream
355 (Wallace 1990). There have been no studies to use such offsets to evaluate Quaternary slip rates along
356 the Matano Fault.

357 The Matano Fault is highly segmented, and lacks a single through-going strand (Fig. 8a). Several
358 linear basins (e.g. Pansu, Matano and Mahalona) lie within or adjacent to the fault zone, often at step-
359 overs between strands. Each basin is 4-6 km wide and 20-30 km long. The Matano basin hosts Lake
360 Matano, which at 590 m deep (Haffner *et al.* 2001), is the deepest lake in Indonesia and the 10th
361 deepest in the world. A fault passing from the northern margin of the Pansu Basin is very prominent
362 as it cuts through ultramafic rocks in the SW corner of Lake Matano, just south of Desa Matano (Fig.
363 8a). The fault then steps to the left to another very prominent fault in the NW of the lake, from where
364 it passes across the Mahalona Basin's northern margin. Rapid subsidence in the lake and earthquake
365 focal mechanisms recording E-W extension close to the lake likely result from this releasing geometry
366 (McCaffrey & Sutardjo 1982). Two major pop-ups associated with uplift, thrusting and exhumation of
367 metamorphics and serpentinite at restraining bends occur east of the Mahalona Basin and west of the
368 Pansu basin (Fig. 8a).

369 A number of consistent left-lateral stream offsets and evidence of stream capture across two fault
370 strands west of Pansu Basin (Fig. 8b) and steep-sided, narrow fault valleys (Fig. 8c), suggest youthful
371 fault activity. Geomorphic indices of oblique basin-bounding faults range from S_{mf} : 1.06-1.28,
372 average V_f : 0.69 (Pansu Basin); S_{mf} : 1.02-1.17, average V_f : 0.78 (Matano Basin); S_{mf} : 1.19, V_f : 0.45
373 (Mahalona Basin); to S_{mf} : 1.08-1.9, average V_f : 0.51 (eastern termination splay), and indicate mostly
374 rapid to moderate tectonic activity.

375 On 15th February 2011 a shallow focus M_w 6.1 earthquake near the western end of Lake Matano
376 (NEIC) had a focal mechanism consistent with left-lateral slip along the Matano Fault. The
377 earthquake caused damage to concrete walls and buildings, including a newly-built hospital in the
378 Mahalona valley (Fig. 8d). The earthquake's location suggests that the prominent fault segment that
379 links the NE corner of Lake Matano with the Mahalona Basin failed (Fig. 8e). 'Surface cracks' were
380 reported by locals at the eastern end of the basin, and though we visited the area in October 2011, a
381 surface rupture could not be located. Close to the lake, very high resolution satellite imagery recently
382 made available (Bing Maps) shows three clear lineaments cutting across boggy ground and low-lying
383 forest (Fig. 8f) along strike from a Matano Fault strand that offsets drainage to the left. While it is not
384 possible to confirm that they represent the 2011 surface rupture, these lineaments appear to be
385 tectonic in origin and are clearly very young. Linking these lineaments with the reported surface
386 cracks in the east, along a topographically clearly defined fault strand, yields a postulated surface
387 rupture length of > 39 km, which is longer than expected for a M_w 6.1 earthquake from empirical
388 relationships (Wells & Coppersmith 1994).

389 *Lawanopo Fault and Lake Towuti*

390 The Lawanopo Fault (Fig. 4) consists of several straight NW-trending fault segments that cross
391 Sulawesi's SE arm south of the Matano Fault. The Lawanopo Fault is used in preference to the
392 Matano Fault by Socquet *et al.* (2006) as the southern margin of the 'East Sula Block'. However,
393 discontinuous and eroded fault traces along strands of the Lawanopo Fault system suggest that it has
394 been mostly inactive during the Quaternary (Bellier *et al.* 2006; Natawidjaja & Daryono 2014).
395 Nonetheless, recent earthquakes close to Kendari may indicate that at least some strands of the
396 Lawanopo Fault system remain active. An M_w 7.5 earthquake in the Banda Sea 170 km SE of Kendari
397 on 19th October 2001 had a strike-slip focal mechanism, and may have originated on the projected
398 offshore trace of the Lawanopo Fault (Yeats 2010).

399 Like the Matano Fault, the Lawanopo Fault is highly segmented and there is no through-going strand
400 at the surface (Fig. 4). Mountain front sinuosity values on the few segments associated with adjacent
401 basins range from 1.21 to 1.75, and valley depth/width ratios average 0.55-0.83, indicating moderate
402 to slow tectonic activity.

403 Lake Towuti, the largest of the Malili Lakes, occupies an intermontane basin at 318 m elevation and
404 has a maximum water depth of 203 m (Haffner *et al.* 2001). The basin lies in the wedge between the
405 Matano and Lawanopo faults, and is itself cut by linear fault strands that internally deform the wedge
406 (Fig. 4). Two prominent curvilinear faults lie along the south and east of the lake (Fig. 8a). The
407 closest, trending NE-SW and downthrown to the NW, forms the linear eastern lake boundary, and is
408 marked by a number of fans prograding into the lake. Its high mountain front sinuosity (2.04) and
409 valley depth/width ratios (1.22) suggest slow tectonic activity. However, a large earthquake along this
410 >25 km long structure could cause a substantial tsunami or seiche in the lake. The second fault, to the
411 east, is longer still (>55 km) and highly continuous. It intersects the Lawanopo Fault at a small angle,
412 and may directly transfer slip away from that structure. Mountain front sinuosity ranges from 1.03-
413 1.15, suggesting maximal to rapid tectonic activity, though valley floors are rather rounded (V_f
414 average is 0.49). Lake Towuti would rapidly fill with sediment if it were not actively subsiding,
415 therefore the bounding normal faults must be considered to be active during the Quaternary.

416 *Kolaka Fault*

417 The Kolaka Fault (Simandjuntak *et al.* 1984, 1994; Suroño 1994) (Fig. 9a) lies along the southern
418 margin of the Mengkoka mountains, and is sub-parallel to the Lawanopo Fault to its north. It is
419 equivalent to the *Mendoke Fault* of Bellier *et al.* (2006). Hamilton (1979) interpreted the fault as a
420 SW-dipping thrust, Bellier *et al.* (2006) considered the fault as a pre-Early Pleistocene strike-slip
421 continuation of the Palu-Koro Fault, but there is little evidence to support either hypothesis. One
422 strand of the Kolaka Fault is sealed by 4.4 ± 0.2 Ma dacites, potentially placing a limit on the timing
423 of faulting (White *et al.* 2014).

424 The fault is composed of several NE-SW-trending gently arcuate segments up to 45 km long in map
425 view. Along Bone Bay coast and at Kolaka town the downthrown side is to the south, the easternmost
426 segment is downthrown to the north (Fig. 9a). The polarity shift occurs across a 10 km wide relay
427 straddling the Anggowala mountains. The orientation of these two apparently normal fault systems is
428 kinematically consistent with sinistral slip along the overall Kolaka trend.

429 Geomorphic indices are highest closest to Kolaka town, where S_{mf} values of 1.22 to 1.30 and V_f
430 values of 0.23-1.68 suggest that there is rapid to slow active dip-slip across the fault, which has clear
431 surface expression and is marked by triangular facets (Fig. 9c). Along strike to the NW a series of
432 linear valleys and low ridges near Lasusua may be a continuation of the Kolaka Fault (Fig. 9b). An
433 absence of fault scarps or clearly displaced features makes fault activity hard to evaluate, but meander
434 confinement within a linear graben across the Lasusua alluvial plain and asymmetric subsidence
435 highlighted by the river's proximity to the bounding fault suggests recent fault activity (Fig. 9d).

436 Faults downthrown to the WSW at the western end of the Kolaka Fault have very low S_{mf} and V_f
437 values (1.05, 1.25 respectively), deeply incised streams and well developed triangular facets,
438 suggesting Quaternary dip-slip. These faults face into Bone Bay and may be related to basin-bounding
439 extensional structures accommodating subsidence in the bay (Camplin & Hall 2014).

440 *Balantak Fault*

441 A prominent ENE-trending linear structure, the Balantak Fault lies at the eastern end of Sulawesi's
442 east arm and separates the Batui thrust system in the south from mountainous highlands in the north
443 (Fig. 10a). It has been considered to be part of the Batui thrust system (Silver *et al.* 1983b) but its
444 remarkably straight outcrop, field observations (Simandjuntak 1986) and along-strike alternation
445 between local uplift and subsidence suggest that it is a steep, possibly strike-slip fault.

446 Onshore, where the fault bends gently to the right, small apparently Quaternary basins are developed
447 (Fig. 10b). Where the fault bends gently to the left there is uplift. Both observations are kinematically
448 compatible with a dextral shear sense. One of the zones of Quaternary subsidence is shown in Fig.
449 10c. A basin-bounding fault at a small clockwise angle from the regional Balantak Fault trend is
450 crossed by streams that show no systematic offset, suggesting dominant dip-slip. To the north, a
451 prominent lineament crosses the basin, expressed by lines of vegetation and slightly darker (moister?)
452 soil. This lineament's parallelism with the Balantak Fault to the east and its negligible topographic
453 relief suggests it is the through-going strike-slip fault strand. Although stream avulsion across the flat-
454 topped basin is too dynamic to preserve meaningful offsets, the clear expression of the fault in the
455 young sediments suggests the Balantak Fault has been active during the Quaternary.

456 The Balantak Fault's termination system offshore to the east of Poh Head is composed of left-stepping
457 segments separated by folds and thrusts (Fig. 10d). Contraction between left-stepping main segments,

458 an apparently antithetic sinistral fault, and the orientation of folds and thrusts are all kinematically
459 compatible with dextral shear along the Balantak Fault (Watkinson *et al.* 2011). Earthquakes located
460 onshore and west of Poh Head also suggest right lateral and reverse slip parallel to the Balantak Fault
461 (Fig. 10a). However, a swarm of offshore earthquakes between Peleng and Taliabu to the east have
462 focal mechanisms which support sinistral slip along the Balantak trend. This apparent contradiction is
463 discussed in Watkinson *et al.* (2011). Here we conclude that the geologic and geomorphic evidence
464 supports long-term Quaternary dextral slip. Further work is required to understand the significance of
465 a small number of contradictory seismological signals in the area.

466 The Balantak Fault is almost continuous for 54 km from Balantak town in the east to Poh Bay in the
467 west, where it likely continues just offshore for another >30 km. Extending to include the dextral fault
468 system offshore to the SE makes the fault up to 250 km long. The onshore fault scarp has
469 exceptionally low S_{mf} values, from 1.04 to 1.22 (Fig. 10b), with correspondingly low average V_f
470 values of 0.36, suggesting maximal to moderate tectonic activity.

471 *Gorontalo Fault*

472 The Gorontalo Fault (Katili 1973) (Fig. 11a), has been considered to be one of the major block-
473 bounding structures of Sulawesi (e.g. Socquet *et al.* 2006; Molnar & Dayem 2010). Geodetic
474 modelling suggests 11 mm/yr dextral slip rate and 10 km locking depth; however, as observation
475 points are widely spaced, it remains possible that GPS data record rotation of the entire north arm of
476 the island rather than discrete slip across a fault (Socquet *et al.* 2006). There is little modern shallow
477 seismicity in the Gorontalo area, suggesting that the fault is inactive or remains locked (Fig. 11a).

478 The fault is composed of several branching segments, including major ~30 km long segments south
479 and north of Gorontalo city (Fig. 11b). Limboto lake lies in the 7 km wide step-over between these
480 two segments, indicating local transtension. The fault is expressed by highly eroded scarps passing
481 along the Tomini Bay coast and bounding the Gorontalo/Limboto depression. Geomorphic indices
482 suggest that the segments experience slow to minimal tectonic activity, with S_{mf} values ranging from
483 1.83 to 2.36 and an average V_f of 1.28. Though there is considerable human development within the
484 Gorontalo/Limboto depression which may obscure neotectonic activity, there appears little evidence
485 of deformation within the Quaternary sediment fill, except for the presence of Limboto lake
486 subsidence at the releasing step-over.

487 *Western Tomini Bay bounding faults*

488 A series of faults along the margin of Tomini Bay show evidence of recent activity. The faults are
489 arcuate and generally mark the boundary between mountainous ground along Sulawesi's narrow
490 'neck' and Tomini Bay, which is up to 2 km deep and contains a sedimentary succession up to 10 km
491 thick (Jablonski *et al.* 2007; Pholbud *et al.* 2011). Extension and mantle decompression across the bay
492 is associated with Plio-Pleistocene volcanism in the Togian Islands and possibly with modern
493 volcanism at Una Una volcano (Cottam *et al.* 2011) supporting recent extensional faulting and
494 lithospheric thinning both on and offshore (Pholbud *et al.* 2011).

495 The northernmost bounding fault bounds the 2.5 km high Molino Metamorphic Complex (Fig. 11c), a
496 suite of quartzofeldspathic mica schists and gneisses that may be an exhumed metamorphic core
497 complex (van Leeuwen *et al.* 2007). The faults dip north and south on the north and south sides of the
498 complex respectively, and have crystalline basement in their footwalls. The southern segment has a
499 curvilinear trace more than 75 km long, with extremely low S_{mf} values (1.05) and well-developed

500 triangular facets at the end of V-shaped valleys with V_f values of 0.33-0.64 within an uplifted footwall
 501 block. On this basis, combined with no evidence of strike-slip, it is interpreted as a normal fault.

502 Further SW, Tomini Bay bounding faults are crossed by a number of fan deltas prograding into the
 503 bay which are surprisingly short (<3 km), given the potential upstream sediment source, suggesting
 504 rapid and recent hangingwall subsidence (Fig. 11d, e). Segments further south along the 'neck' have
 505 higher S_{mf} values (1.66) and fan delta lobe length increases to over 10 km, suggesting less significant
 506 recent subsidence (Fig. 11f).

507 At the southern end of the neck, a NE-dipping fault system, including the Tambarama Fault (Pholbud
 508 *et al.* 2011) forms an apparently continuous arcuate trace at Parigi (Fig. 4), marking the boundary
 509 between the Palu Metamorphic Complex onshore (van Leeuwen & Muhandjo 2005) and Tomini Bay
 510 subsidence offshore. S_{mf} values are generally high (2.77 to 3.25), though a short northern segment is
 511 less sinuous at 1.32. A well-developed apron of fan deltas extends 6 km from the mountain front.

512 **Maluku and North Maluku**

513 Maluku and North Maluku are composed of numerous islands affected by disparate neotectonic
 514 processes. In the north, Halmahera (Fig. 1) and the Sangihe Arc are involved in the active collision of
 515 two accretionary complexes above the subducted Molucca Sea slab, where the Sangihe forearc is
 516 being thrust eastwards over the Halmahera forearc (e.g. Silver & Moore 1978; Hamilton 1979; Hall
 517 1987; Hall *et al.* 1995). The entire system accommodates 80 mm/yr of the 105 mm/yr Philippine Sea
 518 Plate-Sundaland convergence (Rangin *et al.* 1999). Splays of the left-lateral Sorong Fault pass
 519 through and to the south of Halmahera and Bacan, where there is abundant modern seismicity (e.g.
 520 Ali & Hall 1995; Hall *et al.* 1995) (Fig. 1).

521 South of Bacan, islands with Australian continental basement such as the Banggai-Sula Islands and
 522 Obi, are bounded by strands of the Sorong Fault and were for a long time considered to have been
 523 translated from New Guinea along a 1900 km long Sorong Fault passing from northern Papua New
 524 Guinea towards Sulawesi (e.g. Visser & Hermes 1962; Audley-Charles *et al.* 1972; Hamilton 1979;
 525 Silver & Smith 1983; Pigram *et al.* 1985; Garrard *et al.* 1988; Hutchison 1989). New interpretations,
 526 based on evidence of extreme crustal extension and mantle exhumation, mantle tomography and
 527 geodynamic models (e.g. Spakman & Hall 2010; Spencer 2011; Hall 2011; Pownall *et al.* 2014),
 528 suggest that those islands, together with others along the northern Banda Arc such as Buru and Seram,
 529 were part of a continental spur that was fragmented during Miocene-Pliocene times by Banda Sea
 530 rollback-driven lower crustal delamination.

531 Quaternary extension in Maluku appears to be as important as it is in Sulawesi, despite a collisional
 532 overall tectonic setting. Young metamorphic core complexes exhumed in Seram (Pownall *et al.* 2013)
 533 and possibly Buru (Roques 1999) are associated with low angle and steep normal faults. A significant
 534 component of the seismic moment release in Maluku is by normal and strike-slip earthquakes,
 535 alongside important thrusting in the Molucca Sea and north Seram (e.g. Rangin *et al.* 1999). Finally,
 536 sinistral transpression through Seram accommodates Australia-Pacific convergence and links into the
 537 Tarera-Aiduna Fault of West Papua (e.g. Rangin *et al.* 1999; Stevens *et al.* 2002; Teas *et al.* 2009).

538 *Banggai-Sula Islands*

539 The Banggai-Sula Islands (Fig. 10a) occupy a fragment of continental crust of Australian affinity that
 540 has collided with the east arm of Sulawesi (e.g. Audley-Charles *et al.* 1972; Hamilton 1979; Pigram *et*

541 *al.* 1985; Garrard *et al.* 1988). The South Sula-Sorong Fault was interpreted by Hamilton (1979) to
542 follow the break in slope south of Taliabu and pass between Mangole and Sanana. North of the
543 Banggai-Sula Islands the North Sula-Sorong Fault (e.g. Hamilton 1979; Norvick 1979; Silver *et al.*
544 1983b; Sukanto & Simundjuntak 1983), previously considered to pass from the Bird's Head, past
545 Obi, and along the north margin of the Banggai-Sula Islands towards Sulawesi's east arm, cannot be
546 detected in new geophysical data and must lie below the Molucca Sea collision complex to the north
547 (Ferdian *et al.* 2010; Watkinson *et al.* 2011).

548 Despite the density of deformation in the area, immediately north of the Banggai-Sula margin there is
549 very little shallow seismicity (Engdahl *et al.* 1998; Rangin *et al.* 1999; Beaudouin *et al.* 2003),
550 indicating that there are few active structures, that deformation is largely aseismic, or that the main
551 faults have interseismic periods which exceed instrumental records. This is a marked contrast to the
552 abundant shallow seismicity associated with the Molucca Sea collisional zone further north. However,
553 a number of focal mechanisms north and south of the islands indicate that there is some residual left-
554 lateral slip on E-W to NW-SE trending faults (Fig. 10a).

555 Mangole Island appears to be bordered along its north and south sides by several linear E-W trending
556 normal faults, indicated by straight traces and well-developed triangular facets (Fig. 12a, b). Mountain
557 front sinuosity values range from 1.11 to 1.57, and V_f is from 0.44-0.55 suggesting that some of the
558 structures have been active during the Quaternary. Sanana Island, topographically orthogonal to
559 Mangole, is bounded by NNW-SSE trending faults that can be traced offshore in multibeam
560 bathymetry. The most prominent fault, on the east coast, forms a well defined scarp over 20 km long,
561 dipping and down-thrown to the east, making it likely to be a normal fault (Fig. 12c). Triangular
562 facets, hanging valleys, deeply incised streams (Fig. 12d) and an absence of subaerial prograding fan
563 delta tops wider than about 400 m suggest rapid recent eastward subsidence along the fault, supported
564 by S_{mf} values of 1.27 to 1.34.

565 Taliabu Island (Fig. 10a) is cut by a number of E-W and N-S trending Quaternary faults. North-south
566 trending faults in the west have particularly fresh geomorphic expression. A north coast bedding-
567 parallel dip-slope dips 6° into the Molucca Sea (Fig. 13a). Offshore to the north a planar detachment
568 surface 34 km wide exactly corresponds to the Taliabu dip-slope onshore, and represents a submarine
569 slope failure (Watkinson *et al.* 2011). Both onshore and offshore slopes appear to be part of a single
570 large glide surface of a mega-debris slide that translated much of north Taliabu at least 37 km north
571 into the Molucca Sea, likely causing a significant tsunami.

572 The north Taliabu dip-slope is truncated by several prominent E-W trending faults that dip steeply
573 north. Geomorphic expression is very fresh (Fig. 13b) – footwall crests are only slightly eroded, in
574 most cases drainage runs parallel to fault scarps and has not cut across them, except for a few
575 prominent high order streams. The faults displace the dip-slope, and so must post-date the mega-
576 debris slide. Though we have no absolute constraint on the timing of the slide, reef build-ups are
577 conspicuously poorly-developed along the section of coast at the foot of the dip-slope, but are
578 extensive along the coast and small islands either side. The slide must have happened recently enough
579 that corals have been unable to fully recolonise the new coastline, suggesting that the post-slide
580 normal faults are late Quaternary and likely still active.

581 *Sorong Fault from Obi to Waigeo*

582 Westward splaying segments of the Sorong Fault emanate from the western Bird's Head and pass
583 close to the islands of Salawati, Misool, Obi, Bacan, south Halmahera, and Waigeo (e.g. Katili 1975;
584 Hamilton 1979; Ali & Hall 1995) (Fig. 1). Though there is debate about whether the Sorong Fault

585 onshore West Papua is tectonically active (discussed below in *Sorong Fault in West Papua*), at the
586 latitude of Obi there is 19 ± 8 mm/yr left lateral displacement between Ternate and the Bird's Head
587 that may be accommodated by one or more strands of the Sorong Fault (Bock *et al.* 2003). Seismicity
588 is limited in the islands immediately west of the Bird's Head, but intense seismicity occurs around
589 Obi, Bacan and south Halmahera (Rangin *et al.* 1999), which may be where sinistral strain is
590 transferred from Seram into the Molucca Sea.

591 *Seram fold and thrust belt*

592 Between northern Seram and the Bird's Head is a broad zone of transpression linked to convergence
593 between Australia and the Pacific plate (Fig. 1). A deep bathymetric trough, the Seram Trough, lies
594 150 km north of Seram island, and curves around the Banda Sea, linking to the Timor Trough and
595 ultimately the Java Trench. The Seram Trough has been interpreted as a subduction trench (e.g.
596 Hamilton 1979), a foredeep ahead of a fold and thrust belt (e.g. Audley-Charles 1986), and a hinge
597 zone marking the northern limit of delaminated and subducted lower continental crust (Spakman &
598 Hall 2010).

599 Convergence across the Seram Trough is presently 20 mm/yr (Rangin *et al.* 1999; Stevens *et al.* 2002)
600 and is associated with intense seismicity generated by shallow thrust faulting (McCaffrey 1989;
601 Engdahl *et al.* 1998) mainly concentrated along the northern edge of Seram (Fig. 14a), and entirely in
602 the western part of the fold belt (Teas *et al.* 2009).

603 Seram is centred on a belt of high mountains (>3 km elevation), which include tracts of continental
604 metamorphics, ultramafic rocks and Earth's youngest exposed ultra-high temperature granulites,
605 exhumed since 16 Ma (Pownall *et al.* 2014). Plio-Pleistocene Wahai and Fufa formations onlap the
606 elevated pre-Pliocene succession forming low plains along the northern coast (Pairault *et al.* 2003),
607 and are themselves overlain by modern alluvial and reef deposits. Within these plains there is
608 evidence of active contraction.

609 On the north coast of Seram, onshore fold growth affects modern drainage, suggesting that the folds
610 have been active during the Quaternary (Fig. 15a). Three large rivers draining the northern slopes of
611 the Kobipoto Mountains are deflected from a linear route to the coast by two sets of segmented E-W
612 to NW-SE trending hills. Progressive migration of the rivers away from the hill tips is recorded by a
613 trail of abandoned and filled river channels left behind the deflected river, expressed by oxbow shaped
614 fields and areas of vegetation (Fig. 15b, c). Larger hills, like that in the centre of Fig. 15a, cause more
615 deflection than smaller folds, like that in the east which only deflects Wai (*stream*) Kobi slightly. In
616 all cases the abandoned channels are located upslope of the modern river, suggesting that progressive
617 uplift is forcing river avulsion. This tendency for the hills to grow symmetrically from a central axis,
618 their elongate morphology and their asymmetry (steep northern slopes, shallow southern slopes)
619 supports the interpretation that they are the surface expression of shallow, north-vergent fault
620 propagation folds above south-dipping thrusts (Fig. 15d).

621 Abandoned meander channels and point bars on the coastal plain in the central part of Fig. 15d are not
622 associated with any obvious modern river, but seem to originate at the foot of the central frontal
623 thrust. Abandoned remnants of a comparably large river can also be observed in an uplifted valley
624 immediately to the south, and directly north of a fourth major north flowing river, which presently
625 abruptly curves around the eastern tip of the fault before joining Wai Musi. It is interpreted that the
626 abandoned channels here represent a river which flowed directly north before the fold developed. An
627 uplifted valley across the mid-point of the fold shows that the river attempted to down-cut as the fold

628 grew, but was ultimately thwarted by a high uplift rate, and swung east to be captured by Wai Musi.
629 Deep lateral incision by the captured river into the back limb of the fold (Fig. 15b), suggests that the
630 fold growth, and presumably underlying thrust activity, is ongoing.

631 A series of abandoned channels east of Wai Musi, the easternmost of which link to Wai Kobi,
632 indicates that river itself may previously have been a tributary to Wai Kobi, before being deflected to
633 the west and ultimately cut off from the trunk stream, presumably by uplift above the eastern frontal
634 thrust.

635 Such evidence of recent hangingwall uplift and tectonic folding, together with the low relief of the
636 range front, leads to the conclusion that the faults are youthful low-angle south to SW-dipping thrusts,
637 supported by focal mechanisms along the north coast (Fig. 14a). Uplifted coastal terraces in the
638 foreland of the onshore thrusts and a conspicuously wide coastal plain (Fig. 15d) suggest additional
639 young uplift north of the onshore thrusts, perhaps in response to a third set of active faults just
640 offshore. This is consistent with modern thrust activity within the broad fold and thrust belt offshore
641 (e.g. Engdahl *et al.* 1998; Teas *et al.* 2009) and a 1629 mega-thrust earthquake likely originating in
642 the Seram Trough (Liu & Harris 2013).

643 *Kawa Fault*

644 The Kawa Fault (Pownall *et al.* 2013) lies in the prominent ESE-WNW-trending deep linear valley
645 that passes through central Seram (Fig. 14a), occupied by the Kawa River. The fault broadly separates
646 upper-greenschist to mid-amphibolite facies Tehoru Formation rocks in the south from generally
647 higher grade metamorphics of the Saku and Taunusa complexes in the north (Gemeraad 1946;
648 Tjokrosapoetro *et al.* 1993; Pownall *et al.* 2013). The Kawa Fault coincides with the position of
649 strongly mylonitic garnet-bearing Tehoru Formation schists with a steeply-dipping foliation
650 considered by Linthout *et al.* (1991) to record dextral shear, but now recognised to have been
651 intensely folded and possibly originating in a low-angle normal fault, resulting in complexly re-
652 orientated kinematic indicators (Pownall *et al.* 2013).

653 A brittle fault zone up to 2 km wide (Pownall *et al.* 2013) overprints the mylonitic rocks and controls
654 the modern topography (Fig. 16a, b). Fault strands are generally parallel to mylonitic foliation, and
655 contain abundant serpentinite slivers and smears. Mid-way along the fault is a prominent right-step
656 associated with uplift and a major drainage divide, pointing to local transpression due to left-lateral
657 slip. Stream offsets measured from Landsat and Google Earth imagery along the fault (Fig. 16a) range
658 from 66 to 605 m of left lateral offset (22 measurements) to 62 to 334 m of right lateral offset (5
659 measurements). Most measurements have high uncertainty, increased by Seram's extremely humid
660 climate and thick forest cover. Nonetheless, some measurements, for example 268 m and 253 m left
661 lateral offset (e.g. Fig. 16c), are considered robust because: a) they lie on fault segments that are well
662 defined (narrow linear valleys with other independent evidence of a fault origin such as triangular
663 facets, steps/bends with corresponding uplift/subsidence appropriate to river offset sense); b) there is
664 no evidence of stream capture; and c) upstream and downstream valleys have a similar geomorphic
665 character. A left-lateral shutter ridge displacement and a NW-SE-trending fold within the Kawa River
666 delta (Fig. 16a) support recent sinistral shear. A few earthquakes close to the western end of the fault
667 yield CMT solutions suggesting dextral slip along NW-SE-trending planes, while one close to the
668 westernmost splay indicates sinistral slip (Fig. 14a).

669 The fault zone splays as it enters Taluti Bay in the east (Fig. 16a). Splay strands are associated with
670 well-developed triangular facets that record Quaternary normal faulting (Fig. 16d). The two major

671 splays have low S_{mf} values: 1.10 in the north and 1.33 in the south, and an average V_f of 0.27,
672 indicating rapid to moderate tectonic activity. The Kawa river flows hard against the southern splay
673 suggesting active subsidence along that segment, despite its higher S_{mf} indicating slower tectonic
674 activity than in the north. However, the river's position may also be influenced by landslips, debris
675 flows and anticline growth in the northern part of its valley. In the west the fault splays north of
676 Elaputih Bay, attaining a total onshore length of 90 km, or 120 km including a possible splay fault
677 along the north coast of Taluti Bay (Fig. 14a).

678 Although the fault zone is thickly forested, numerous landslip scars can be recognised along the fault,
679 indicating recent seismicity (Fig. 16a). Additionally, the eastern termination is characterised by a
680 series of discontinuous tilted blocks suggestive of slope failure along the southern margin of the
681 Manusela Mountains (Fig. 16a). A M 7.8 earthquake in 1899 triggered landslides that caused a 12 m
682 high local tsunami at Tehoru (www.ngdc.noaa.gov; Brune *et al.* 2010), though it is unclear whether
683 the source was the Kawa Fault or a more distant earthquake. However, all evidence points to the
684 Kawa Fault being active during the Quaternary and capable of generating large earthquakes.

685 *Other active faults of Seram*

686 Along strike from the Kawa Fault on the east side of Taluti Bay, a fault zone occupies the valleys of
687 Wai Masumang and Wai Bobol, and is here termed the Bobol Fault (Fig. 14a). It is highly segmented,
688 though with a total onshore length of 100 km and possible along-strike continuity with the Kawa
689 Fault, it is a significant structure. Four large basins are developed along its length, each bounded by
690 ESE-WNW to SE-NW trending normal faults. Mountain front sinuosity along these structures ranges
691 from 1.26 in the central section to 1.99 in the west, and average V_f is 1.66, indicating moderate to
692 slow tectonic activity. There are a number of stream offsets both across the basin bounding faults and
693 across parallel faults in adjacent mountains (Fig. 16e). Convincing displacements are all left-lateral,
694 and range from 310 m to 2.06 km (Fig. 16f). Most strike-slip fault segments within the fault zone are
695 parallel to the Kawa Fault, and the two fault systems appear to be tectonically related and part of a
696 broader zone of active left-lateral shear linking to the Tarera-Aiduna Fault in West Papua.

697 The southern margin of Seram is locally formed by linear mountain fronts flanked by narrow fan
698 deltas not more than 1 km wide. The mountain fronts' steep, linear aspect, high topographic relief,
699 and topographic lineaments that cross the fans parallel to the mountain front (Fig. 14b) suggests that
700 the mountain front is defined by Quaternary normal faults. However, the coastal range is rather deeply
701 eroded, with S_{mf} values of 1.84 to 2.08 and average V_f of 1.62, indicating slow tectonic activity.
702 Earthquake focal mechanisms towards the west of the coastal fault system in the region of Elaputih
703 Bay support shallow focus, broadly south-directed steep normal faulting (Fig. 14a).

704 A number of other small suspected normal fault systems occur around the SW coast of Seram,
705 including those bounding the Ambon islands. One fault along the northern coast of Hitu (Fig. 14a) is
706 particularly steep and straight, with a S_{mf} of 1.16 and well developed triangular facets along its 16 km
707 long trace. A NE-SW trending lineament that passes through Ambon city marks the southern coast of
708 Ambon Bay (Fig. 14c) and is associated with a zone of fault breccia and foliated gouge several metres
709 thick (Fig. 14d). A M7.6 earthquake occurred on 8th October 1950 close to the south coast of Ambon
710 (Bath & Duda 1979), though it is unlikely that such an event could have been caused by the relatively
711 short, dominantly normal faults visible onshore.

712 *Buru*

713 Buru consists of a presumed Palaeozoic continental metamorphic basement flanked by a Mesozoic
714 sedimentary succession (Tjokrosoepetro *et al.* 1993), both of which are likely continuous with similar
715 units in Seram (e.g. Pigram & Panggabean 1984; Linthout *et al.* 1989). Young K-Ar ages of 4-5 Ma
716 (Linthout *et al.* 1989) and an apatite fission track central age of 2.5 ± 0.5 Ma suggest late Neogene
717 exhumation, possibly accommodated by low angle normal faults (Roques 1999) as similarly
718 postulated for western Seram (Pownall *et al.* 2013).

719 Intense shallow seismicity associated with Seram terminates abruptly in Manipa Strait, east of Buru
720 (Fig. 17a). A broad belt of earthquakes in Manipa Strait possess CMT solutions indicating either
721 NNE-SSW dextral events or WNW-ESE sinistral events, including a 14th March 2006 M_w 6.7
722 earthquake 25 km offshore. Most earthquakes have a component of reverse slip, others are pure thrust
723 earthquakes with a NW-SE trend.

724 Most of Buru's sparse population lives in the NE of the island, including the major town, Namlea. A
725 5-10 km wide system of NW-SE trending faults cuts through the town, across Kayeli Bay, and defines
726 the coastline (Fig. 17b). The faults are expressed in remote sensing data by linear hills and sag ponds
727 at releasing right step-overs, notably at Jikumerasa (Fig. 17c). Fault strands that cut through basement
728 metamorphic rocks and alluvial fans show consistent stream offsets, and pass directly into Quaternary
729 alluvium and control modern river channels (Fig. 17d). Stream offsets of up to 85 m across individual
730 strands are mostly right-lateral, where they are left lateral there is clear evidence for stream capture.
731 Variation in offset sense and amount is to be expected - streams are dynamic and are not passively
732 offset like pre-kinematic geologic markers. The process of offset, beheading and capture, leading to
733 stream offsets of zero or opposite to the fault's shear sense, is well documented and widely observable
734 in active faults worldwide (e.g. Wallace 1968; Sieh & Jahns 1984; Huang 1993; Walker & Allen
735 2012). All these features imply Quaternary NW-SE trending dextral fault activity in NE Buru, despite
736 the apparent discordance with the few earthquake focal mechanisms recorded.

737 A broad fault zone 65 km long almost bisects Buru from the NE to SW (Figs. 17a & 18a). Identified
738 as left lateral on early geological maps (e.g. Tjokrosoepetro *et al.* 1981), little else is known about the
739 fault zone, here termed Rana Fault. Danau (lake) Rana, in the centre of Buru, occupies an
740 intermontane basin within a right step-over between two segments of the Rana Fault, suggesting that
741 the fault is dextral. West of Wadule, Wa (river) Geren is abruptly diverted 90° from a broad oversized
742 valley that would have taken it to the coast in the NE of the island, into a narrow and steep sided
743 canyon (Fig. 18a) that links with Wa Apu and empties into Kayeli Bay further south (Fig. 17a). This
744 pronounced capture of a northern drainage basin by a relatively minor tributary of Wa Apu appears to
745 have been triggered by uplift at a left bend in the Rana Fault immediately east of the capture point
746 (Fig. 18a), again suggesting Quaternary dextral shear.

747 Upstream of the Wa Geren stream capture, the Rana Fault has exceptionally fresh geomorphic
748 expression (Fig. 18b, c), with pronounced triangular facets and very low S_{mf} values, from 1.01 to 1.18
749 along the southern valley slope and a correspondingly low average V_f of 0.25, all suggesting maximal
750 to rapid tectonic rate. There are a number of beheaded and offset streams along the southern valley
751 slope, though there is no consistent tectonic lateral offset. In two places, the axial river has migrated
752 systematically eastwards, leaving behind abandoned channels uplifted up to 10 m above the modern
753 river channel (Fig. 18c). The uplift defines a pair of low amplitude right-stepping en-echelon
754 periclinal folds, consistent with Quaternary right-lateral shear. There is abundant evidence of re-vegetated
755 landslip scars in the surrounding hills close to the fault.

756 A ~10 m high scarp along the base of alluvial fans in the valley, visible in high resolution
757 DigitalGlobe satellite imagery from Google Earth, has the appearance of a normal fault surface
758 rupture (Fig. 18d, e). The valley is relatively thinly vegetated and the scarp, discontinuous over ~7.5
759 km, is well preserved. Though in places it is parallel to the modern river valley, the linear scarp also
760 crosses higher ground, proving that it is not simply an erosional feature. By analogy with proven
761 historical earthquake surface ruptures with similar topographic expression, for example the 1857 Lone
762 Pine earthquake (Beanland & Clark 1994) and the 1609 Hongyazi earthquake (Xu *et al.* 2010), the
763 Buru scarp may have formed during the last few hundred years. The entire 10 m throw could have
764 developed during a single M7.5 earthquake according to empirical relationships (Wells &
765 Coppersmith 1994), or during a number of smaller events, similar to the Star Valley Fault at Afton,
766 Wyoming, where an 11 m high scarp formed during three late Quaternary earthquakes (Piety *et al.*
767 1992) – perhaps a more likely scenario given the relatively short length of the Rana Fault.

768 Elsewhere in Buru other steep normal faults' geomorphic expression suggests rapid to moderate
769 tectonic activity. Faults associated with the Rana Lake basin have S_{mf} values of 1.33 to 1.49 (Fig. 2j).
770 Short fault segments in the SE of the island have S_{mf} values of 1.23 and 1.44, while those on the
771 extreme east coast are more eroded, with S_{mf} values of 1.99 and 2.14 (Fig. 2k), indicating that they
772 have been less active during the Quaternary.

773 **Papua and West Papua**

774 Oblique convergence at an angle of ~60° between Australia and the Pacific is accommodated across
775 Papua and West Papua in a complex zone of strain partitioning between shortening and left-lateral
776 shear (e.g. Abers & McCaffrey 1988; McCaffrey 1996). West of about 138°E shortening is largely
777 accommodated on a variety of structures in the New Guinea Trench and Manokwari Trough, in the
778 Mamberamo fold-thrust belt, and in the central Highlands to the south (e.g. Milsom *et al.* 1992;
779 Puntodewo *et al.* 1994; Stevens *et al.* 2002). The largest earthquake to occur in eastern Indonesia
780 since 1938 was the tsunamigenic 17th February 1996 M_w 8.2 Biak earthquake, which was also the
781 largest thrust event worldwide since 1977 (Henry & Das 2002) and may have been associated with the
782 1979 M7.9 Yapen earthquake (Okal 1999).

783 Left-lateral strain of up to 80 mm/yr resulting from oblique Australia-Pacific convergence is
784 accommodated across a 300 km wide zone of sinistral shear (Stevens *et al.* 2002) focused on the
785 Yapen Fault system in the north, and stepping across Cenderawasih Bay to the Tarera-Aiduna Fault
786 system in the south, largely bypassing the antecedent Sorong Fault in West Papua (e.g. Puntodewo *et al.*
787 1994; McCaffrey 1996; Stevens *et al.* 2002; Bock *et al.* 2003). Left-lateral shear is passed from the
788 Tarera-Aiduna Fault westwards into Maluku via the highly transpressive Seram fold-thrust belt (Teas
789 *et al.* 2009).

790 As in Sulawesi, Maluku and North Maluku, extension is important within the overall convergent
791 orogen. Cenderawasih Bay and the adjacent Waipoga Basin contain thick sediment piles (e.g. Dow &
792 Sukanto 1984; Pubellier *et al.* 1999; Charlton 2010), and metamorphic core complex exhumation at
793 the Wandamen Peninsula (e.g. Bailly *et al.* 2009) indicates extreme lithospheric stretching. While
794 extension may be related to processes within the wide left-lateral shear zone (Stevens *et al.* 2002),
795 lessons from Sulawesi suggest that far-field subduction-related mechanisms may also be significant.

796 *Sorong Fault in West Papua*

797 The Sorong Fault in West Papua is marked by a 15 km wide zone of pronounced linear ridges and
798 valleys trending ENE from northern Salawati, through Sorong city and into the deep valley cutting
799 across the northernmost mainland towards Manokwari in the east (Fig. 19a). Hamilton (1979)
800 questioned whether this structure was significant in post-Miocene tectonics, pointing out that parts of
801 it were covered by post-Miocene strata, and it is now generally considered to be inactive (e.g.
802 Puntodewo *et al.* 1994; Decker *et al.* 2009; Charlton 2010).

803 There is little significant seismicity along much of the fault and geodetic measurements suggest that
804 both sides of the fault are broadly moving together and with the Pacific (e.g. Puntodewo *et al.* 1994;
805 Stevens *et al.* 2002), with slight residual left-lateral motion between Sorong and Fakfak GPS stations
806 possibly accommodated on the Sorong Fault or the Koor Fault to the north (Bock *et al.* 2003).
807 However, the Sorong GPS station is south of important strands of the Sorong Fault, which lie offshore
808 to the north, coming onshore at Mega, and the station is certainly south of the Koor Fault, leaving
809 substantial uncertainty in the amount of present-day left-lateral strain accommodated across this zone.
810 April 1937 M 6.9 and April 1944 M 7.2 and 7.4 earthquakes relocated by Okal (1999) were located
811 on the onshore Sorong Fault 50-100 km west of Manokwari, and had focal mechanisms indicating
812 left-lateral shear. Apparent right lateral motion between Sorong and Biak GPS stations, taken to lie on
813 opposite sides of the Sorong Fault (Puntodewo *et al.* 1994) is complicated by other structures such as
814 the Ransiki and Yapen Faults, which also lie between the stations.

815 Numerous convincing left-lateral stream offsets of up to 300 m are documented in the central part of
816 the fault valley (Dow & Sukamto 1984) (Fig. 20a). Similar sized displacements of Wallace Creek
817 crossing the San Andreas Fault have been dated to 13,259 years (Sieh & Jahns 1984). It is unclear
818 how long such offsets can be preserved in the landscape of an environment like West Papua, but it is
819 unlikely they are pre-Quaternary. Given that few such offsets are preserved in the more obviously
820 active faults of eastern Indonesia such as the Palu-Koro and Matano faults, the Sorong Fault examples
821 must reflect relatively recent and significant strike-slip. Mountain front sinuosity along those
822 segments of the fault associated with vertical motions is also conspicuously low, ranging from 1.16 to
823 1.17 along segments NNE of Sorong city; to 1.14 along the central section where Dow and Sukamto
824 (1984) measured displaced streams, and where triangular facets and shutter ridges are well developed.
825 In the east S_{mf} values of 1.20 and 1.33 also suggest active tectonics. Faults adjacent to flat-topped
826 Quaternary basins associated with Sorong Fault releasing geometries are interpreted to be dominantly
827 normal faults (Fig. 20a), and these structures have generally higher S_{mf} values, including 1.60, 1.61,
828 1.74 and 2.79. Average V_f for all these fault segments is 1.15, consistent with moderate to slow
829 tectonic activity.

830 *Koor Fault and Ransiki Fault*

831 The Koor Fault is an E-W trending structure 20-30 km north of the Sorong Fault (Fig. 19a), which lies
832 within a boundary zone between the oceanic Pacific plate and continental crust in the south (Dow &
833 Sukamto 1984). The NNW-trending Ransiki Fault (Fig. 19a) has been viewed as a dextral shear zone
834 linking the easternmost Sorong Fault and the Yapen Fault (e.g. Robinson & Ratman 1978; Milsom *et*
835 *al.* 1992; Charlton 2010).

836 Like the Sorong Fault in West Papua, both the Koor and Ransiki faults have been considered to be
837 inactive (e.g. Hamilton 1979; Puntodewo *et al.* 1994). However, a shallow M 7.6 earthquake on 10th
838 October 2002 at the southern end of the Ransiki Fault (Fig. 19b) had a focal mechanism and
839 aftershock distribution consistent with dextral slip along the Ransiki Fault (NEIC); though the

840 possibility of sinistral slip along a NE-SW trending splay of the Yapen Fault cannot be excluded.
841 Topographic and bathymetric data from the intersection (Fig. 19b) could be interpreted to show the
842 two structures curving gently into each other, leading to the possibility of contraction in the Ransiki
843 area.

844 Mountain front sinuosity measured along two splays of the southern Ransiki Fault yields values of
845 2.64 for a clearly inactive ~N-S trending southwestern strand, and 1.06 for the linear fault bounding
846 the southern margin of Ransiki delta (Figs. 2p and 19b). The very low S_{mf} and the asymmetric
847 position of the Ransiki River close to the fault scarp (Fig. 20b) support recent extensional activity
848 along the fault. A 2 m high coseismic surface rupture formed close to the fault scarp during the 2002
849 earthquake, and was associated with subsidence of the delta that flooded a low-lying church (D. Gold,
850 pers. comm. 2013), visible in satellite imagery to be coincident with a large region of flooded forest
851 (Fig. 20c).

852 *Yapen Fault*

853 The Yapen Fault (Fig. 21a) is a highly linear E-W trending structure that crosses the 320 km wide
854 northern Cenderawasih Bay, and is similar in character to the Sorong Fault in West Papua (e.g.
855 Hamilton 1979; Dow & Sukanto 1984). In the east, the Yapen Fault vanishes into the Mamberamo
856 delta (Fig. 21a), where it forms a subtle linear valley delineated by active mud volcanoes (Dow &
857 Sukanto 1984) and may dissipate into the Mamberamo fold-thrust belt (Puntodewo *et al.* 1994). In
858 the west the Yapen Fault has an unclear termination, variously interpreted as being dextrally offset
859 from the Sorong Fault along the Ransiki Fault (Puntodewo *et al.* 1994; Charlton 2010),
860 linking/terminating against the Ransiki Fault (Milsom *et al.* 1992) and being unconnected to inactive
861 Ransiki/onshore Sorong faults, but transferring strain south to the Wandamen fault system (Bailly *et*
862 *al.* 2009).

863 Geodetic measurements indicate a fast left-lateral slip rate of 46 ± 12 mm/yr across the Yapen Fault
864 (Bock *et al.* 2003), expressed by intense seismicity and focal mechanisms indicating left-lateral slip
865 along E-W trending subvertical planes (e.g. Okal 1999; Stevens *et al.* 2002). The 12th September 1979
866 M 7.9 tsunamigenic earthquake on the south coast of Yapen island (Fig. 21a) was associated with
867 sinistral slip along a ESE-WNW trending plane focused at a depth of 5 km and likely to have caused 2
868 m of displacement (Okal 1999).

869 The Randaway Fault zone (Dow & Hartono 1982) is a set of NW-SE trending faults onshore Yapen
870 that link to strands of the Yapen Fault in the north (Fig. 21b). Interpreted as post Plio-Pleistocene
871 normal faults, they have previously been used to support a period of right-lateral shear along the
872 Yapen Fault zone (Charlton 2010). However, we see no geomorphic evidence of significant normal
873 faulting along the Randaway trend – instead a small linear basin and lake near the northern tip of the
874 Randaway Fault lies at a left step-over, and a deeply incised stream is offset to the left by almost 1 km
875 – both evidence of Quaternary sinistral shear (Fig. 21b).

876 Although the north coast of Yapen is remarkably straight and clearly fault controlled, the main fault
877 mostly lies just offshore to the north, meaning that geomorphic indices could not be usefully
878 measured along the Yapen Fault. Multibeam bathymetry east of the island shows the Yapen Fault
879 expressed by a straight, narrow lineament marked by pressure ridges and parallel to a prominent set of
880 curvilinear normal faults (Fig. 21c). Splays of the fault curving to the WSW delimit at least two
881 rhomboidal pull-apart basins. At the western limit of the multibeam data a splay appears to enter a
882 third pull-apart basin which is associated with a prominent N-S trending sidewall fault. It is
883 significant that this structure is parallel to and 60 km north of the Wandamen Peninsula – perhaps

884 support for southward transfer of sinistral shear from the Yapen Fault via a region of E-W extension
885 as proposed by Bailly *et al.* (2009).

886 *Mamberamo fold-thrust belt*

887 The Mamberamo fold-thrust belt (Fig. 21a) likely accommodates some Australia-Pacific shortening in
888 eastern Papua, and lies north of the highland thrust belt of central New Guinea (e.g. Dow & Sukamto
889 1984). Unlike the complex oblique convergence and strain partitioning further west, the belt contains
890 relatively simple NW-trending active structures oriented normal to convergence (McCaffrey 1996).
891 Despite intense and widespread seismicity, less than 15 mm/yr of shortening occurs across the
892 Mamberamo belt, leaving much of the remaining 45 mm/yr Australia-Pacific convergence and 100
893 mm/yr of left lateral motion to offshore structures to the north and the Highlands thrust belt to the
894 south (Puntodewo *et al.* 1994; McCaffrey 1996; Bock *et al.* 2003) (Fig. 1).

895 *Wandamen Peninsula faults*

896 The Wandamen Peninsula projects into Cenderawasih Bay from the eastern edge of the Lengguru fold
897 belt, and is bounded on east and west sides by N-S trending faults (Fig. 22). We refer here specifically
898 to these faults, not to the Wandamen Fault Zone of Dow & Sukamto (1984) that connects the Sorong
899 Fault with the Tarera-Aiduna Fault system via the Ransiki Fault.

900 The peninsula is considered to represent the exhumed internal zone of the Lengguru fold belt, and is
901 composed of an amphibolite-eclogite grade metamorphic dome rising to over 2 km elevation
902 (Robinson *et al.* 1990; Bailly *et al.* 2009; Charlton 2010) that may be a metamorphic core complex
903 (e.g. Hill *et al.* 2002). Seismicity and GPS vectors either side of Cenderawasih Bay (Stevens *et al.*
904 2002) suggest active extension accommodated on N-S trending structures close to the Wandamen
905 Peninsula, which may connect to the western releasing termination array of the Yapen Fault in the
906 north (Fig. 21c).

907 Normal faults bounding the peninsula are expressed by curvilinear en echelon segments up to 20 km
908 long trending N-S to NNW-SSE. These make up the east and west detachment systems of Bailly *et al.*
909 (2009). Triangular facets, hanging valleys and V-shaped valleys are common and indicate rapid
910 tectonic activity (Fig. 22b). Two tiers of hanging valleys on the eastern fault system's eroded scarp
911 are defined by changes in valley width or orientation at common elevations along the scarp. They
912 likely record variation in tectonic rate or climate during exhumation of the fault surface. Mountain
913 front sinuosity values of four segments on the east side are uniform at 1.25, 1.28 and 1.29, with one
914 more eroded segment of 1.72. Fan deltas are well developed at relays between the fault segments,
915 notably at Goni, and another smaller delta 21 km further north (Fig. 22a). As well as localising
916 sediment transport, the relays are likely to be sites of active displacement minima, allowing subaerial
917 delta progradation on the hangingwall.

918 On the west of the peninsula S_{mf} values range from 1.05 to 1.43, indicating maximal to rapid tectonic
919 activity. A 21 km long section of the western fault system passing through Wasior shows evidence of
920 recent normal faulting (Fig. 22c). Upper modern fan deltas are abruptly terminated by a linear scarp,
921 above which are narrow truncated palaeofans. Rivers vertically incised into footwall palaeofans show
922 little evidence of lateral erosion, and small landslides are localised along the over-steepened scarp.
923 The scarp is marked by a linear change in topography, lines of vegetation, and frequently an abrupt
924 change from meandering rivers upstream to anatomising rivers downstream of the scarp. A southern
925 continuation of the Wandamen fault system bounds the eastern margin of the Wasimi delta, and has
926 an S_{mf} value of 2.33, indicating slow to minimal tectonic activity.

927 *Other circum-Cenderawasih Bay structures*

928 The locus of active Australia-Pacific left-lateral strain partitioning shifts from the Yapen Fault system
 929 to the Tarera-Aiduna fault system across Cenderawasih Bay, defining a 300 km wide shear zone that
 930 involves a complex array of Quaternary faults within the two bounding strike-slip zones (e.g. Stevens
 931 *et al.* 2002; Bock *et al.* 2003). Along the eastern margin of Cenderawasih Bay, the NE-trending
 932 Lowlands Fault Zone (bounding the Waipoga Trough of Visser & Hermes (1962)) and the Paniai
 933 Fault Zone are associated with thrust and left-lateral strike-slip earthquakes (Fig. 23), offset drainage
 934 and high fault scarps, indicating modern tectonic activity (Pubellier *et al.* 1999; Stevens *et al.* 2002).
 935 The faults have a soft linkage with the Tarera-Aiduna Fault system in the south, and splays curve into
 936 parallelism with the Yapen Fault and Mamberamo fold-thrust belt in the north.

937 The Lengguru fold belt (Visser & Hermes 1962) lies SW of Cenderawasih Bay and the Wandamen
 938 Peninsula, east of Bintuni Bay and the Bomberai Peninsula, and is bounded by the Tarera-Aiduna
 939 Fault system in the south (Fig. 23). Compressional deformation terminated during the Pleistocene
 940 (Decker *et al.* 2009), and the belt is presently largely inactive, except for a few earthquakes related to
 941 gravitational collapse (Bailly *et al.* 2009), often with a left-lateral component related to residual
 942 Tarera-Aiduna strain.

943 *Tarera-Aiduna Fault*

944 The Tarera-Aiduna Fault (Visser & Hermes 1962) is an E-W trending left-lateral shear zone that
 945 forms the southern boundary of the Lengguru fold belt, and passes offshore to the west, north of the
 946 Aru Trough (Fig. 23). The Tarera-Aiduna Fault *sensu stricto* is part of a wide system of faults that
 947 pass, via a diffuse zone of sinistral transpression, into the Seram fold-thrust belt in the west (Teas *et*
 948 *al.* 2009). The fault system is at least 130 km long onshore (Fig. 24), expressed by straight lineaments
 949 clearly visible on satellite imagery (Hamilton 1979) and a set of en-echelon folds (Katili 1986).
 950 Including possible soft linkage to Seram via sinistral transpression within the Seram fold-thrust belt,
 951 imaged in multibeam bathymetric data (Teas *et al.* 2009), the whole fault system may be over 700 km
 952 long. Geodetic measurements show high relative motion between the Birds Head north of the Tarera-
 953 Aiduna Fault, and GPS stations south of the fault, for example at Aru and Timika (Bock *et al.* 2003).
 954 Earthquake focal mechanisms showing sinistral slip along E-W trending vertical planes (e.g. Seno &
 955 Kaplan 1988) suggest that the motion onshore is seismic and occurs along a broad zone (Fig. 23).
 956 West of the Bomberai peninsula seismicity is largely absent, suggesting either a wide zone of
 957 aseismic deformation linking the Tarera-Aiduna Fault with the Seram sinistral transpression (Teas *et*
 958 *al.* 2009), a region of seismic deformation with recurrence times longer than the instrumental record,
 959 or no structural connection between the two regions.

960 The onshore Tarera-Aiduna Fault has geomorphic expression typical of a major strike-slip fault zone
 961 (Fig. 24a). In the west it passes across a low-lying mangrove plain with minimal topographic relief. It
 962 is possible to trace several fault strands from linear features revealed by abandoned river channels and
 963 coastline segments (Fig. 24b). Its central section is expressed by a series of linear ridges of moderate
 964 relief bounding a wide rhomboidal basin (Fig. 24c), across which the captured Aru River passes into
 965 the Uruma River in the south. The river is abruptly deflected as it crosses two prominent fault strands,
 966 with 65-75 m left-lateral displacement, which may reflect recent Tarera-Aiduna Fault slip (Fig. 24d,
 967 e), although this offset is rather speculative.

968 An asymmetric graben developed at the eastern termination of the Tarera-Aiduna Fault is bounded by
 969 NE-SW trending normal faults (Fig. 24f). Rivers pressed hard against the NW-dipping bounding
 970 faults and a SE-dipping set of antithetic faults indicate active subsidence. The easternmost Tarera-

971 Aiduna Fault itself has a significant dip-slip component, forming the northern margin of an 800 m
 972 high ridge. The Tarera-Aiduna Fault and the eastern bounding normal fault have S_{mf} values of 1.08
 973 and 1.21 respectively, indicating that they are both active. Bounding faults along the northern margin
 974 of the rhomboidal basin, including segments which correspond to Hamilton's (1979) Aria River Fault,
 975 have S_{mf} values of 1.63, 1.91 and >4.00 , pointing to slow to inactive tectonics.

976 **Discussion**

977 *Challenges*

978 Identification of Quaternary/modern fault activity in eastern Indonesia has historically proven difficult
 979 (e.g. Hamilton 1979; Dow & Sukanto 1984; Puntodewo *et al.* 1994; Socquet *et al.* 2006; Bailly *et al.*
 980 2009; Teas *et al.* 2009). In part this is because eastern Indonesia cannot be well described in terms of
 981 rigid plate tectonics, involving instead diffuse boundaries and boundary linkages, lithospheric strength
 982 heterogeneity and lower crustal flow (Hall 2011). All the fault zones in the region that are relatively
 983 well-constrained by geodetic data display strain gradients that can be explained in terms of multiple
 984 fault strands, distributed deformation, or elastic strain surrounding a locked fault (e.g. Walpersdorf *et*
 985 *al.* 1998; Ranging *et al.* 1999; Stevens *et al.* 2002; Bock *et al.* 2003; Socquet *et al.* 2006). Poor
 986 historical earthquake records and few palaeoseismic data mean that it is difficult to distinguish
 987 between these options, and so attention is naturally focused on geomorphologically prominent faults
 988 and lineaments or structures with instrumentally recorded seismicity. Faults or segments of fault
 989 systems with recurrence intervals greater than the short period of instrumental or even historical
 990 seismic records inevitably remain undocumented.

991 Additional challenges to Quaternary fault identification include thick forest over most of the islands
 992 (e.g. Pubellier *et al.* 1999), the abundance of important structures located entirely offshore and not
 993 readily available for study (e.g. Silver *et al.* 1983b; Henry & Das 2002; Teas *et al.* 2009; Liu & Harris
 994 2013), rapid erosion of tectonic landforms in the humid environment, rapid burial of coseismic
 995 features by high sediment flux (e.g. Suggate & Hall 2003), and the high density of active and inactive
 996 structures within a large region (e.g. Puntodewo *et al.* 1994; Stevens *et al.* 2002).

997 Of 27 fault systems described here, none can be confidently described as inactive during the
 998 Quaternary. Eleven show evidence of 'maximal' tectonic activity according to the classification
 999 summarised in McCalpin (2009), and a further five show evidence of 'rapid' tectonic activity (Table
 1000 3). It is important to note that Quaternary faults discussed here are not exhaustive – there are
 1001 numerous other active faults in the region, and major offshore seismic sources such as the Molucca
 1002 Sea collision complex, the Banda Sea and Molucca Sea subducted slabs, and ongoing subduction of
 1003 the Celebes Sea (e.g. Cardwell & Isacks 1978; Silver & Moore 1978; Cardwell *et al.* 1980; Silver *et*
 1004 *al.* 1983a; Engdahl *et al.* 1998) that also need to be taken into account in any hazard analysis.

1005 *Quaternary fault geometry and earthquakes*

1006 The largest earthquakes in eastern Indonesia have been thrust and mega-thrust events, including those
 1007 of the Seram Trough (1629, $M > 8.5$), the Banda Sea (1938, $M > 8.0$) and Biak (1996, M_w 8.2) (e.g.
 1008 Wichmann 1918; Henry & Das 2002; Okal & Reymond 2003; Liu & Harris 2013). But many major
 1009 historical earthquakes in the studied region have occurred on strike-slip faults, including the Sorong
 1010 Fault (1944, M 7.5), the Yapen Fault (1979, M 7.9) the Ransiki Fault (2002, M 7.6) and perhaps the
 1011 Kawa Fault (1899, M 7.8) (e.g. Okal 1999; Brune *et al.* 2010; NEIC). Sixteen of the studied faults are
 1012 dominantly strike-slip, an additional five may have a substantial strike-slip component (Table 3).

1013 Often being long, straight, geometrically simple and subvertical, strike-slip faults are capable of
1014 generating large, shallow and damaging earthquakes; for example the 1906 M 7.7 San Francisco
1015 earthquake (e.g. Wald *et al.* 1993), the 2001 M_w 7.8 Kunlun Shan earthquake (e.g. Lin *et al.* 2003),
1016 and the 2002 M_w 7.9 Denali earthquake (e.g. Haeussler *et al.* 2004).

1017 A critical barrier to lateral rupture propagation and hence earthquake magnitude even on straight
1018 strike-slip faults is the presence of discontinuities, or step-overs (e.g. Segal & Pollard 1980; Sibson
1019 1985; Barka & Cadinsky-Cade 1988). The majority of historical strike-slip earthquake ruptures are
1020 arrested by step-overs wider than 3-5 km (Lettis *et al.* 2002; Wesnousky 2006). For example, the 1999
1021 M_w 7.1 Düzce earthquake ruptured a 40 km segment of the North Anatolian Fault (Aydin & Kalafat
1022 2002) and terminated in the >4 km wide Eften releasing bend in the west and the 4-5 km wide
1023 Bakacak releasing step-over in the east (Duman *et al.* 2005). Straight, continuous faults are therefore
1024 capable of generating larger earthquakes than curved or segmented faults, of generating ruptures that
1025 penetrate below the seismogenic layer (King & Wesnousky 2007) and of sustained supershear rupture
1026 propagation, causing enhanced ground motions (Robinson *et al.* 2010). Eastern Indonesia's major
1027 strike-slip faults show a variety of levels of segmentation, which may be viewed as an indication of
1028 their structural maturity, with high cumulative displacements empirically known to remove fault zone
1029 complexities (e.g. Wesnousky 1988; Stirling *et al.* 1996; King & Wesnousky 2007). Other properties
1030 such as block rotation and pre-existing weaknesses may complicate this simple relationship.

1031 The Matano Fault is an example of a structurally immature fault zone. Its onshore length of 195 km is
1032 punctuated by three major basins, each one 4-6 km wide, and two major restraining bends. The
1033 resultant maximum potential rupture length is 90 km (Table 3). Empirical rupture length-magnitude
1034 relationships (Wells & Coppersmith 1994) suggest a potential M 7.4 earthquake for such a rupture
1035 length. Uncertainties in this estimate include the unknown ability of a rupture to bypass the relatively
1036 gentle restraining bend east of the Mahalona basin, the possibility of a through-going strike-slip fault
1037 at seismogenic depths below Lake Matano, the effect on fault strength of widespread serpentinite
1038 smears along the fault zone, and the unknown length to which the fault continues offshore to the east.

1039 The Sorong Fault in West Papua, part of the fault system at the southern end of the Philippine Sea
1040 Plate, is a much more established fault zone with a long history of slip (e.g. Ali & Hall 1995),
1041 reflected in an apparent absence of step-overs >1 km and a continuous, straight onshore length of 420
1042 km equating to a potential M >8.0 earthquake if the entire linked system failed. The M_w 7.9 Yapen
1043 earthquake of 1979 ruptured an unknown length of the potentially 420 km long quasi-continuous
1044 Yapen Fault (Okal 1999) showing that such a scenario is possible. Despite evidence that most left-
1045 lateral strain is focused south of the Sorong Fault in West Papua, a conservative slip-rate estimate of 2
1046 mm/yr could accumulate 2 m elastic displacement across the northern Bird's Head (similar to the
1047 1979 Yapen earthquake release (Okal 1999)) in 1000 years. Even if all of this occurred west of the
1048 1937 and 1944 earthquakes, and assuming complete stress release during those events, the remaining
1049 ~200 km western portion of the fault could still generate a M >7.7 earthquake.

1050 The apparently very young and highly segmented Tarera-Aiduna fault zone and structures in the near-
1051 offshore Seram fold-thrust belt (Teas *et al.* 2009) and onshore Seram (Kawa and Bobol faults), could
1052 be part of a single soft-linked fault system, and seem to partition much of the present-day left-lateral
1053 motion between Australia and the Bird's Head. This fault system may thus be taking over the Pre-
1054 Pleistocene role of the Sorong Fault. Although there is no through-going fault on the scale of the
1055 Sorong Fault yet, the individual components of the Tarera-Aiduna Fault and left-lateral faults in
1056 Seram are each capable of generating M >7 earthquakes, and geomorphic observations suggest that
1057 they have all been active during the Quaternary, even if some segments (e.g. Bobol Fault) lack

1058 instrumental seismicity records. A major uncertainty in assessing the Tarera-Aiduna Fault system is
1059 the type and degree of linkage along its segments. The longest segment onshore with geomorphic
1060 evidence for rapid activity is 60 km long, and may be traced, via an abrupt releasing bend 3 km wide,
1061 another 30 km to the east. Assuming rupture is not terminated by the bend, a M 7.4 earthquake is
1062 possible on this 90 km long segment. It is reasonable to assume the fault passes some distance
1063 offshore before the next terminating step-over, so the maximum magnitude is likely to be larger.

1064 Similarly, maximum potential magnitudes for observed quasi-continuous segments of the Kawa and
1065 Bobol faults of southern Seram are 7.5 and 7.4 respectively, but a continuous rupture linking across
1066 Taluti Bay could achieve a length of 240 km and an earthquake magnitude of 7.8. The 1899 M 7.8
1067 event which caused slope failure north of Tehoru and a tsunami around Taluti Bay could have
1068 originated from such a rupture.

1069 Previously the Palu valley has been considered to represent a pull-apart basin between two strands of
1070 the Palu-Koro Fault (Bellier *et al.* 2001, 2006; Beaudouin *et al.* 2003; Socquet *et al.* 2006). The width
1071 between the two strands would be about 6 km, ample to terminate earthquake rupture, limiting the
1072 maximum length and magnitude of Palu-Koro Fault earthquakes to the segments north and south of
1073 Palu valley. However, the possibility of a continuous, buried cross-basin fault system within the Palu
1074 valley as proposed here has significant implications for seismic hazard assessment in the densely
1075 populated valley. A continuous cross-basin fault within the Palu valley, as seen in analogue models
1076 (e.g. Wu *et al.* 2009) and natural strike-slip basins (e.g. Clonard Basin, Haiti (Mann *et al.* 1995))
1077 means the Palu-Koro Fault may be straighter and more continuous than previously suggested, and
1078 palaeoseismic trenches across the border faults may not record major historic strike-slip earthquakes.
1079 The postulated buried and locked section alone is 50 km long, thus capable of generating a M 7.0
1080 earthquake. The total onshore length of the Palu-Koro Fault between Leboni valley and Palu city,
1081 lacking step-overs wider than 1 km and bends greater than 5°, is 135 km. As such, the Palu-Koro
1082 Fault must qualify as a ‘fault superhighway’, potentially capable of sustained supershear rupture
1083 speeds (Robinson *et al.* 2010) and earthquakes up to M 7.6.

1084 Other smaller structures which are geologically less significant because they are either not associated
1085 with instrumental seismicity (e.g. Sapu valley fault system), have very low geomorphic tectonic
1086 activity indices (e.g. Gorontalo Fault), or are composed of short and discontinuous fault segments
1087 (e.g. Namlea fault system) are of particular importance from a hazard analysis perspective because of
1088 their proximity to large population centres with little to no earthquake resistance. Similarly, structures
1089 such as the Kolaka Fault, which has its most geomorphologically youthful segment bounding steep
1090 uplifted topography immediately adjacent to Kolaka town, may also be associated with secondary
1091 seismic hazards such as landslides. Large earthquakes along many of the faults, particularly the Palu-
1092 Koro, Matano and Balantak faults and the Molino, Towuti and Wandamen Peninsula boundary faults,
1093 may also trigger local tsunamis, as has been already demonstrated in Palu and Taluti bays (e.g.
1094 Prasetya *et al.* 2001; Brune *et al.* 2010).

1095 **Conclusions**

1096 Neotectonic deformation in eastern Indonesia is rarely focused on discrete shear zones bounding rigid
1097 blocks as it is often interpreted to be. The pattern of seismicity and the broad distribution of
1098 Quaternary faults suggests continuum mechanics more closely approximates the region than rigid
1099 microplates (e.g. Thatcher 1995). All of the studied faults show geomorphic evidence of Quaternary

1100 tectonic activity, even in areas where high strain rates are not inferred from geodetic measurements
1101 (e.g. Buru, south Seram, northern West Papua).

1102 The zone of left-lateral deformation that includes the Yapen Fault, the Tarera-Aiduna Fault and strike-
1103 slip associated with the Seram fold-thrust belt is perhaps the most active on/near-shore fault system of
1104 eastern Indonesia as recorded by instrumental seismicity and geodetics. However, in terms of seismic
1105 risk, the Palu-Koro Fault is considered to be the most significant structure due to its proximity to Palu
1106 city, the possibility of a cross-basin fault system close to the city, the fault's unpredictability due to its
1107 poorly known seismic history, and its potential to cause large shallow focus supershear earthquakes.
1108 Additional factors increasing Palu-Koro Fault risk include the possibility of liquefaction in the deep
1109 Quaternary sedimentary basin on which Palu city is built, and the low-lying city's vulnerability to
1110 tsunami travelling down narrow Palu Bay.

1111 The Sorong Fault in West Papua should be viewed as the wildcard of eastern Indonesian active
1112 tectonics. Though GPS measurements appear to show little sinistral strike-slip motion, or even a
1113 degree of dextral slip, station locations in Sorong and Biak cannot resolve Sorong-Yapen-Ransiki
1114 fault complexity and may omit shear to the north. Convincing left-lateral stream offsets and low
1115 mountain front sinuosity values show that the fault has been active during the Quaternary. A dearth of
1116 seismicity, rather than indicating that the fault is benign, may instead indicate that it is locked and
1117 accumulating elastic strain. Magnitude 6.9, 7.2 and 7.4 earthquakes in 1937 and 1944, located on the
1118 fault west of Manokwari, prove that the fault is capable of generating large earthquakes. The Sorong
1119 Fault's contribution to the seismic hazard of West Papua should not be underestimated, particularly
1120 given its proximity to large towns such as Sorong and Manokwari.

1121 There is great potential for palaeoseismic study of some of the faults discussed in this study to
1122 confirm Quaternary activity and to provide more detailed answers to questions about seismic hazards,
1123 particularly characteristic earthquake sizes and recurrence intervals. It is recommended that trenching
1124 work is carried out across possible surface ruptures identified along the Matano, Balantak, Rana,
1125 Ransiki and Wandamen Peninsula faults. Geophysical studies to image shallow fault strands in the
1126 Quaternary sedimentary fill of several strike-slip basins, including the Palu, Sapu and Mahalona
1127 valleys, would help to confirm the existence of cross-basin strike-slip fault systems that may pose a
1128 previously unrecognised seismic hazard.

1129 **Acknowledgements**

1130 We are grateful to TGS (www.tgs.com) who provided the multibeam data, to John Decker, Phil Teas
1131 and the crew of the Shakti dive boat for support and valuable discussions during Banda Sea fieldwork.
1132 Alfend Rudyawan, Dave Gold, Ferry Yulian, Ega Abang Surya Nugraha, Jonathan Pownall and
1133 Benjamin Sapiie are thanked for their assistance and contributions to the ideas discussed here. Two
1134 anonymous reviewers are thanked for detailed and constructive reviews which considerably improved
1135 the final manuscript. Recent fieldwork was funded by the SE Asia Research Group, Royal Holloway
1136 University of London.

1137 **References**

1138 ABERS, G. & MCCAFFREY, R. 1988. Active deformation in the New Guinea Fold-and-Thrust Belt:
1139 seismicological evidence for strike-slip faulting and basement-involved thrusting. *Journal of*
1140 *Geophysical Research*, **93**, 13,332-13,354.

- 1141 AHMAD, W. 1975, Geology along the Matano Fault Zone, East Sulawesi, Indonesia. Regional
1142 Conference on the Geology and Mineral resources of South East Asia, Jakarta.
- 1143 ALI, J. R. & HALL, R. 1995. Evolution of the boundary between the Philippine Sea Plate and
1144 Australia: Palaeomagnetic evidence from eastern Indonesia. *Tectonophysics*, **251**, 251-275.
- 1145 AUDLEY-CHARLES, M. G. 1986. Timor-Tanimbar Trough: the foreland basin to the evolving Banda
1146 orogen. In: ALLEN, P. A., & HOMEWOOD, P. (eds.) *Foreland Basins* 8. International
1147 Association of Sedimentologists, Special Publication, 91-102.
- 1148 AUDLEY-CHARLES, M. G., CARTER, D. J. & MILSOM, J. 1972. Tectonic development of Eastern
1149 Indonesia in relation to Gondwanaland dispersal. *Nature*, **239**, 35-39.
- 1150 AYDIN, A. & KALAFAT, D. 2002. Surface Ruptures of the 17 August and 12 November 1999 Izmit
1151 and Duzce Earthquakes in Northwestern Anatolia, Turkey: Their Tectonic and Kinematic
1152 Significance and the Associated Damage. *Bulletin of the Seismological Society of America*,
1153 **92**, 95-106.
- 1154 BAILLY, V., PUBELLIER, M., RINGENBACH, J-C., DE SIGOYER, J. & SAPIN, F. 2009. Deformation zone
1155 'jumps' in a young convergent setting; the Lengguru fold-and-thrust belt, New Guinea Island,
1156 *Lithos*, **113**, 306-317.
- 1157 BARKA, A. & KADINSKY-CADE, K. 1988. Strike-slip fault geometry in Turkey and its influence on
1158 earthquake activity. *Tectonics*, **7**, 663-684.
- 1159 BATH, M. & DUDA, S. J. 1979. Some Aspects of Global Seismicity. Report No. 1-79, Seismological
1160 Institute, Uppsala, Sweden. 41pp.
- 1161 BEANLAND, S. & CLARK, M. 1994, The Owens Valley fault zone, eastern California, and surface
1162 rupture associated with the 1872 earthquake: U.S. Geological Survey Bulletin 1982, 29 pp.
- 1163 BEAUDOUIN, T. 1998. Tectonique active et sismotectonique du système de failles décrochantes de
1164 Sulawesi Central. Thèse de Doctorat, Université Paris-Sud, 343 pp.
- 1165 BEAUDOUIN, T., BELLIER, O. & SEBRIER, M. 2003. Present-day stress and deformation fields within
1166 the Sulawesi Island area (Indonesia): geodynamic implications. *Bulletin de la Société*
1167 *Géologique de France*, **174**, 305-317.
- 1168 BELLIER, O., BEAUDOUIN, T., SEBRIER, M., VILLENEUVE, M., BAHAR, I., PUTRANTO, I., PRATOMO,
1169 E., MASSAULT, M. & SEWARD, D. 1998. Active faulting in central Sulawesi (eastern
1170 Indonesia). In: WILSON, P., & MICHEL, G. W. (eds.) *The Geodynamics of S and SE Asia*
1171 (*GEODYSSSEA Project*), GeoForshingsZentrum, Potsdam, Germany. 276-312.
- 1172 BELLIER, O., SEBRIER, M., BEAUDOUIN, T., VILLENEUVE, M., BRAUCHER, R., BOURLES, D., SIAME,
1173 L., PUTRANTO, E. & PRATOMO, I. 2001. High slip rate for a low seismicity along the Palu-
1174 Koro active fault in central Sulawesi (Indonesia). *Terra Nova*, **13**, 463-470.
- 1175 BELLIER, O., SÉBRIER, M., SEWARD, D., BEAUDOUIN, T., VILLENEUVE, M. & PUTRANTO, E. 2006.
1176 Fission track and fault kinematics analyses for new insight into the Late Cenozoic tectonic
1177 regime changes in West-Central Sulawesi (Indonesia). *Tectonophysics*, 413, 201-220.
- 1178 BOCK, Y., PRAWIRODIRDJO, L., GENRICH, J. F., STEVENS, C. W., MCCAFFREY, R., SUBARYA, C.,
1179 PUNTODEWO, S. S. O. & CALAIS, E. 2003. Crustal motion in Indonesia from Global
1180 Positioning System measurements. *Journal of Geophysical Research*, **108**, 2367.

- 1181 BRUNE, S., BABEYKO, A. Y., LADAGE, S. & SOBOLEV, S. V. 2010. Landslide tsunami hazards in the
1182 Indonesian Sunda Arc. *Natural Hazards Earth Systems Science*, **10**, 589-604.
- 1183 BULL, W. B. 1978. Geomorphic tectonic activity classes of the south front of the San Gabriel
1184 Mountains, California. Unpublished Final Report, U.S. Geological Survey, Contract No. 14-
1185 08-0001-G-394, 59 pp.
- 1186 BULL, W. B. 2007. Tectonic Geomorphology of Mountains: A New Approach to Paleoseismology.
1187 Blackwell Publishing, Malden, MA, USA. 316 pp.
- 1188 BULL, W. B. & MCFADDEN, L. D. 1977. Tectonic geomorphology north and south of the Garlock
1189 fault, California. In: DOEHERING, D. O. (ed) *Geomorphology in arid regions*. Proceedings at
1190 the Eighth Annual Geomorphology Symposium. State University of New York, Binghamton,
1191 NY, pp. 115–138.
- 1192 BURCHFIEL, B. C., ROYDEN, L. H., VAN DER HILST, R. D., HAGER, B. H., CHEN, Z., KING, R. W., LI,
1193 C., LÜ, J., YAO, H. & KIRBY, E. 2008. A geological and geophysical context for the
1194 Wenchuan earthquake of 12 May 2008, Sichuan, People's Republic of China. *Geological
1195 Society of America Today*, **18**, 4-11.
- 1196 CAMPLIN, D. J. & HALL, R. 2014. Neogene history of Nene Gulf, Sulawesi, Indonesia. *Marine and
1197 Petroleum Geology*, **57**, 88-108.
- 1198 CARDWELL, R. K. & ISACKS, B. L. 1978. Geometry of the subducted lithosphere beneath the Banda
1199 Sea in eastern Indonesia from seismicity and fault plane solutions. *Journal of Geophysical
1200 Research*, **83**, 2825-2838.
- 1201 CARDWELL, R. K., ISACKS, B. L. & KARIG, D. E. 1980. The Spatial Distribution of Earthquakes, Focal
1202 Mechanism Solutions, and Subducted Lithosphere in the Philippine and Northeastern
1203 Indonesian Islands. In: HAYES, D. E. (ed) *The Tectonic and Geologic Evolution of Southeast
1204 Asian Seas and Islands*. American Geophysical Union, Geophysical Monograph, **23**, 1-35.
- 1205 CHARLTON, T. R. 2010. The Pliocene-Recent anticlockwise rotation of the Bird's Head, the opening
1206 of the Aru Trough – Cenderawasih Bay sphenochasm, and the closure of the Banda double
1207 arc. In: *Proceedings Indonesian Petroleum Association, 34th Annual Convention and
1208 Exhibition*. IPA10-G-008.
- 1209 CHEN, W-P. & HSU, L. 2013. Historic seismicity near the source zone of the great 2008 Wenchuan
1210 earthquake: Implications for seismic hazards. *Tectonophysics*, **584**, 114-118.
- 1211 COTTAM, M. A., HALL, R., FORSTER, M.A. & BOUDAGHER-FADEL, M. K. 2011. Basement character
1212 and basin formation in Gorontalo Bay, Sulawesi, Indonesia: new observations from the
1213 Togian Islands. In: HALL, R., COTTAM, M. A. & WILSON, M. E. J. (eds.) *The SE Asian
1214 Gateway: History and Tectonics of the Australia–Asia Collision*. Geological Society, London,
1215 Special Publications, **355**, 177–202.
- 1216 DECKER, J., BERGMAN, S. C., TEAS, P. A., BAILLIE, P. & ORANGE, D. L. 2009. Constraints on the
1217 tectonic evolution of the Bird's Head, West Papua. In: *Proceedings Indonesian Petroleum
1218 Association, 33rd Annual Convention and Exhibition*, IPA09-G139.
- 1219 DEHBOZORGI, M., POURKERMANI, M., ARIAN, M., MATKAN, A. A., MOTAMEDI, H. & HOSSEINIASL,
1220 A. 2010. Quantitative analysis of relative tectonic activity in the Sarvestan area, central
1221 Zagros, Iran. *Geomorphology*, **121**, 329-341.

- 1222 DEMETS, C. GORDON, R., ARGUS, D. & STEIN, S. 1994. Effects of recent revisions to the geomagnetic
1223 reversal time scale on estimates of current plate motions. *Geophysical Research Letters*, **21**,
1224 2191–2194.
- 1225 DOW, D. B. & HARTONO, U. 1982. The nature of the crust underlying Cenderawasih (Geelvink) Bay,
1226 Irian Jaya. *Proceedings of the Indonesian Petroleum Association*, **11**, 203-210.
- 1227 DOW, D. B. & SUKAMTO, R. 1984. Western Irian Jaya: the end-product of oblique plate convergence
1228 in the Late Tertiary. *Tectonophysics*, **106**, 109-139.
- 1229 DUMAN, T. Y., EMRE, O., DOGAN, A. & OZALP, S. 2005. Step-Over and Bend Structures along the
1230 1999 Duzce Earthquake Surface Rupture, North Anatolian Fault, Turkey. *Bulletin of the*
1231 *Seismological Society of America*, **95**, 1250–1262, doi: 10.1785/0120040082.
- 1232 ENGDAHL, E. R., VAN DER HILST, R. & BULAND, R. 1998. Global teleseismic earthquake relocation
1233 with improved travel times and procedures for depth determination. *Bulletin of the*
1234 *Seismological Society of America*, **88**, 722-743.
- 1235 ESHGHI, S. & ZARE, M. 2003. Bam (SE Iran) earthquake of 26 December 2003, M_w 6.5: A
1236 preliminary reconnaissance report.
1237 http://www.iiees.ac.ir/English/bam_report_english_recc.html. [14th January 2016].
- 1238 FERDIAN, F., HALL, R. & WATKINSON, I. 2010. A structural re-evaluation of the north Banggai-Sula
1239 area, eastern Indonesia. In: *Proceedings Indonesian Petroleum Association, 34th Annual*
1240 *Convention*, IPA07-G-009, 1–20.
- 1241 FU, B., NINOMIYA, Y., LEI, X., TODA, S. & AWATA, Y. 2004. Mapping active fault associated with the
1242 2003 M_w 6.6 Bam (SE Iran) earthquake with ASTER 3D images. *Remote Sensing of*
1243 *Environment*, **92**, 153-157.
- 1244 GARRARD, R. A., SUPANDJONO, J. B. & SURONO. 1988. The geology of the Banggai-Sula
1245 microcontinent, eastern Indonesia. *Proceedings Indonesian Petroleum Association, 17th*
1246 *Annual Convention*, 23-52.
- 1247 GERMERAAD, J. H. 1946. Geology of central Seran. In: Rutten, L. & Hotz, W. (eds). Geological,
1248 petrographical, and palaeontological results of explorations, carried out from September 1917
1249 till June 1919 in the island of Ceram, 135 pp., de Bussy, Amsterdam.
- 1250 GOVERS, R. & WORTEL, M. J. R. 2005. Lithosphere tearing at STEP faults: Response to edges of
1251 subduction zones. *Earth and Planetary Science Letters*, **236**, 505– 523.
- 1252 HAEUSSLER, P. J., SCHWARTZ, D. P., DAWSON, T. E., STENNER, H. D., LIENKAEMPER, J. J., SHERROD,
1253 B. & PERSONIUS, S. F. 2004. Surface rupture and slip distribution of the Denali and
1254 Totschunda faults in the 3 November 2002 M 7.9 earthquake, Alaska. *Bulletin of the*
1255 *Seismological Society of America*. **94**, S23-S52.
- 1256 HAFFNER, G. D., HEHANUSSA, P. E. & HARTOTO, D. 2001. The biology and physical processes of
1257 large lakes of Indonesia: Lakes Matano and Towuti. In: MUNAWAR, M. & HECKY, R. E. (eds.)
1258 *The Great Lakes of the World (GLOW): Food-web, health and integrity*, Ecovision World
1259 Monograph Series, Backhuys Publishers, Leiden, The Netherlands, 183-192.
- 1260 HALL, R. 1987. Plate boundary evolution in the Halmahera region, Indonesia. *Tectonophysics*, **144**,
1261 337-352.
- 1262 HALL, R. 1996. Reconstructing Cenozoic SE Asia. In: HALL, R., & BLUNDELL, D. J. (eds.) *Tectonic*
1263 *Evolution of SE Asia*. Geological Society, London, Special Publications, **106**, 153-184.

- 1264 HALL, R. 2002. Cenozoic geological and plate tectonic evolution of SE Asia and the SW Pacific:
1265 computer-based reconstructions, model and animations. *Journal of Asian Earth Sciences*, **20**,
1266 353-434.
- 1267 HALL, R. 2011. Australia–SE Asia collision: plate tectonics and crustal flow. In: HALL, R., COTTAM
1268 M. A. & WILSON M. E. J. (eds). *The SE Asian Gateway: History and Tectonics of the*
1269 *Australia–Asia Collision*. Geological Society, London, Special Publications, **355**, 75–109.
- 1270 HALL, R. 2012. Late Jurassic–Cenozoic reconstructions of the Indonesian region and the Indian
1271 Ocean. *Tectonophysics*, **570**, 1-41.
- 1272 HALL, R., FULLER, M., ALI, J. R. & ANDERSON, C. D. 1995. The Philippine Sea Plate: Magnetism and
1273 Reconstructions. In: TAYLOR, B. & NATLAND, J. H. (eds). *Active Margins and Marginal*
1274 *Basins: A Synthesis of Western Pacific Drilling Results*. American Geophysical Union
1275 Monograph, **88**, 371-404.
- 1276 HAMILTON, W. 1979. Tectonics of the Indonesian region. *U.S. Geological Survey Professional Paper*,
1277 **1078**, 345 pp.
- 1278 HARRIS, R. A. 1992. Peri-collisional extension and the formation of Oman type ophiolites in the
1279 Banda Arc and Brooks Range. In: PARSON, L. M., MURTON, B. J. & BROWNING, P. (eds.)
1280 *Ophiolites and their modern oceanic analogues*. Geological Society, London, Special
1281 Publications, **60**, 301-325.
- 1282 HENNIG, J., ADVOKAAT, E., RUDYAWAN, A. & HALL, R. 2014. Large Sediment Accumulations and
1283 Major Subsidence Offshore; Rapid Uplift On Land: Consequences of Extension of Gorontalo
1284 Bay and Northern Sulawesi. In: *Proceedings Indonesian Petroleum Association, 38th Annual*
1285 *Convention and Exhibition*, IPA14-G-304.
- 1286 HENRY, C. & DAS, S. 2002. The M_w 8.2, 17 February 1996 Biak, Indonesia, earthquake: Rupture
1287 history, aftershocks, and fault plane properties. *Journal Of Geophysical Research*, **107**,
1288 Doi:10.1029/2001jb000796.
- 1289 HILL, K. C., HOFFMAN, N., LUNT, P. & PAUL, R. 2002. Structure and Hydrocarbons in the Sareba
1290 block, "Bird's Neck", West Papua. *Proceedings Indonesian Petroleum Association, 28th*
1291 *Annual Convention*, 227-248.
- 1292 HOLZER, L. T. & SAVAGE, J. C. 2013. Global Earthquake Fatalities and Population. *Earthquake*
1293 *Spectra*, **29**, 155-175.
- 1294 HUANG, W. 1993. Morphologic patterns of stream channels on the active Yishi Fault, southern
1295 Shandong Province, Eastern China: implications for repeated great earthquakes in the
1296 Holocene. *Tectonophysics*, **219**, 283–304.
- 1297 HUTCHISON, C. S. 1989, Geological Evolution of South-East Asia, Clarendon Press, Oxford. 368 pp.
- 1298 JABLONSKI, D., PRIYONO, P., WESTLAKE, S. & LARSEN, O. A. 2007. Geology and exploration
1299 potential of the Gorontalo basin, central Indonesia – eastern extension of the North Makassar
1300 Basin? *Proceedings Indonesian Petroleum Association, 31st Annual Convention and*
1301 *Exhibition*. IPA07-G-083.
- 1302 KATILI, J. A. 1970. Additional evidence of transcurrent faulting in Sumatra and Sulawesi. *Bandung*
1303 *National Institute of Geology and Mining Bulletin*, **3**, 15-28.

- 1304 KATILI, J. A. 1973. On fitting certain geological and geophysical features of the Indonesian island arc
1305 to the new global tectonics. *In: COLEMAN, P. J. (ed.) The Western Pacific: island arcs,*
1306 *marginal seas, geochemistry.* Western Australia University Press, 287-305.
- 1307 KATILI, J. A. 1975. Volcanism And Plate Tectonics in the Indonesian Island Arcs. *Tectonophysics,*
1308 **26**, 165-188.
- 1309 KATILI, J. A. 1986. Geology and hydrocarbon potential of the Arafura Sea. *In: HALBOUTY, M. T.*
1310 *(ed.) Future Petroleum Provinces of the World, AAPG Memoir, 40,* 487-501.
- 1311 KAVALIERIS, I., VAN LEEUWEN, T.M. & WILSON, M. 1992. Geological setting and styles of
1312 mineralization, north arm of Sulawesi, Indonesia. *Journal of Southeast Asian Earth Sciences,*
1313 **7**, 113–130.
- 1314 KELLER, E. A. 1986. Investigation of active tectonics: use of surficial Earth processes. *In: WALLACE,*
1315 *R. E. (Ed.) Active Tectonics, Studies in Geophysics.* National Academy Press, Washington,
1316 DC, 136–147.
- 1317 KING, G. C. P. & WESNOUSKY, S. G. 2007. Scaling of fault parameters for continental strike-slip
1318 earthquakes. *Bulletin of the Seismological Society of America, 97,* 1833–1840.
- 1319 LACASSIN, R., REPLUMAZ, A. & LELOUP, P. H. 1998. Hairpin river loops and slip-sense inversion on
1320 Southeast Asian strike–slip faults. *Geology, 26,* 703–706.
- 1321 LETTIS, W., BACHHUBER, J., WITTER, R., BRANKMAN, C., RANDOLPH, C. E., BARKA, A., PAGE, W. D.
1322 & KAYA, A. 2002. Influence of Releasing Step-Overs on Surface Fault Rupture and Fault
1323 Segmentation: Examples from the 17 August 1999 Izmit Earthquake on the North Anatolian
1324 Fault, Turkey. *Bulletin of the Seismological Society of America, 92,* 19-42.
- 1325 LIN, A., KIKUCHI, M. & FU, B. 2003. Rupture segmentation and process of the 2001 M_w 7.8 central
1326 Kunlun earthquake, China. *Bulletin of Seismological Society of America, 93,* 2477-2492.
- 1327 LINTHOUT, K., HELMERS, H., SOPAHEL UWAKAN, J. & SURYA NILA, E. 1989. Metamorphic complexes
1328 in Buru and Seram, northern Banda Arc. *Netherlands Journal of Sea Research, 24,* 345-356.
- 1329 LINTHOUT, K., HELMERS, H. & ANDRIESSEN, P. A. M. 1991. Dextral strike-slip in Central Seram
1330 and 3-4.5 Ma Rb/Sr ages in pre-Triassic metamorphics related to Early Pliocene
1331 counterclockwise rotation of the Buru-Seram microplate (E. Indonesia). *Journal of Southeast*
1332 *Asian Earth Sciences, 6,* 335-342.
- 1333 LIU, Z. Y.-C. & HARRIS, R. A. 2013. Discovery of possible mega-thrust earthquake along the Seram
1334 Trough from records of 1629 tsunami in eastern Indonesian region. *Natural Hazards, 72,*
1335 1311-1328.
- 1336 MANN, P. 2007. Global catalogue, classification and tectonic origins of restraining- and releasing
1337 bends on active and ancient strike-slip fault systems. *In: CUNNINGHAM, W. D. & MANN, P.*
1338 *(eds.) Tectonics of Strike-Slip Restraining and Releasing Bends.* Geological Society, London,
1339 Special Publications, **290**, 13–142.
- 1340 MANN, P., TAYLOR, F. W., LAWRENCE EDWARDS, R. & TEH-LUNG KU. 1995. Actively evolving
1341 microplate formation by oblique collision and sideways motion along strike-slip faults: An
1342 example from the northeastern Caribbean plate margin. *Tectonophysics, 246,* 1-69.
- 1343 MCCAFFREY, R. 1989. Seismological constraints and speculations on Banda arc tectonics.
1344 *Netherlands Journal of Sea Research, 24,* 141-152.

- 1345 MCCAFFREY, R. 1996. Slip partitioning at convergent plate boundaries of SE Asia. *In*: HALL, R. &
 1346 BLUNDELL, D. J. (eds.) *Tectonic Evolution of Southeast Asia*. Geological Society, London,
 1347 Special Publications, **106**, 3-18.
- 1348 MCCAFFREY, R. & SUTARDJO, R. 1982. Reconnaissance microearthquake survey of Sulawesi,
 1349 Indonesia. *Geophysical Research Letters*, **9**, 793-796.
- 1350 MCCALPIN, J. P. (ed.). 2009. Palaeoseismology, 2nd Ed. International Geophysics Series, 95.
 1351 Burlington, USA. 613 pp.
- 1352 MICHETTI, A. M., AUDEMARD, F. A. & MARCO, S. 2005. Future trends in palaeoseismology:
 1353 Integrated study of the seismic landscape as a vital tool in seismic hazard analyses.
 1354 *Tectonophysics*, **408**, 3-21.
- 1355 MILSOM, J., MASSON, D., NICHOLS, G., SIKUMBANG, N., DWIYANTO, B., PARSON, L. & KALLAGHER,
 1356 H. 1992. The Manokwari Trough and the western end of the New Guinea Trench. *Tectonics*,
 1357 **11**, 145-153.
- 1358 MOLNAR, P. & DAYEM, K. E. 2010. Major intercontinental strike-slip faults and contrasts in
 1359 lithospheric strength. *Geosphere*, **6**, 444-467.
- 1360 NATAWIDJAJA, D. H. & DARYONO, M. R. 2014. The Lawanopo Fault, Central Sulawesi, East
 1361 Indonesia. 4th International Symposium on Earthquake and Disaster Mitigation 2014 (ISED
 1362 2014). AIP Conference Proceedings 1658. 030001-1 – 030001-23. Doi: 10.1063/1.4915009.
- 1363 NATIONAL GEOPHYSICAL DATA CENTER / WORLD DATA SERVICE (NGDC/WDS): Significant
 1364 Earthquake Database. National Geophysical Data Center, NOAA. doi:10.7289/V5TD9V7K.
 1365 [23rd April 2014].
- 1366 NEIC - NATIONAL EARTHQUAKE INFORMATION CENTRE. <http://earthquake.usgs.gov/regional/neic/>
 1367 [10th August 2014].
- 1368 NORVICK, M. S. 1979. The tectonic history of the Banda arcs, eastern Indonesia: a review. *Journal of*
 1369 *the Geological Society of London*, **136**, 519-527.
- 1370 OKAL, E. A. 1999. Historical seismicity and seismotectonic context of the great 1979 Yapen and Biak,
 1371 Irian Jaya earthquakes. *Pure and Applied Geophysics*, **154**, 633– 675.
- 1372 OKAL, E. A. & REYMOND, D. 2003. The mechanism of great Banda sea earthquake of 1 February
 1373 1938: applying the method of preliminary determination of focal mechanism to a historical
 1374 event. *Earth and Planetary Science Letters*, **216**, 1–15.
- 1375 PAIRAULT, A. A., HALL, R. & ELDERS, C. F. 2003. Tectonic Evolution of the Seram Trough,
 1376 Indonesia. *Proceedings Indonesian Petroleum Association, 29th Annual Convention*, 355-
 1377 370.
- 1378 PAVLIDES, S. B. 1989. Looking for a definition of neotectonics. *Terra Nova*, **1**, 233–235.
 1379 doi:10.1111/j.1365-3121.1989.tb00362.x.
- 1380 PELINOVSKY, E., YULIADI, D., PRASETYA, G. & HIDAYAT, R. 1997. The 1996 Sulawesi tsunami.
 1381 *Natural Hazards*, **16**, 29-38.
- 1382 PIETY, L., SULLIVAN, J. T. & ANDERS, M. H. 1992. Segmentation and paleoseismicity of the Grand
 1383 Valley Fault, southeastern Idaho and western Wyoming. *In*: LINK, P. K., KUNTZ, M. A. &
 1384 PLATT, L. B. (eds) *Regional Geology of Eastern Idaho and Western Wyoming*. Geological
 1385 Society of America Memoir. **179**, 155-182.

- 1386 PIGRAM, C. J. & PANGGABEAN, H. 1984. Rifting of the eastern margin of the Australian continent and
1387 the origin of some microcontinents in Indonesia. *Tectonophysics*, **107**, 331-353.
- 1388 PIGRAM, C. J., SURONO & SUPANDJONO, J. B. 1985. Origin of the Sula Platform, eastern Indonesia.
1389 *Geology*, **13** 246-248.
- 1390 PHOLBUD, P., HALL, R., ADVOKAAT, E., BURGESS, P. & RUDYAWAN, A. 2012. A new interpretation
1391 of Gorontalo Bay, Sulawesi. In: *Proceedings Indonesian Petroleum Association, 36th Annual*
1392 *Convention*, IPA12-G-029, 197-224.
- 1393 POWNALL, J. M., HALL, R. & WATKINSON, I. M. 2013. Extreme extension across Seram and Ambon,
1394 eastern Indonesia: Evidence for Banda slab rollback. *Solid Earth*, **4**, 277-314.
- 1395 POWNALL, J. M., HALL, R., ARMSTRONG, R. A. & Forster, M. A. 2014. Earth's youngest known
1396 ultrahigh-temperature granulites discovered on Seram, eastern Indonesia. *Geology*, **42**, 279-
1397 282.
- 1398 PRASETYA, G. S., DE LANGE, W. P. & HEALY, T. R. 2001. The Makassar Strait Tsunamigenic Region,
1399 Indonesia. *Natural Hazards*, **24**, 295-307.
- 1400 PUBELLIER, M., DESFONTAINES, B., CHOROWICZ, J., RUDANT, J-P. & PERMANA, H. 1999. Active
1401 denudation morphostructures from SAR ERS-1 images (SW Irian Jaya). *International*
1402 *Journal of Remote Sensing*, **20**, 789-800.
- 1403 PUNTODEWO, S. S. O., MCCAFFREY, R., CALAIS, E., BOCK, Y., RAIS, J., SUBARYA, C., POEWARIARDI,
1404 R., STEVENS, C., GENRICH, J., FAUZI, ZWICK, P. & WDOWINSKI, S. 1994. GPS measurements
1405 of crustal deformation within the Pacific-Australia plate boundary zone in Irian Jaya,
1406 Indonesia. *Tectonophysics*, **237**, 141-153.
- 1407 QUIGLEY, M., VAN DISSEN, R., LITCHFIELD, N., VILLAMOR, P., DUFFY, B., BARRELL, D., FURLONG,
1408 K., STAHL, T., BILDERBACK, E. & NOBLE, D. 2012. Surface rupture during the 2010 M_w 7.1
1409 Darfield (Canterbury) earthquake: Implications for fault rupture dynamics and seismic-hazard
1410 analysis. *Geology*, **40**, 55-58.
- 1411 RAMÍREZ-HERRERA, M. T. 1998. Geomorphic Assessment of Active Tectonics in the Acambay
1412 Graben, Mexican Volcanic Belt. *Earth Surface Processes and Landforms*, **23**, 317-332.
- 1413 RANGIN, C., LE PICHON, X., MAZZOTTI, S., PUBELLIER, M., CHAMOT-ROOKE, N., AURELIO, M.,
1414 WALPERSDORF, A., & QUEBRAL, R. 1999. Plate convergence measured by GPS across the
1415 Sundaland/Philippine Sea Plate deformed boundary: the Philippines and eastern Indonesia.
1416 *Geophysical Journal International*, **139**, 296-316.
- 1417 ROBINSON, D. P., DAS, S. & SEARLE, M. P. 2010. Earthquake fault superhighways. *Tectonophysics*,
1418 **493**, 236-243.
- 1419 ROBINSON, G. P. & RATMAN, N. 1978. The stratigraphic and tectonic development of the Manokwarai
1420 area, Irian Jaya. *BMR Journal of Australian Geology & Geophysics*, **3**, 19-24.
- 1421 ROBINSON, G. P., RYBURN, R. J., HARAHAP, B. H., TOBING, S. L. & ACHDAN, A. 1990. Geology of
1422 the Steenkool Sheet area, Irian Jaya. 1:250,000 scale. Geological Research and Development
1423 Centre, Bandung, Indonesia.
- 1424 ROCKWELL, T. K., KELLER, E. A. & JOHNSON, D. L. 1984. Tectonic geomorphology of alluvial fans
1425 and mountain fronts near Ventura, California. In: MORISAWA, M. (ed) *Tectonic*
1426 *Geomorphology*. Proceedings of the 15th Annual Geomorphology Symposium. Allen and
1427 Unwin Publishers, Boston, MA, 183-207.

- 1428 ROQUES, D. 1999. The metamorphic core of Buru. Report No. 204, Southeast Asia Research Group,
1429 London. 49 pp.
- 1430 ROYDEN, L. H. 1993. Evolution of retreating subduction boundaries formed during continental
1431 collision. *Tectonics*, **12**, 629 – 638.
- 1432 RUDYAWAN, A. 2011. Tectonostratigraphy and Structural Style of The South Banggai – Sula Block
1433 and NW Banda Basin, Indonesia. Unpublished MSc. Thesis, University of London, London,
1434 UK.
- 1435 SEGAL, P. & POLLARD, D. D. 1980. Mechanics of discontinuous faults. *Journal of Geophysical*
1436 *Research*, **85**, 4337-4350.
- 1437 SENO, T. & KAPLAN, D. E. 1988. Seismotectonics of western New Guinea. *Journal of Physics of the*
1438 *Earth*, **36**, 107-124.
- 1439 SIBSON, R. H. 1985. Stopping of earthquake ruptures at dilational fault jogs. *Nature*, **316**, 248-251.
- 1440 SIEH, K. E. & JAHNS, R. H. 1984. Holocene activity of the San Andreas fault at Wallace Creek,
1441 California. *Journal of Geophysical Research*, **95**, 883–896.
- 1442 SILVA, P. G., GOY, J. L., ZAZO, C. & BARDAJÍ, T. 2003. Fault-generated mountain fronts in southeast
1443 Spain: geomorphologic assessment of tectonic and seismic activity. *Geomorphology*, **50**, 203–
1444 225.
- 1445 SILVER, E. A. & MOORE, J. C. 1978. The Molucca Sea collision zone, Indonesia. *Journal of*
1446 *Geophysical Research*, **83**, 1681-1691.
- 1447 SILVER, E. A., MCCAFFREY, R. & SMITH, R. B. 1983a. Collision, rotation and the initiation of
1448 subduction in the evolution of Sulawesi, Indonesia. *Journal of Geophysical Research*, **88**,
1449 9407-9418.
- 1450 SILVER, E. A., MCCAFFREY, R., JOYODIWIRYO, Y. & STEVENS, S. 1983b. Ophiolite emplacement by
1451 collision between the Sula Platform and the Sulawesi Island Arc, Indonesia. *Journal of*
1452 *Geophysical Research*, **88**, 9419-9435.
- 1453 SIMANDJUNTA, T. O. 1986. *Sedimentology and tectonics of the collision complex in the East Arm of*
1454 *Sulawesi, Indonesia*. PhD Thesis, University of London, 374 pp.
- 1455 SIMANDJUNTA, T. O., SURONO & SUKIDO. 1984. *Geological Report of the Kolaka Quadrangle*, 394
1456 *Sulawesi, Scale 1:250,000*. Open file report, Indonesian Geological Research and
1457 Development Centre, Bandung, 50 pp.
- 1458 SIMANDJUNTA, T. O., SURONO & SUKIDO. 1994. Geological Map of the Kolaka Quadrangle,
1459 Sulawesi, 1:250,000 scale. Geological Research and Development Centre, Bandung,
1460 Indonesia.
- 1461 SOCQUET, A., VIGNY, C. CHAMOT-ROOKE, N., SIMONS, W., RANGIN, C. & AMBROSIUS, B. 2006.
1462 India and Sunda plates motion and deformation along their boundary in Myanmar determined
1463 by GPS. *Journal of Geophysical Research*, **111**: doi:10.1029/2005JB003877.
- 1464 SOHONI, P. S. MALIK, J. N., MERH, S. S. & KARANTH, R. V. 1999. Active Tectonics Astride Katrol
1465 Hill Zone, Kachchh, Western India. *Journal of the Geological Society of India*, **53**, 579-586.
- 1466 SPAKMAN, W. & HALL, R. 2010. Surface deformation and slab-mantle interaction during Banda Arc
1467 subduction rollback. *Nature Geoscience*, **3**, 562-566.

- 1468 SPENCER, J. E. 2010. Structural analysis of three extensional detachment faults with data from the
1469 2000 Space-Shuttle Radar Topography Mission. *Geological Society of America Today*, **20**, 4-
1470 10.
- 1471 SPENCER, J. E. 2011. Gently dipping normal faults identified with Space Shuttle radar topography
1472 data in central Sulawesi, Indonesia, and some implications for fault mechanics. *Earth and*
1473 *Planetary Science Letters*, **308**, 267-276.
- 1474 STEIN, S., GELLER, R. J. & LIU, M. 2012. Why earthquake hazard maps often fail and what to do about
1475 it. *Tectonophysics*, **562-563**, 1-25.
- 1476 STEVENS, C. W., MCCAFFREY, R., BOCK, Y., GENRICH, J. F., VIGNY, C., SUBARYA, C., PUNTODEWO,
1477 S. S. O. & FAUZI. 1999. GPS evidence for rapid rotations about a vertical axis in a collisional
1478 setting: the Palu fault of Sulawesi, Indonesia. *Geophysical Research Letters*, **26**, 2677-2680.
- 1479 STEVENS, C. W., MCCAFFREY, R., BOCK, Y., GENRICH, J. F., PUBELLIER, M. & SUBARYA, C. 2002.
1480 Evidence for block rotations and basal shear in the world's fastest slipping continental shear
1481 zone in NW New Guinea. In: STEIN, S. & FREYMUELLER, J. (eds.) *Plate Boundary Zones*.
1482 American Geophysical Union Geodynamics Series, **30**, 87-99.
- 1483 STIRLING, M. W., WESNOUSKY, S. G. & SHIMAZAKI, K. 1996. Fault trace complexity, cumulative slip,
1484 and the shape of the magnitude-frequency distribution for strike-slip faults: A global survey.
1485 *Geophysical Journal International*. **124**, 833-868.
- 1486 SUGGATE, S. & HALL, R. 2003. Predicting sediment yields from SE Asia: A GIS approach. In:
1487 *Proceedings Indonesian Petroleum Association, 29th Annual Convention*, 289-304.
- 1488 SUKAMTO, R. & SIMANDJUNTAK, T. O. 1983. Tectonic relationship between geologic provinces of
1489 western Sulawesi, eastern Sulawesi and Banggai-Sula in the light of sedimentological aspects.
1490 *Bulletin Geological Research and Development Centre, Bandung*, **7**, 1-12.
- 1491 SURONO. 1994. Stratigraphy of the southeast Sulawesi continental terrane, Eastern Indonesia. *Journal*
1492 *of Geology and Mineral Resources*, **4**, 4-11.
- 1493 TEAS, P. A., DECKER, J., ORANGE, D. & BAILLIE, P. 2009. New insight into structure and tectonics of
1494 the Seram Trough from SEASEPTM high resolution bathymetry. In: *Proceedings*
1495 *Indonesian Petroleum Association, 33rd Annual Convention and Exhibition*, IPA09-G091.
- 1496 THATCHER, W. 1995. Microplate versus continuum descriptions of active tectonic deformation.
1497 *Journal of Geophysical Research*, **100**, 3885-3894.
- 1498 TJOKROSAPOETRO, S., BUDHITRISNA, T. & RUSMANA, D. 1981. Geological map of the Buru Island
1499 Quadrangle, Maluku, 1:250,000 scale. Geological Research and Development Centre,
1500 Bandung, Indonesia.
- 1501 TJOKROSAPOETRO, S., ACHDAN, A., SUWITODIRDJO, K., RUSMANA, E. & ABIDIN, H. Z. 1993.
1502 Geological map of the Masohi quadrangle, 2200 Maluku, 1:250000, Geological Research and
1503 Development Centre, Bandung, Indonesia.
- 1504 USGS EARTHQUAKE HAZARDS PROGRAM, EARTHQUAKE INFORMATION BY YEAR. Available from:
1505 <http://earthquake.usgs.gov/earthquakes/eqarchives/year/>. [14th January 2016].
- 1506 VAN LEEUWEN, T. M. & MUHARDJO. 2005. Stratigraphy and tectonic setting of the Cretaceous and
1507 Paleogene volcanic-sedimentary successions in northwest Sulawesi, Indonesia implications
1508 for the Cenozoic evolution of Western and Northern Sulawesi. *Journal of Asian Earth*
1509 *Sciences*, **25**, 481-511.

- 1510 VAN LEEUWEN, T., ALLEN, C.M., KADARUSMAN, A., ELBURG, M., PALIN, J.M., MUHARDJO &
 1511 SUWIJANTO. 2007. Petrologic, isotopic, and radiometric age constraints on the origin and
 1512 tectonic history of the Malino Metamorphic Complex, NW Sulawesi, Indonesia. *Journal of*
 1513 *Asian Earth Sciences*, **29**, 751-777.
- 1514 VECCHIOTTI, F. 2008. Calculating geomorphic indices in SE Asia using a SRTM derived DEM: a
 1515 worked example from West Sulawesi, Indonesia. In: MICHEL, U., CIVCO, D. L., EHLERS, M.
 1516 & KAUFMAN, H. J. (eds.) *Remote Sensing for Environmental Monitoring*, GIS Applications
 1517 and Geology VIII, SPIE Proceedings, **7110**, doi: [10.1117/12.800240](https://doi.org/10.1117/12.800240)
- 1518 VISSER, W. A. & HERMES, J. J. 1962. Geological results of the exploration for oil in Netherlands New
 1519 Guinea. *Verhandelingen Koninklijk Nederlands Geologisch en Mijnbouwkundig*
 1520 *Genootschap, Geologische Serie*, 265 pp.
- 1521 WALD, D. J., KANAMORI, H., HELMBERGER, D. V. & HEATON, T. H. 1993. Source study of the 1906
 1522 San Francisco earthquake. *Bulletin of the Seismological Society of America*. **83**, 981-1019.
- 1523 WALKER, F. & ALLEN, M. B. 2012. Offset rivers, drainage spacing and the record of strike-slip
 1524 faulting: The Kuh Banan Fault, Iran. *Tectonophysics*, **530–531**, 251–263.
- 1525 WALLACE, R. E. 1968. Notes on stream channels offset by the San Andreas fault, southern Coast
 1526 Ranges, California. In: DICKINSON, W. & GRANTZ, A. (eds.) *Conference on Geologic*
 1527 *Problems of San Andreas Fault System. Proceedings: Stanford University Publications in the*
 1528 *Geological Sciences*, **11**, 6-21.
- 1529 WALLACE, R. E. 1986. *Active Tectonics: Impacts on Society*. National Academy Press, Washington,
 1530 D.C., *Studies in Geophysics*. 266 pp.
- 1531 WALLACE, R. E. (ed.). 1990. *The San Andreas fault system, California*. U.S. Geological Survey
 1532 *Professional Paper*, 1515, 283 pp.
- 1533 WALPERSDORF, A., VIGNY, C., SUBARYA, C. & MANURUNG, P. 1998. Monitoring of the Palu-Koro
 1534 Fault (Sulawesi) by GPS. *Geophysical Research Letters*, **25**, 2313-2316.
- 1535 WANG, Y., SIEH, K., SOE THURA TUN, LAI, K.-Y. & THAN MYINT. 2014. Active tectonics and
 1536 earthquake potential of the Myanmar region. *Journal of Geophysical Research: Solid Earth*,
 1537 **119**, 3767-3822. doi:10.1002/2013JB010762.
- 1538 WATKINSON, I. M. 2011. Ductile flow in the metamorphic rocks of central Sulawesi. In: HALL, R.,
 1539 COTTAM, M. A. & WILSON, M. E. J. (eds.) *The SE Asian Gateway: History and Tectonics of*
 1540 *the Australia–Asia Collision*. Geological Society, London, *Special Publications*, **355**, 157–
 1541 176.
- 1542 WATKINSON, I. M., HALL, R. & FERDIAN, F. 2011. Tectonic re-interpretation of the Banggai-Sula–
 1543 Molucca Sea margin, Indonesia. In: HALL, R., COTTAM, M. A. & WILSON, M. E. J. (eds.) *The*
 1544 *SE Asian Gateway: History and Tectonics of the Australia–Asia Collision*. Geological
 1545 Society, London, *Special Publications*, **355**, 203–224.
- 1546 WELLS, D. L. & COPPERSMITH, K. J. 1994. New empirical relationships among magnitude, rupture
 1547 length, rupture width, rupture area, and surface displacement. *Bulletin of the Seismological*
 1548 *Society of America*. **84**, 974-1002.
- 1549 WELLS, S. G., BULLARD, T. F., MENGES, C. M., DRAKE, P. G., KARAS P. A., KELSON, K. I., RITTER, J.
 1550 B. & WESLING, J. R. 1988. Regional Variations in Tectonic Geomorphology Along a

- 1551 Segmented Convergent Plate Boundary, Pacific Coast of Costa Rica. *Geomorphology*, **1**, 239-
1552 265.
- 1553 WESNOUSKY, S. G. 1988. Seismological and structural evolution of strike-slip faults. *Nature*, **335**,
1554 340–342.
- 1555 WESNOUSKY, S. G. 2006. Predicting the endpoints of earthquake ruptures. *Nature*. **444**, 358-360.
- 1556 WHITE, L. T., HALL, R. & ARMSTRONG, R. A. 2014. The age of undeformed dacite intrusions within
1557 the Kolaka fault zone, SE Sulawesi, Indonesia. *Journal of Asian Earth Sciences*, **94**, 105-112.
- 1558 WICHMANN, A. 1918. Die Erdbeben des Indischen Archipels Bis Zum Jahre 1857, (in Dutch),
1559 *Verhandelingen der Koninklijke Akademie van Wetenschappen te Amsterdam*, **20**, 193 pp.
- 1560 WU, J. E., MCCLAY, K., WHITEHOUSE, P. & DOOLEY, T. 2009. 4D analogue modelling of
1561 transtensional pull-apart basins. *Marine and Petroleum Geology*, **26**, 1608-1623.
- 1562 WYSS, M. 2005. Human losses expected in Himalayan earthquakes. *Natural Hazards*, **34**, 305-314.
- 1563 XU, X., YEATS, R. S. & YU, G. 2010. Five short historical earthquake surface ruptures near the silk
1564 road, Gansu Province, China. *Bulletin of the Seismological Society of America*, **100**, 541-561.
- 1565 YEATS, R. 2010. Active Faults of the World. Cambridge University Press, Cambridge, UK. 621 pp.
- 1566 YILDIRIM, C. 2014. Relative tectonic activity assessment of the Tuz Gölü Fault Zone; Central
1567 Anatolia, Turkey. *Tectonophysics*, **630**, 183-192.

1568 **Figure and table captions**

- 1569 **Table 1:** Summary of geomorphic indices used in mountain front analysis, modified after Wells *et al.*
1570 (1988). Both indices after Bull & McFadden (1977) and Bull (1978).
- 1571 **Table 2:** Summary of measurements of mountain front sinuosity and average valley width/height ratio
1572 for analysed fault segments.
- 1573 **Table 3:** Summary of observations made from Quaternary faults in eastern Indonesia, with
1574 hypothetical earthquake magnitudes, styles and tsunami risk.
- 1575 **Fig. 1:** Map of eastern Indonesia showing upper-crustal structures that show geomorphic evidence of
1576 Quaternary tectonic activity, seismicity (1973-2014, focal depths <35 km). CB Cenderawasih Bay;
1577 KF Kolaka Fault; GF Gorontalo Fault; KF Koor Fault; LF Lawanopo Fault; MF Matano Fault;
1578 MFTB Mamberamo fold-thrust belt; MMC Molino metamorphic complex; NSS North Sulawesi
1579 Subduction; PKF Palu-Koro Fault; RS Ransiki Fault; SF Sorong Fault; SFTB Seram fold-thrust belt;
1580 TAF Tarera-Aiduna Fault; YF Yapen Fault. Locations of figures as indicated.
- 1581 **Fig. 2:** Maps showing fault segments analysed for geomorphic indices. Index map at top. Bold lines
1582 are the sinuous mountain front trace (L_{mf}) used in mountain front sinuosity calculations. Basemap is a
1583 90 m SRTM digital elevation model. All maps (a-r) drawn to same scale. Fault segment codes
1584 correspond to codes used in Table 2.
- 1585 **Fig. 3:** Graph of mountain front sinuosity (S_{mf}) versus valley-floor width to valley-height index (V_f)
1586 for studied faults. Grey boxes indicate tectonic activity rates, after McCalpin (2009), with average V_f
1587 marked by the darker grey bar. BK: Balantak Fault; BV: Bada Valley faults; BB: Bobol Fault; EB:
1588 East Buru faults; GO: Gorontalo Fault; KA: Kawa Fault; KD: Kendari faults; KO: Kolaka Fault; LW:

1589 Lawanopo Fault; MA: Matano Fault; ML: Malino boundary faults; MN: Mangole faults; PA: Parigi
 1590 faults; PK: Palu-Koro Fault; PO: Poso faults; RA: Rana Fault; SN: Sanana faults; SV: Sapu Valley
 1591 faults; SG: Sorong Fault; TE: Southern Seram faults; TO: Towuti faults.

1592 **Fig. 4:** Central Sulawesi overview digital elevation model (SRTM), CMT catalogue earthquakes <35
 1593 km depth and structures that show geomorphic evidence of Quaternary tectonic activity. Rivers
 1594 marked in white. Illumination from NE. Location shown in Fig. 1.

1595 **Fig. 5:** a.) The Palu and Sapu valleys showing structures that show geomorphic evidence of
 1596 Quaternary tectonic activity, plus topography and drainage. Mountain front sinuosity values in bold
 1597 italics. For location see Fig. 4. Major drainage basins for Salo Sapu and Salo Wuno are marked,
 1598 separated by uplift at the western end of the Sapu valley fault system. b) View of the Palu-Koro fault
 1599 scarp from the Palu valley, showing geomorphic evidence of Quaternary tectonic activity.

1600 **Fig. 6:** Evidence of a cross-basin fault system within the Palu valley Quaternary fill. a) Overview
 1601 ASTER digital elevation model draped with ESRI imagery layer. Illumination from NW. Palu river
 1602 channels traced from 6 separate images from 2003 to 2015. Inset shows fault pattern developed in an
 1603 analogue model of a releasing bend, modified after Wu et al. (2009), reflected and rotated to mimic
 1604 the Palu valley. Sidewall faults and cross-basin fault system are highlighted in the model and on the
 1605 satellite imagery. b, c) Laterally confined meander belts, interpreted as representing minor subsidence
 1606 within the cross-basin fault system. d) Laterally confined river channels directly along strike from a
 1607 Palu-Koro Fault strand seen to offset alluvial fans in the south of the valley.

1608 **Fig. 7:** Details of the Sapu valley fault system. a) ESRI imagery of the Sapu and central Palu valleys
 1609 showing major structural and geomorphic features, particularly the releasing-restraining double bend
 1610 and re-routing of axial drainage from the NW valley to the Salo Sapu gorge. b) Detail of the Sapu
 1611 valley showing drainage and highlighting fault control of the axial river. Location shown on Fig. 5a.
 1612 c, d) Laterally confined meander belts and lineaments, interpreted as representing minor subsidence
 1613 within the cross-basin fault system. e) Lineated slickenside surface from an exhumed fault core within
 1614 the Sapu restraining bend. Location shown in Fig. 7a. f) Lower hemisphere stereographic projection
 1615 of fault planes (great circles) and slickenside lineations (points) from the fault shown in Fig. 7e.

1616 **Fig. 8:** Details of the Matano Fault. a) Map of the Matano Fault, Lake Towuti and the northern part of
 1617 the Lawanopo Fault. Basemap is ASTER digital elevation model draped with ESRI imagery. Location
 1618 shown in Fig. 4. b) Systematic stream offsets along strands of the Matano Fault west of the Pansu
 1619 Basin. c) Deep, steep-sided valley marking the westernmost Matano Fault NE of Gunung Balease. d)
 1620 Hospital in the Mahalona valley damaged during the 15th February 2011 Mw 6.1 earthquake. e)
 1621 Detail of the eastern Matano and Mahalona valleys, showing features related to the 2011 earthquake,
 1622 and inferred surface rupture extent. ASTER basemap. f) Imagery from Bing Maps showing strong
 1623 topographic lineaments in low ground in the NE corner of Lake Matano, inferred to represent recent
 1624 (2011?) surface ruptures. Location shown in Fig. 8e.

1625 **Fig. 9:** Details of the Kolaka Fault. a) Overview map of the main Kolaka Fault segments. Basemap is
 1626 ASTER digital elevation model draped with ESRI imagery. Location shown in Fig. 1. b) Straight
 1627 segment of the Kolaka Fault associated with linear ridges and valleys. c) Linear fault-bounded
 1628 mountain front and triangular facets indicating Quaternary fault activity at Kolaka town. d)
 1629 Asymmetric axial drainage at a splaying fault segment near the western fault termination, indicating
 1630 Quaternary subsidence along the bounding fault system.

1631 **Fig. 10:** a) East arm of Sulawesi and Banggai-Sula Islands digital elevation model (SRTM),
 1632 multibeam bathymetry, CMT catalogue earthquakes <35 km depth and structures that show
 1633 geomorphic evidence of Quaternary tectonic activity. After Watkinson *et al.* (2011). Location shown
 1634 in Fig. 1. b) Subsidence and uplift associated with releasing and restraining segments of the onshore
 1635 Balantak Fault. ASTER digital elevation model basemap. c) Detail of bounding fault system of a
 1636 Balantak Fault releasing segment, showing a north-dipping normal fault and sub-parallel lineament in
 1637 agricultural land, inferred to represent a through-going strike-slip strand. ESRI imagery basemap. d)
 1638 Detail of the offshore Balantak Fault expressed in multibeam imagery (illumination from NW)
 1639 showing evidence of dextral shear.

1640 **Fig. 11:** a) North arm of Sulawesi digital elevation model (SRTM), CMT catalogue earthquakes <35
 1641 km depth and structures that show geomorphic evidence of Quaternary tectonic activity. Rivers
 1642 marked in white. Location shown in Fig. 1. b) Detail of the onshore Gorontalo Fault and associated
 1643 basins. ASTER digital elevation model draped with ESRI imagery layer. c) Fault system bounding the
 1644 Malino metamorphic complex showing remarkably straight and steep mountain front and well
 1645 developed triangular facets. d) Overview of fan deltas prograding into western Tomini Bay across the
 1646 bounding fault system. e) Narrow fan delta clearly cut by the basin bounding fault, indicating rapid
 1647 subsidence. f) Wide fan delta further south indicating a slower rate of hanging wall subsidence.

1648 **Fig. 12:** Details of Quaternary faults in the Banggai-Sula islands. For locations see Fig. 10a. a) Part of
 1649 the linear normal fault system bounding the southern margin of Mangole island. Google Earth image.
 1650 b) Triangular facets along the north coast of Mangole island. Oblique view in Google Earth. c) Fault
 1651 control along the eastern coast of Sanana island. Image from Google Earth (greyscale inverted for
 1652 clarity). d) Detail of the Sanana fault, showing the extremely linear mountain front, narrow V-shaped
 1653 valleys and triangular facets.

1654 **Fig. 13:** a) Mega-debris slide and post-collapse normal faults, north coast of Taliabu. Basemap is
 1655 SRTM topography onshore and multibeam bathymetry offshore. Location shown in Fig. 10a. b.)
 1656 Oblique perspective view from Google Earth of one of the normal faults on the north slope of Taliabu.
 1657 White arrows mark fault tips. View to the west. Field of view is approximately 1 km in foreground.
 1658 View location and direction indicated by red arrow in Fig. 13a.

1659 **Fig. 14:** a) Seram digital elevation model (SRTM), CMT catalogue earthquakes <35 km depth and
 1660 structures that show geomorphic evidence of Quaternary tectonic activity. Rivers marked in white.
 1661 Offshore structures from Teas *et al.* (2009). Location shown in Fig. 1. b) Normal faults along the
 1662 south coast of Seram, marked by linear mountain front and a prominent lineament crossing a narrow
 1663 fan delta. c) Possible Quaternary fault SW of Ambon, marked by a lineament that crosses volcanic
 1664 hills and Quaternary drift. d) Example of foliated gouge from a thick fault zone located where the
 1665 lineament illustrated in Fig. 14c reaches the coast. Pen is 14 cm long.

1666 **Fig. 15:** Evidence of Quaternary thrusting along the north coast of Seram. a) ESRI image showing a
 1667 number of NE-flowing rivers flowing around linear elevated and forested regions. Location shown in
 1668 Fig. 14a. b, c) Migrating rivers marked by filled channels and oxbow lakes, and incision into uplifting
 1669 regions. Google Earth imagery. d) Interpretation of Fig. 15a. Thick arrows indicate progressive
 1670 migration of river channels, short arrows show coastline regression. Abandoned channels at points A,
 1671 B and C are interpreted to represent the previous route of a river that previously entered the sea at D
 1672 north of a meander plain at C, but was cut off by thrust hangingwall uplift at B, and was forced to
 1673 divert east from point A to join Wai Musi, leaving previous channels abandoned. Other rivers show

1674 lateral migration away from the growing tips of thrusts in response to hangingwall fold growth. See
1675 text for further details.

1676 **Fig. 16:** Strike-slip faults of southern Seram. a) Overview map of the Kawa Fault zone showing
1677 Quaternary fault strands, rivers, river offsets (in metres) and landslips. Left-lateral offsets in black,
1678 right lateral offsets in grey. See Fig. 14a for location. b) ESRI image of the Kawa Fault zone
1679 highlighting its clear geomorphic expression and thick forest cover. c) Representative stream offset
1680 across the main Kawa Fault strand, image from Google Earth. d) View into the Kawa Fault from the
1681 Wai Kawa delta, showing the linear mountain front and triangular facets developed along the northern
1682 strand of the Taluti Bay splay. e) Overview map of the Bobol Fault zone showing Quaternary fault
1683 strands, rivers and left-lateral river offsets (in metres). Bold italic numbers are Smf. See Fig. 14a for
1684 location. f) Representative stream offset across the main Kawa Fault strand, also showing fault control
1685 of river channels. ESRI imagery.

1686 **Fig. 17:** Quaternary fault features in Buru. a) Digital elevation model (SRTM), CMT catalogue
1687 earthquakes <35 km depth and structures that show geomorphic evidence of Quaternary tectonic
1688 activity. Rivers marked in white. Location shown in Fig. 1. b) Overview of topographic lineaments
1689 passing through Namlea and NE Buru. ESRI imagery. c) Detail showing possible sag pond
1690 developed at the releasing step-over between right-stepping fault segments. d) Evidence of strike-slip
1691 faulting along the Namlea lineament trend. Lineaments pass from basement rock through Quaternary
1692 drift, and are associated with systematic right-lateral stream offsets.

1693 **Fig. 18:** Rana Fault, central Buru. a) Overview of the Rana Fault, ASTER GDEM basemap. Rivers
1694 marked in white, with white arrows showing the flow direction of major rivers discussed in the text.
1695 Location shown in Fig. 17a. b) ESRI image of the central part of the Rana Fault. c) Interpretation of
1696 the image in b, showing evidence of Quaternary fault activity. d) Possible fault scarp along the foot of
1697 triangular facets marking the Rana Fault. e) Detail of the possible fault scarp, showing steep dip, fresh
1698 geomorphic expression and straight trace. d & e are oblique views from Google Earth.

1699 **Fig. 19:** a) Bird's Head (West Papua) digital elevation model (SRTM), multibeam bathymetry, CMT
1700 catalogue earthquakes <35 km depth and structures that show evidence of Quaternary tectonic
1701 activity. Rivers marked in white. Location shown in Fig. 1. Offshore structures north of the Koor
1702 Fault from Milsom *et al.* (1992). b.) Detail of the intersection between the Ransiki and Yapen faults,
1703 south of Manokwari. Eastern limit of image is to the east of the main map. SRTM onshore, multibeam
1704 bathymetry offshore.

1705 **Fig. 20:** Evidence of Quaternary fault activity in the Bird's Head. a) Section of the onshore Sorong
1706 Fault showing a basin-bounding normal fault in the north, and two strike-slip fault strands offsetting
1707 streams to the left in the south. Location shown in Fig. 19a. b) Ransiki delta at the southern end of the
1708 Ransiki Fault, showing prominent western normal fault. Location shown in Fig. 19b. c) Region of
1709 coseismic subsidence showing flooded forest and buildings adjacent to the western normal fault.

1710 **Fig. 21:** Northern Papua and Cenderawasih Bay digital elevation model (SRTM), multibeam
1711 bathymetry, CMT catalogue earthquakes <35 km depth and structures that show geomorphic evidence
1712 of Quaternary tectonic activity. Rivers marked in white. Location shown in Fig. 1. b) Expression of
1713 the Yapen and Randaway faults along the northern coast of Pulau Yapen, showing evidence for
1714 Quaternary sinistral slip along the Randaway Fault. Inset shows the topography and major structures
1715 of Yapen. ESRI imagery. c) Multibeam bathymetry detail showing the Yapen Fault to the west of
1716 Pulau Yapen, southern strands appear to transfer to N-S extension via a series of pull-apart basins.

1717 **Fig. 22:** Evidence of Wandamen Peninsula Quaternary fault activity. a) Overview digital elevation
1718 model (SRTM) showing bounding normal faults. Location shown in Fig. 21a. b) Pronounced
1719 triangular facets and hanging valleys along the eastern bounding fault system. ESRI Imagery. c)
1720 Inferred Quaternary fault trace across the top of alluvial fans crossing the western fault system.

1721 **Fig. 23:** Southern West Papua and Cenderawasih Bay digital elevation model (SRTM), multibeam
1722 bathymetry, CMT catalogue earthquakes <35 km depth and structures that show geomorphic evidence
1723 of Quaternary tectonic activity. Rivers marked in white. Location shown in Fig. 1. Offshore structures
1724 from Teas *et al.* (2009).

1725 **Fig. 24:** a.) Map of the onshore Tarera-Aiduna Fault, showing structures that show geomorphic
1726 evidence of Quaternary tectonic activity. Bold italic numbers are Smf. Location shown in Fig. 23. b.)
1727 Detail from greyscale Landsat TM 432 image, showing linear confinement of abandoned River Aru
1728 channels, indicating strike-slip strands across the plain. c.) Major strand of the Tarera-Aiduna Fault
1729 bounding a steep-sided ridge and rhomboidal basin. d & e) Possible river offset across the Tarera-
1730 Aiduna Fault. f) Termination extensional fault array developed at the eastern end of the main Tarera-
1731 Aiduna fault strand. d, e & f from ESRI imagery.

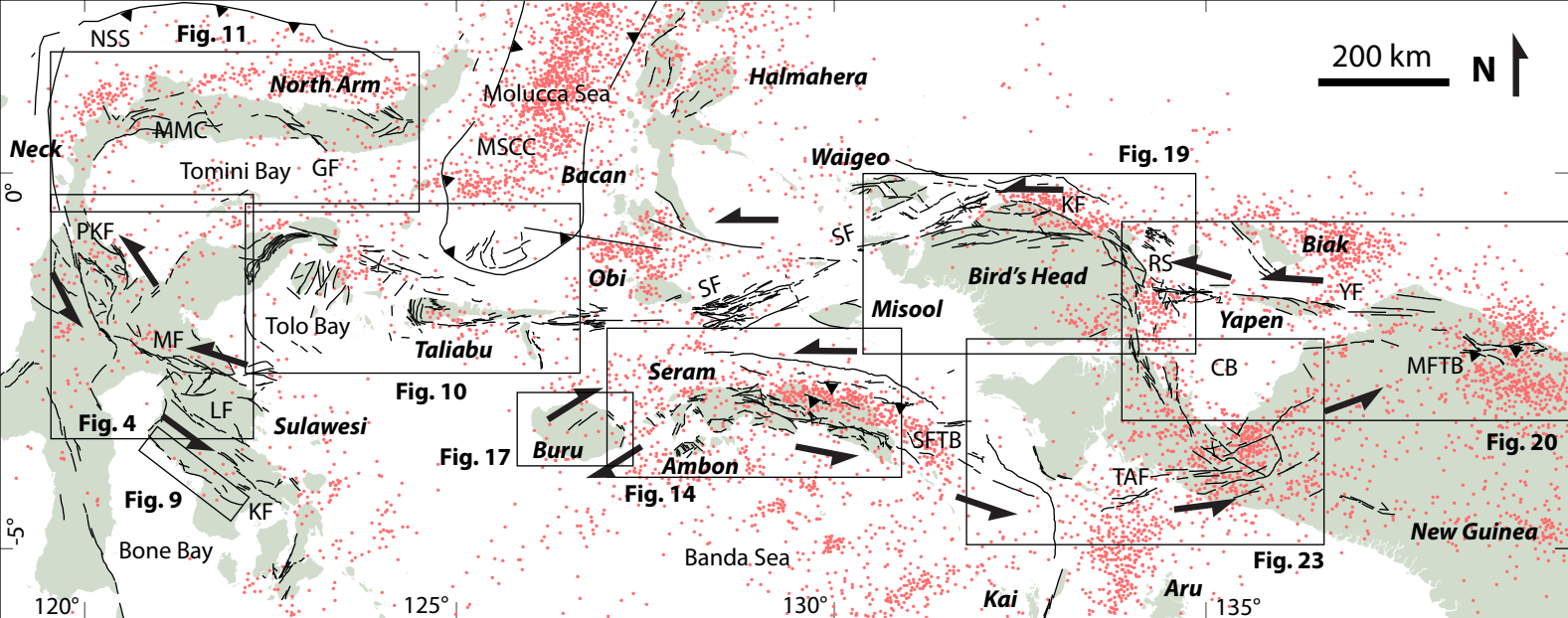


Fig. 1

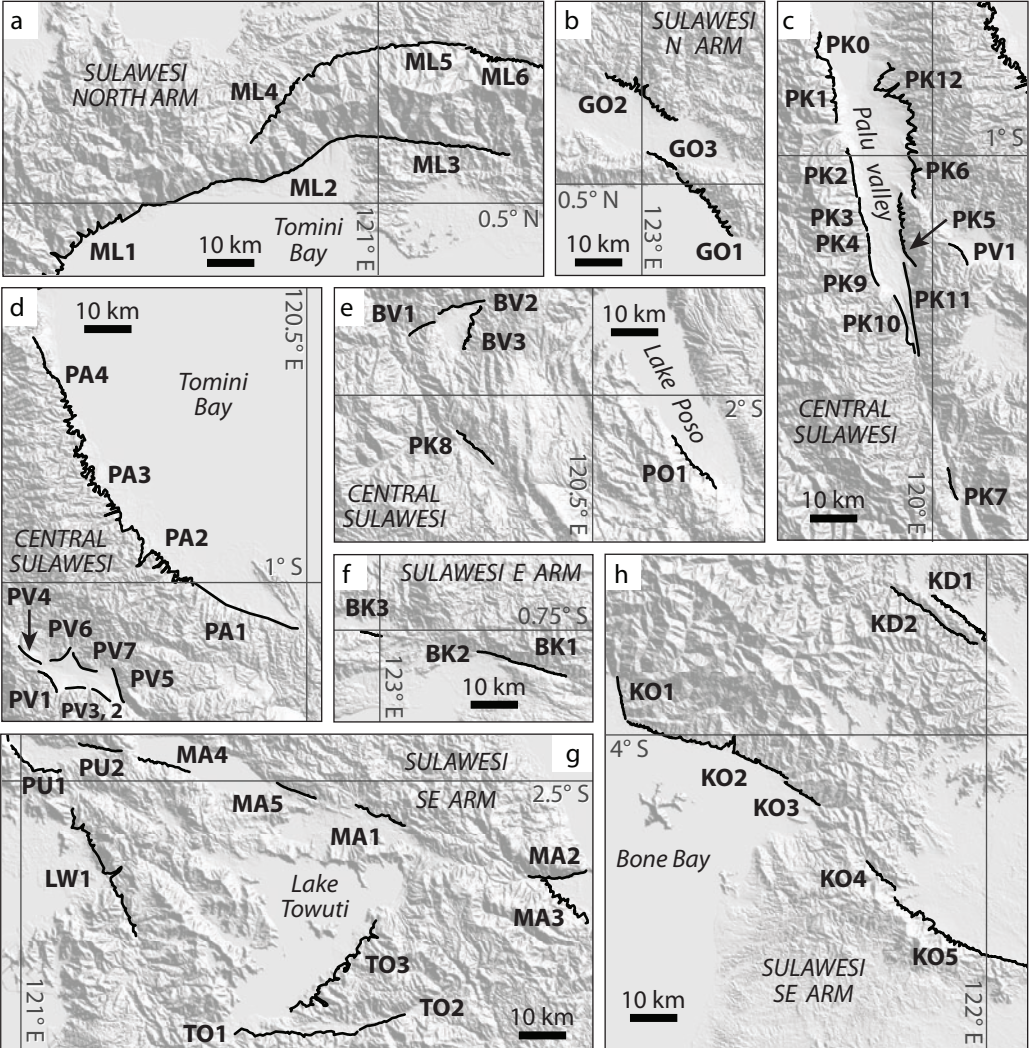


Fig. 2 (PAGE 1)

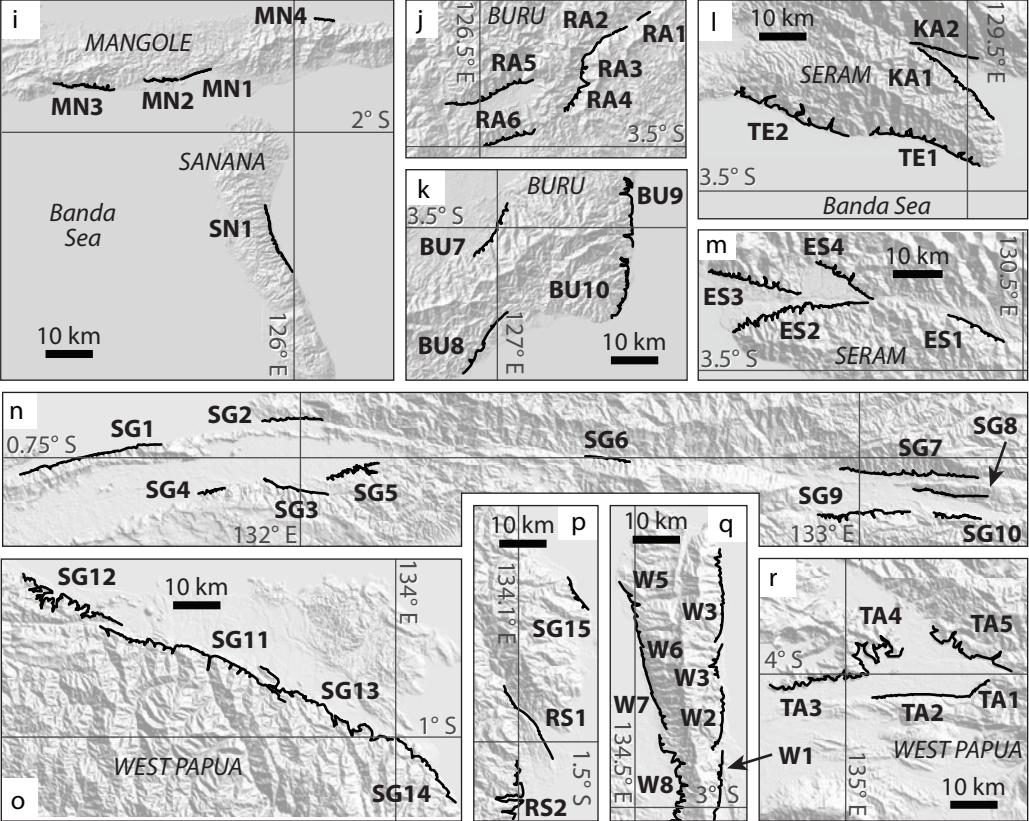
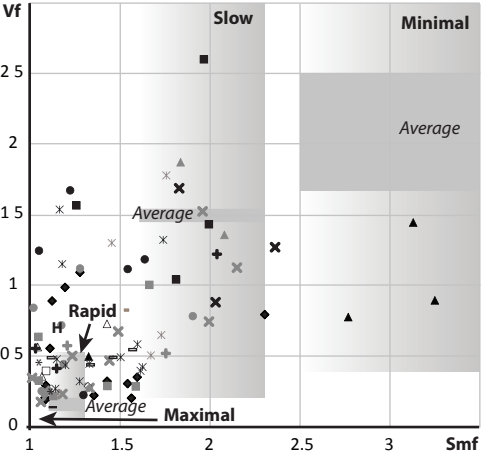


Fig. 2 (PAGE 2)



● AMF * BKF - BNF × BOF × BUF △ BVF ■ ESF × GOF

◆ KAF ⊕ KDF ● KOF - LWF ● MAF ■ MLF - MNF ▲ PAF

◆ PKF ◇ POF □ PVF × SGF ▲ TEF ⊕ TOF

Fig. 3

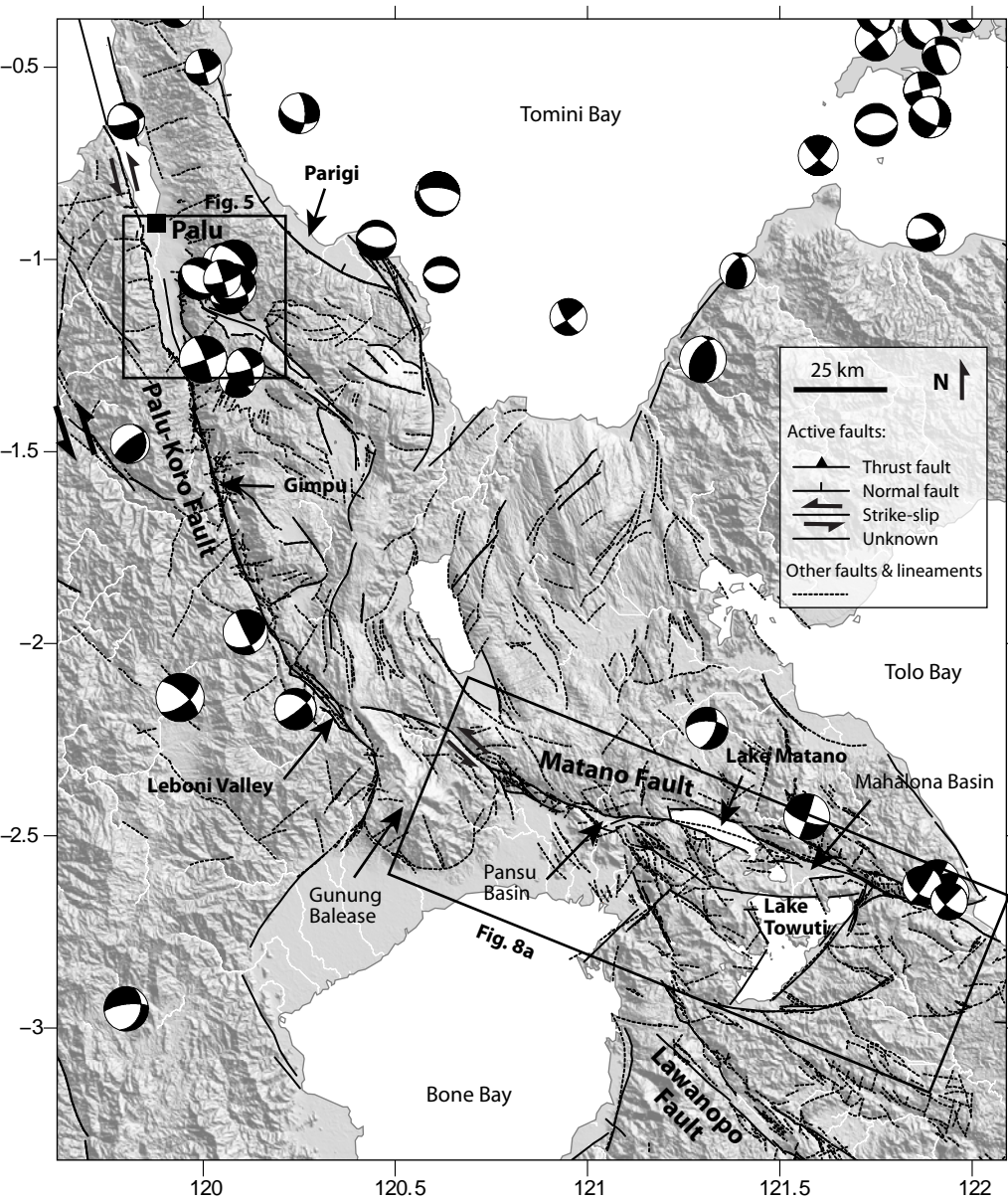


Fig. 4

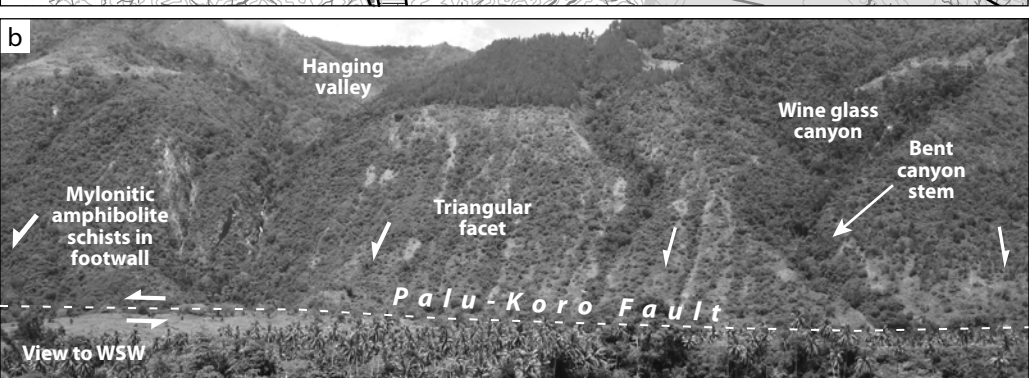
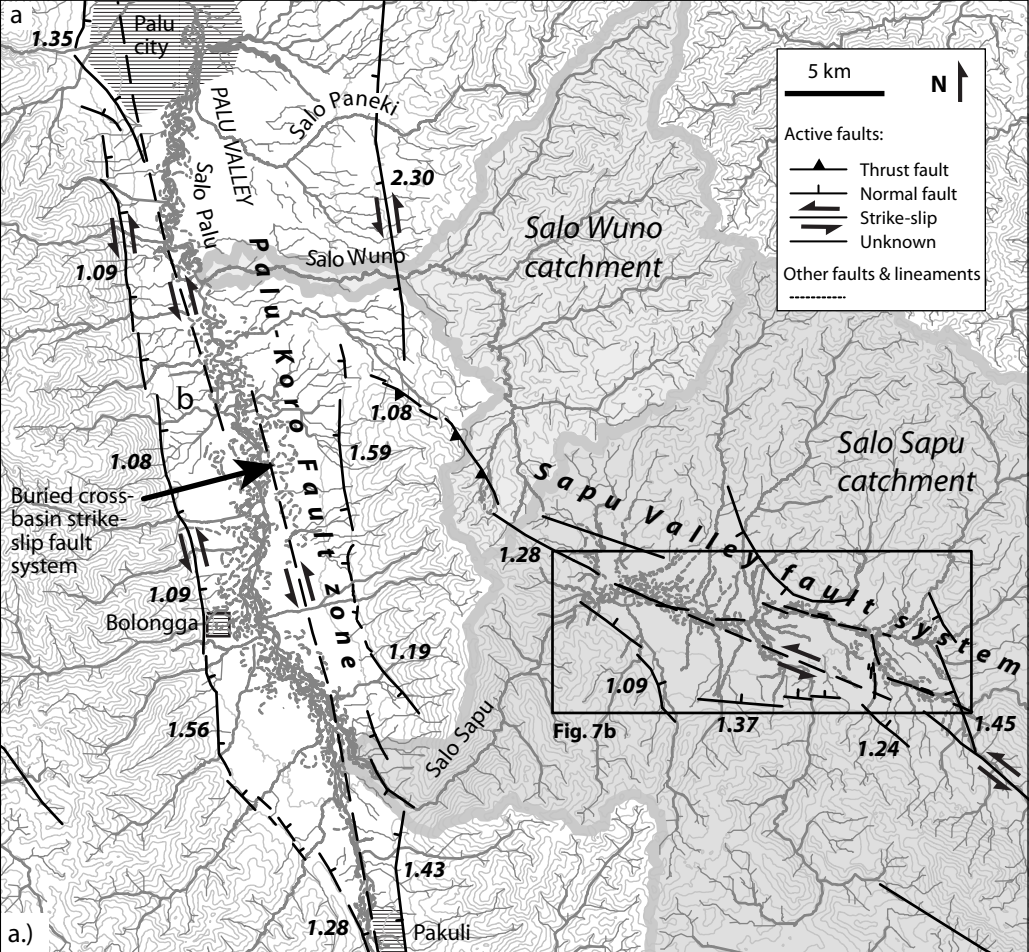


Fig. 5

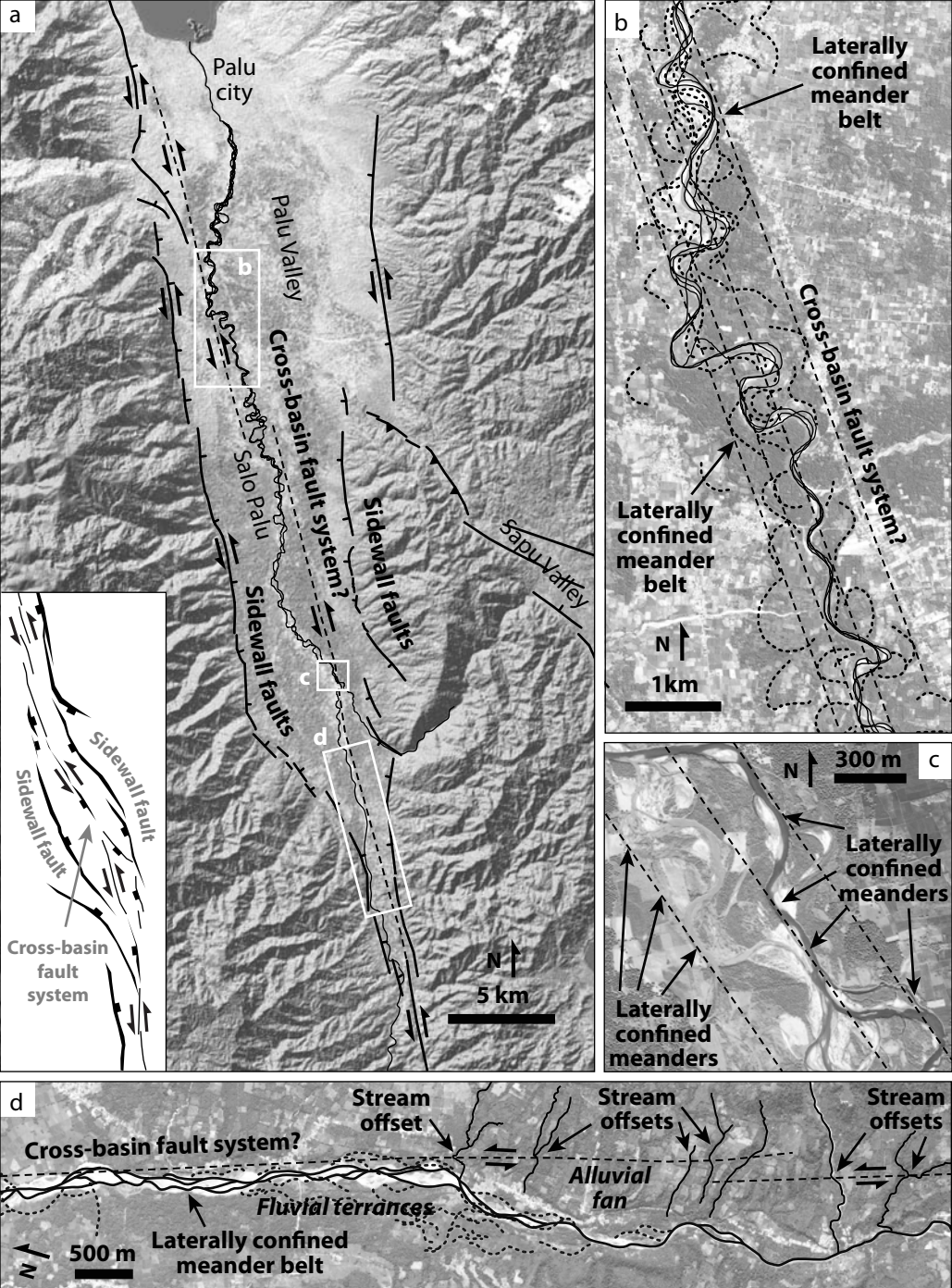
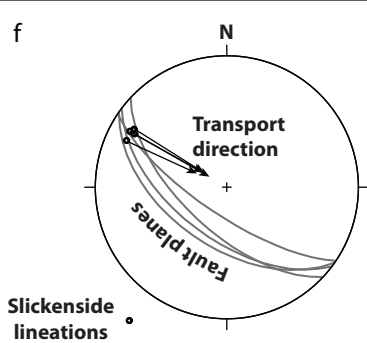
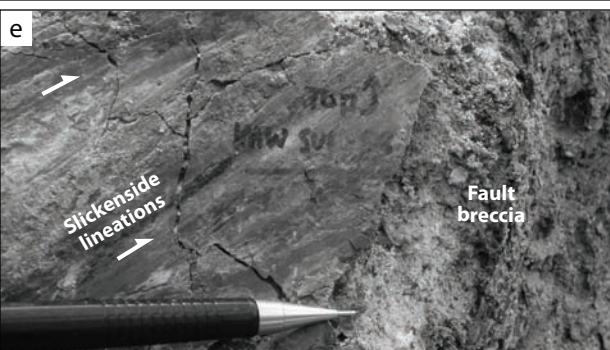
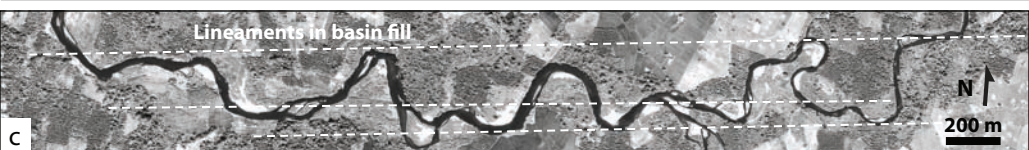
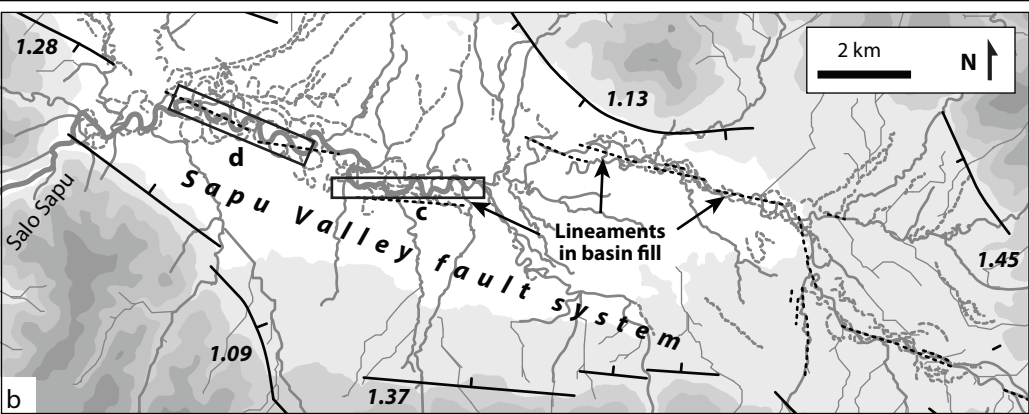
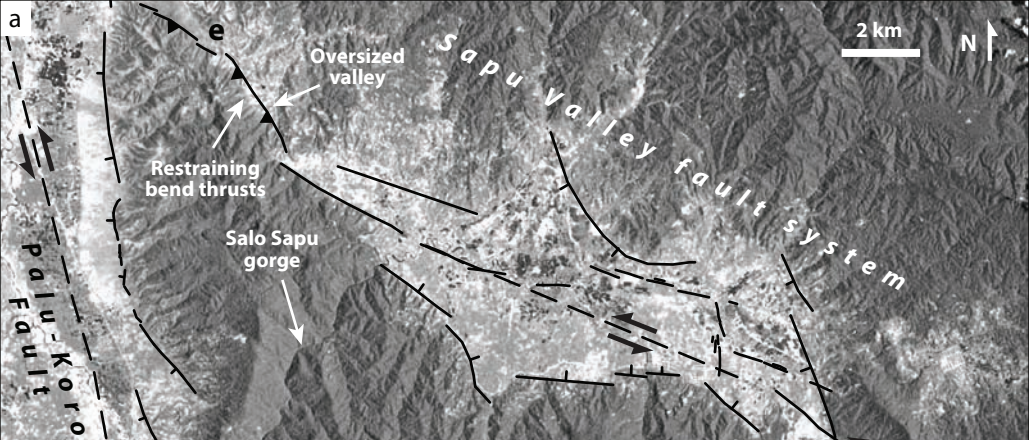


Fig. 6



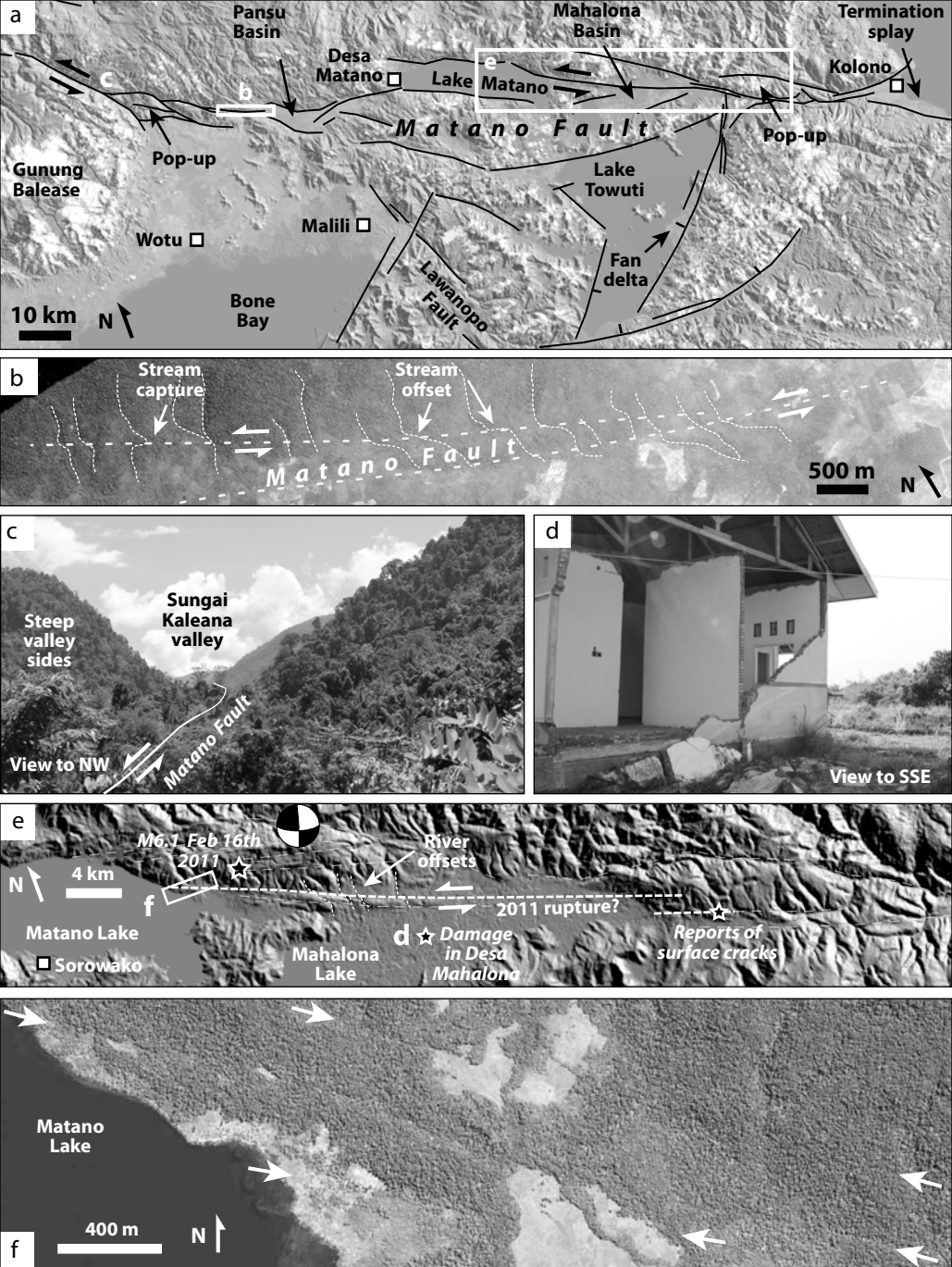


Fig. 8

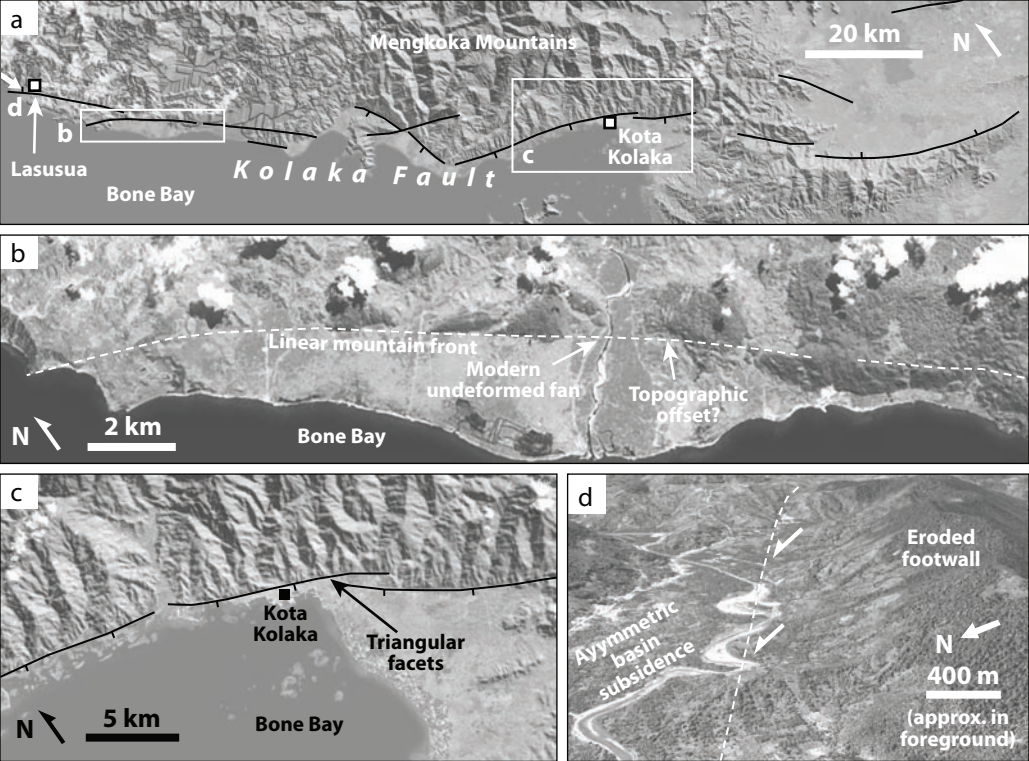


Fig. 9

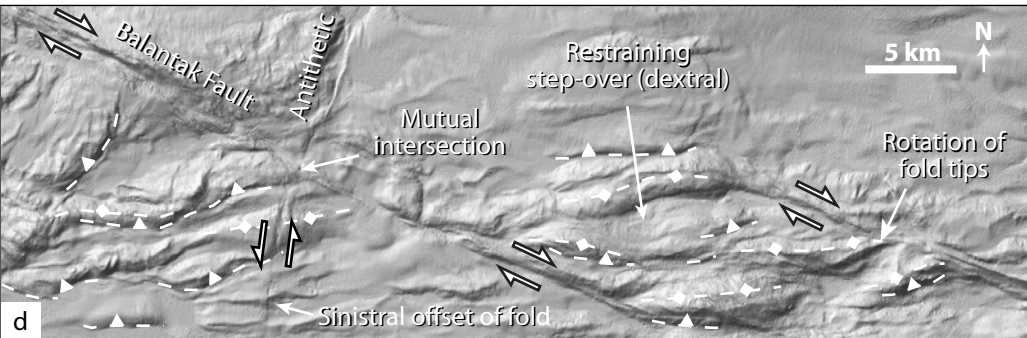
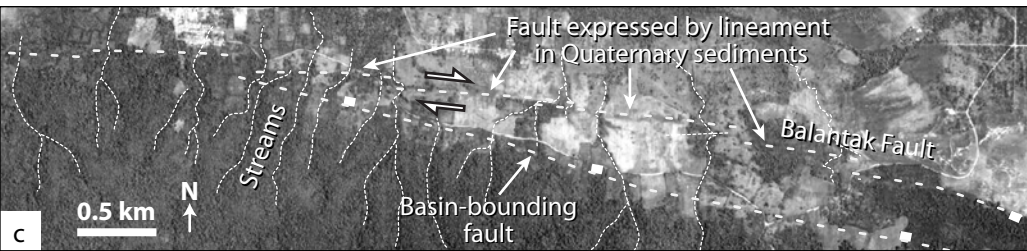
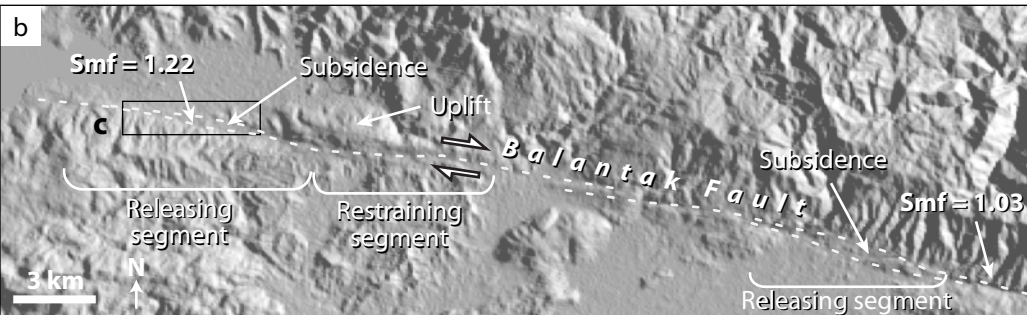
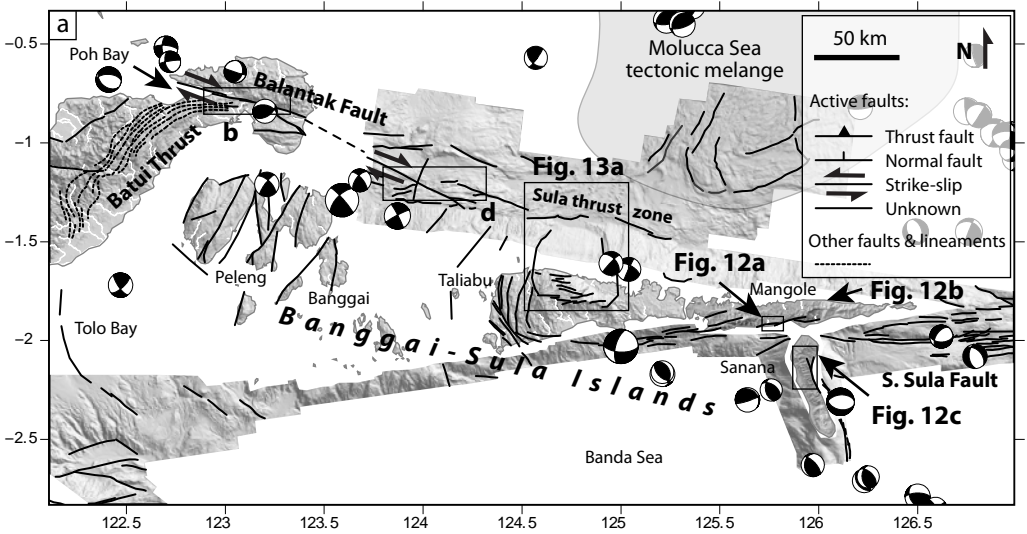
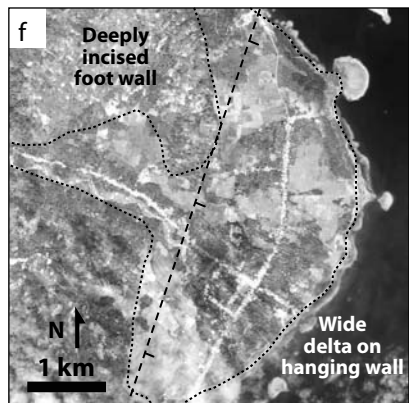
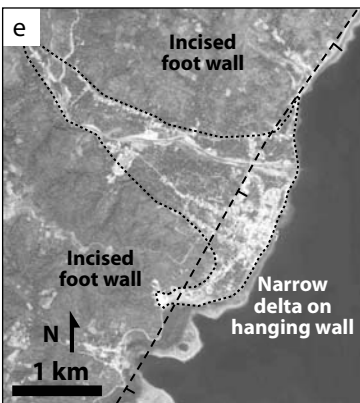
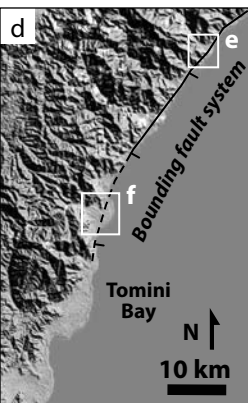
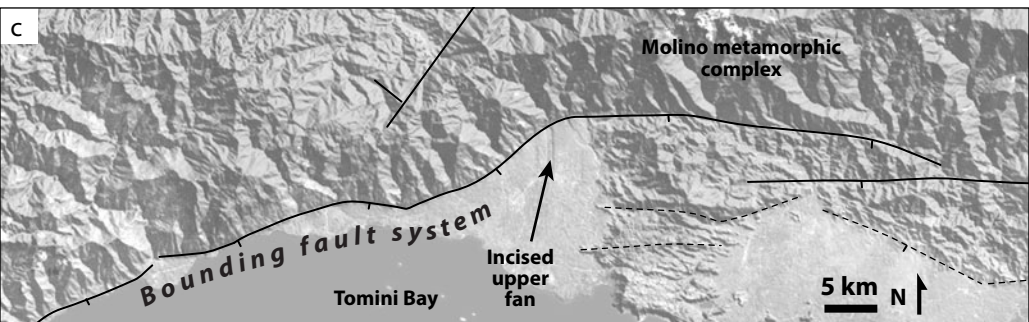
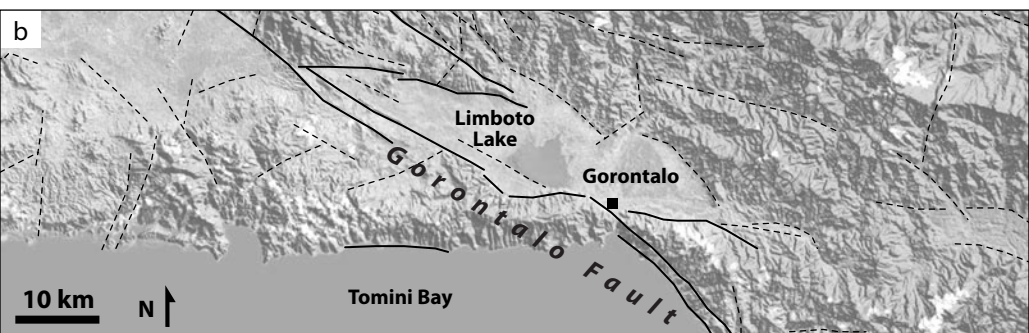
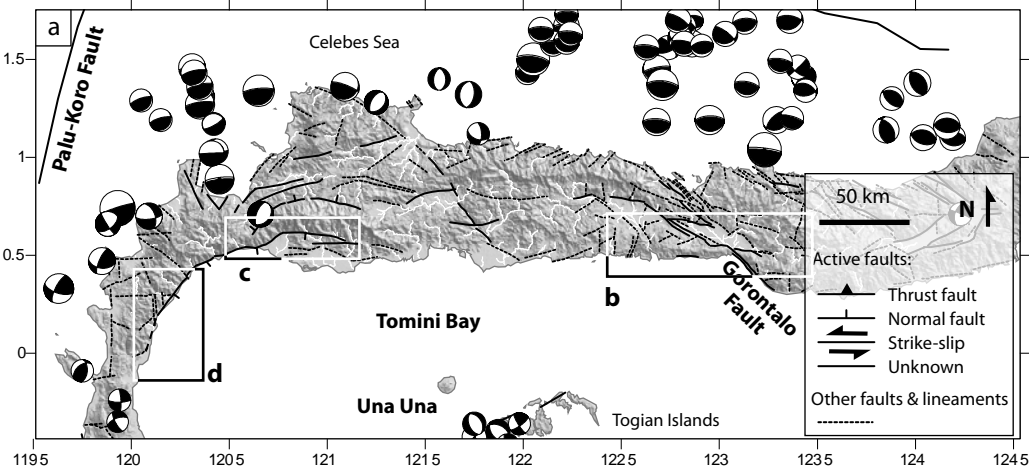


Fig. 10



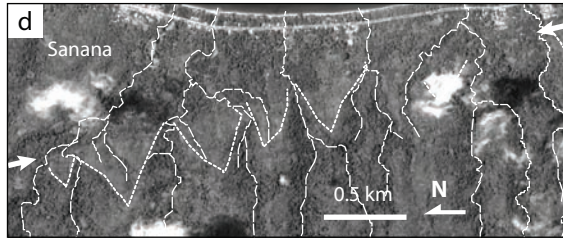
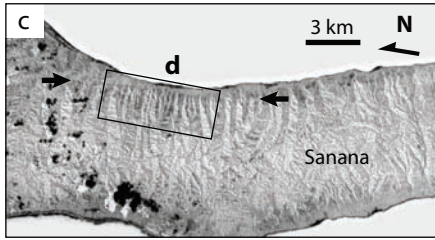
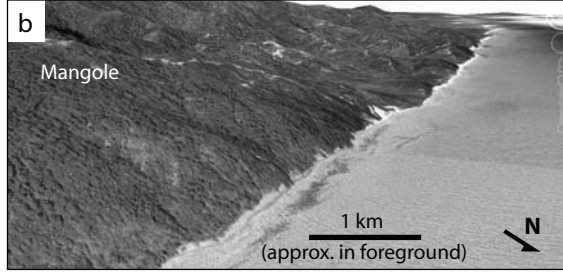
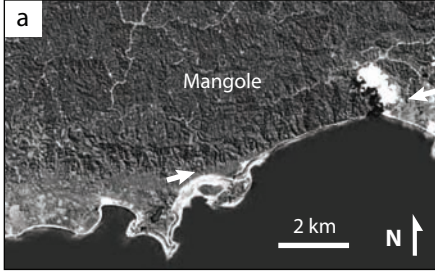


Fig. 12

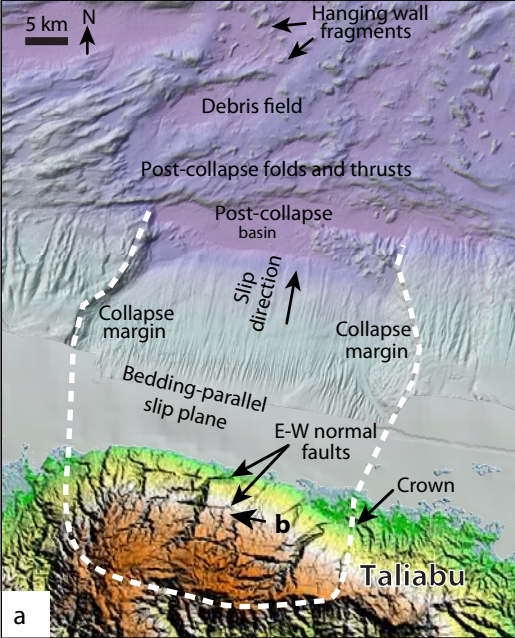


Fig. 13

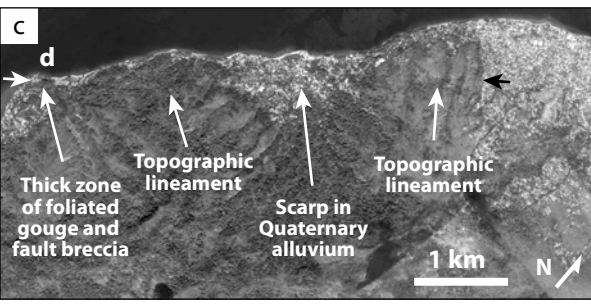
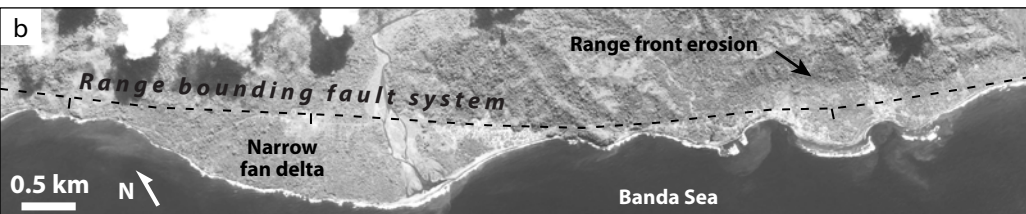
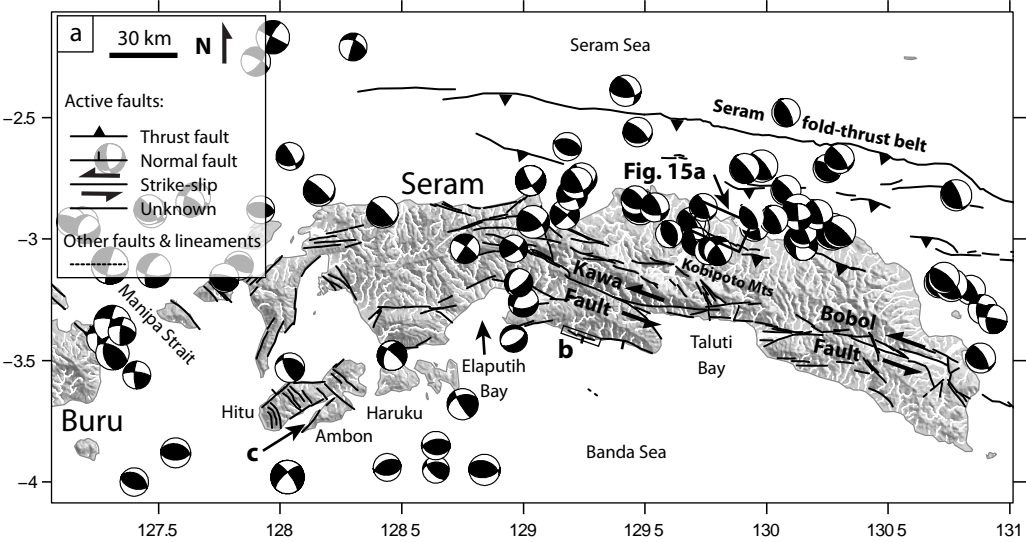
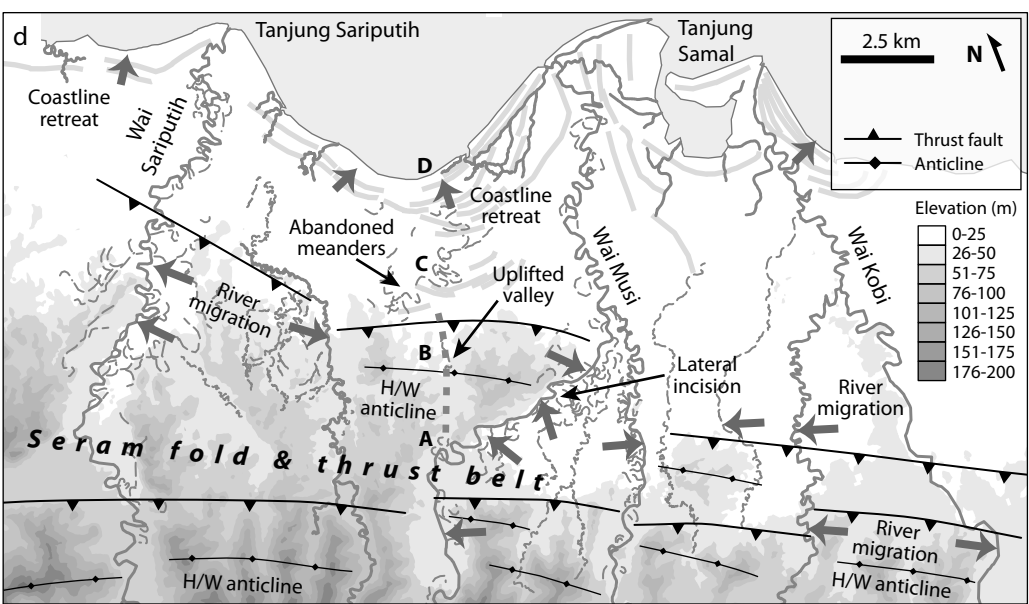
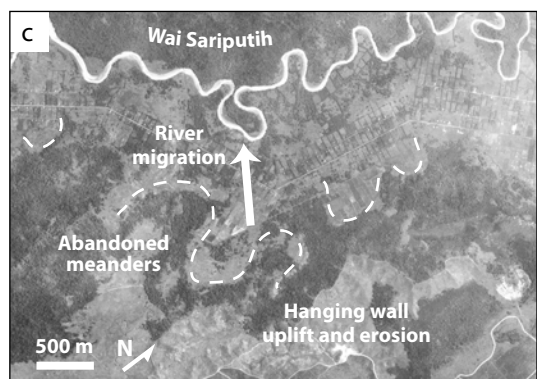
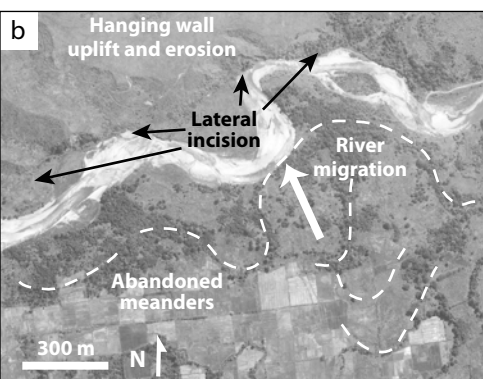


Fig. 14



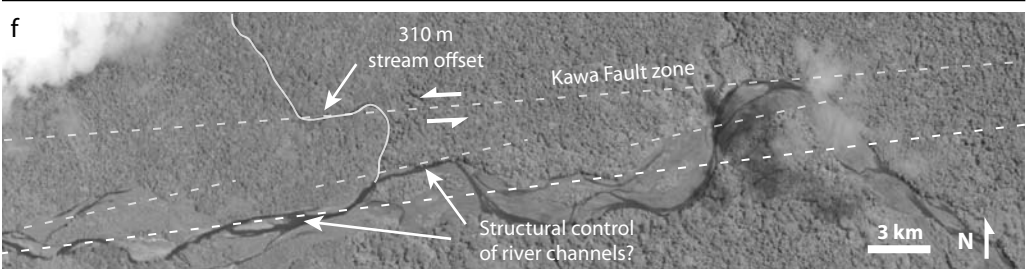
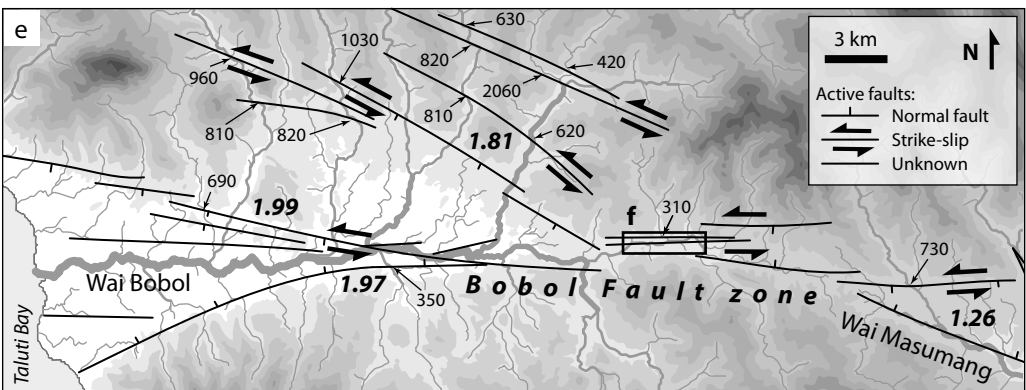
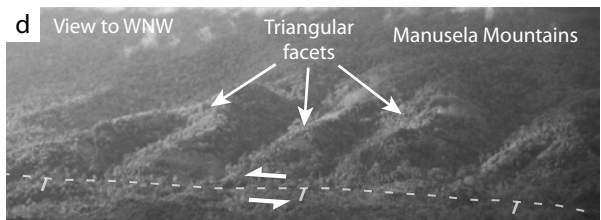
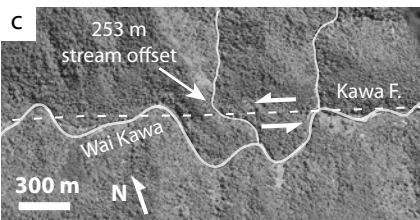
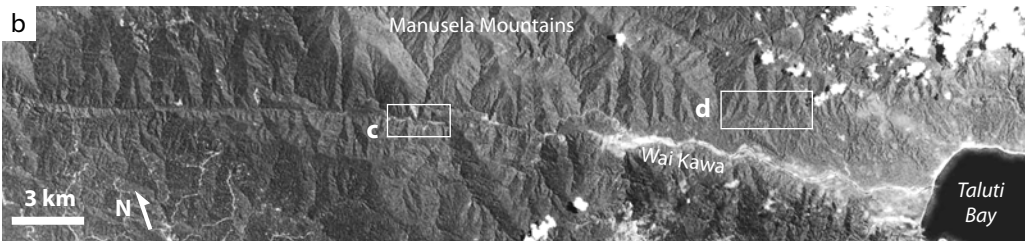
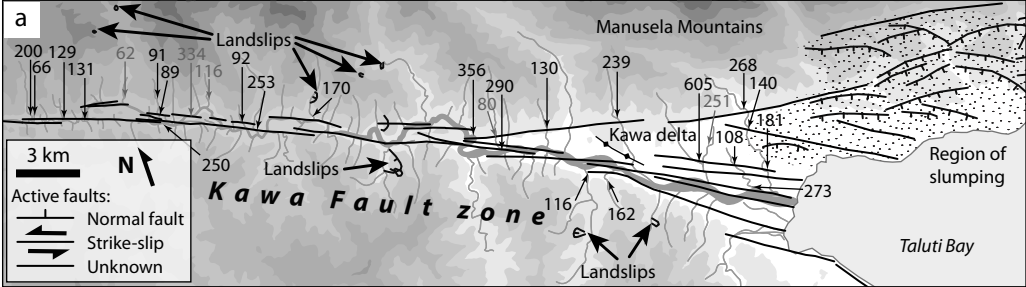


Fig. 16

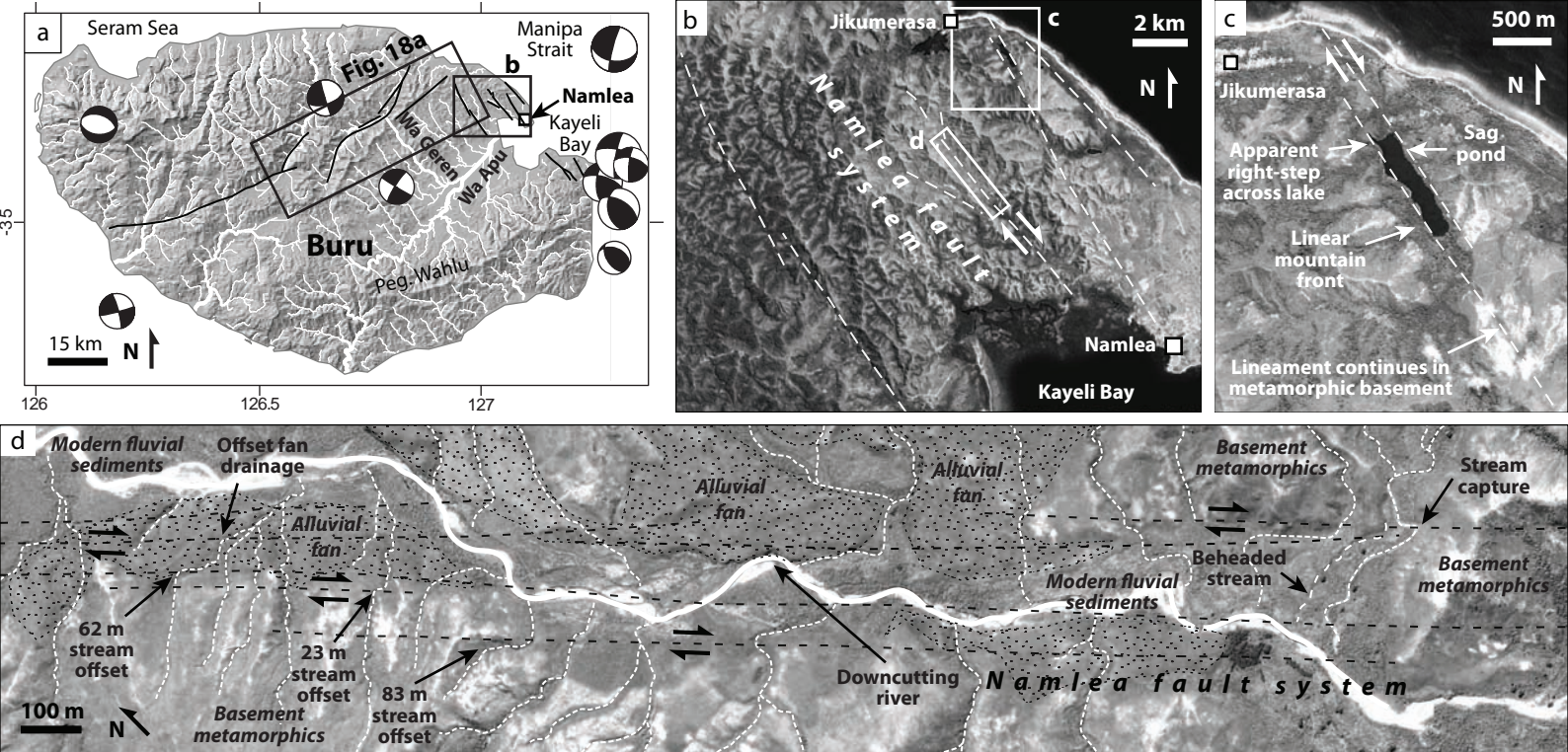


Fig. 17

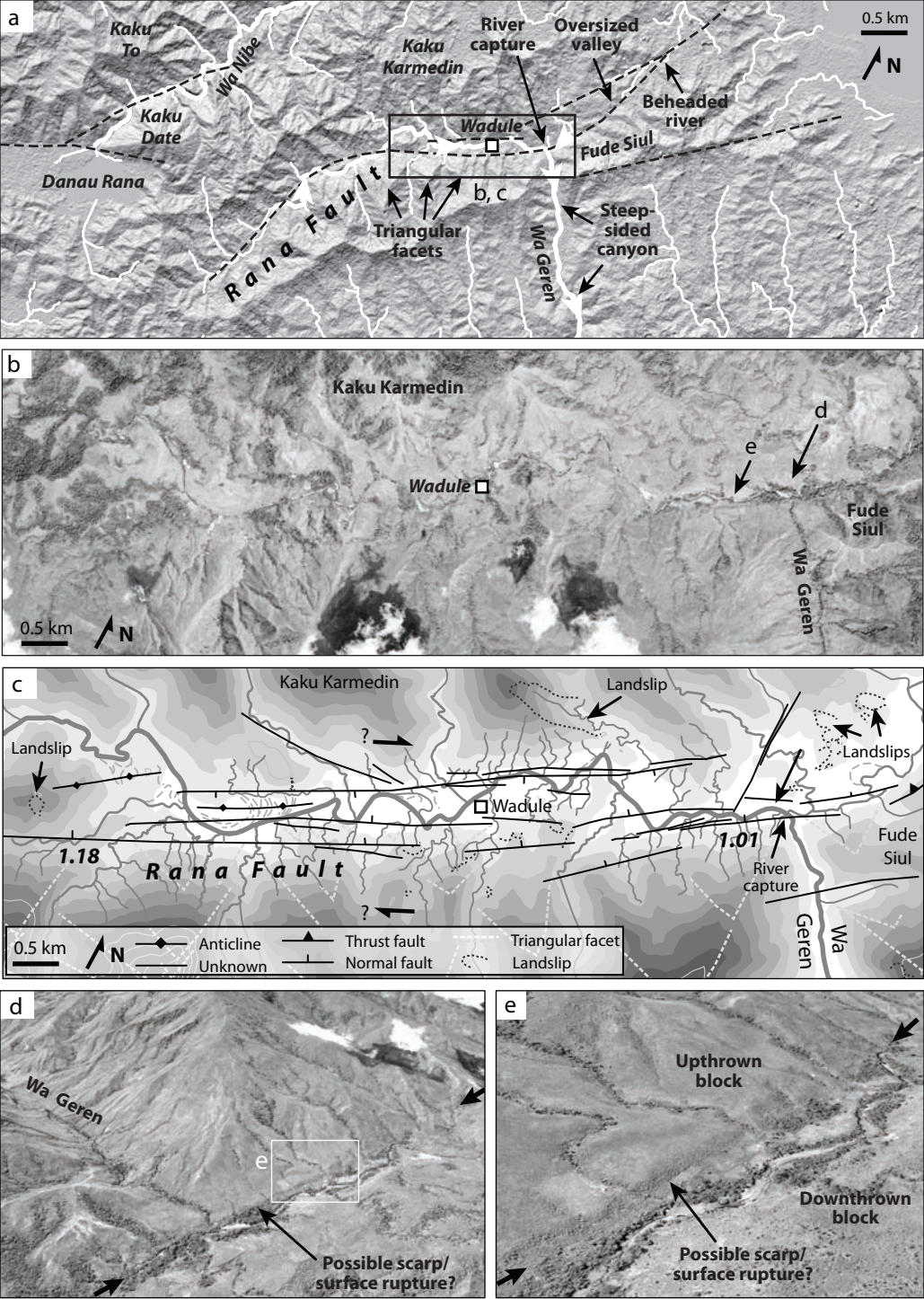


Fig. 18

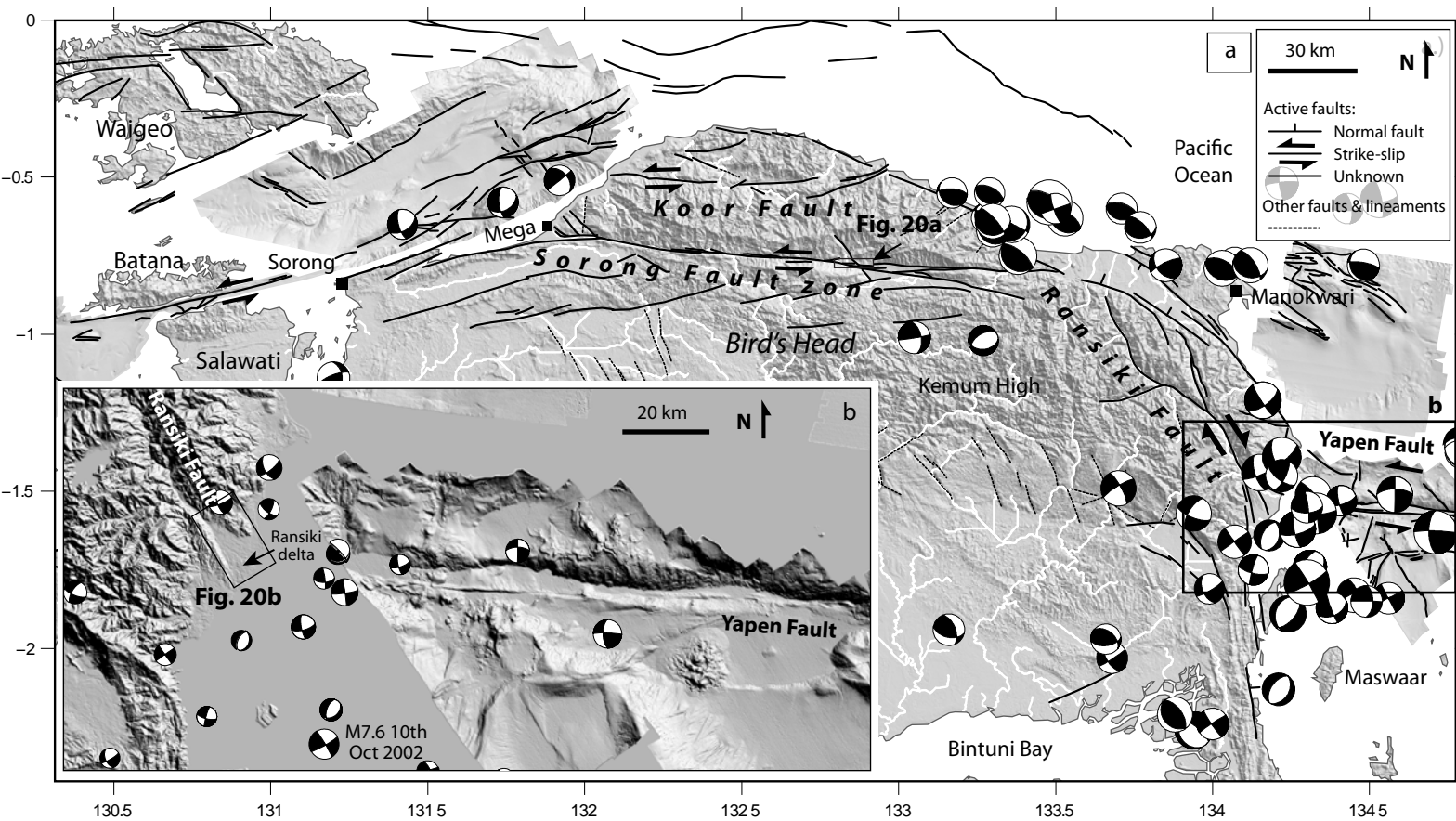


Fig. 19

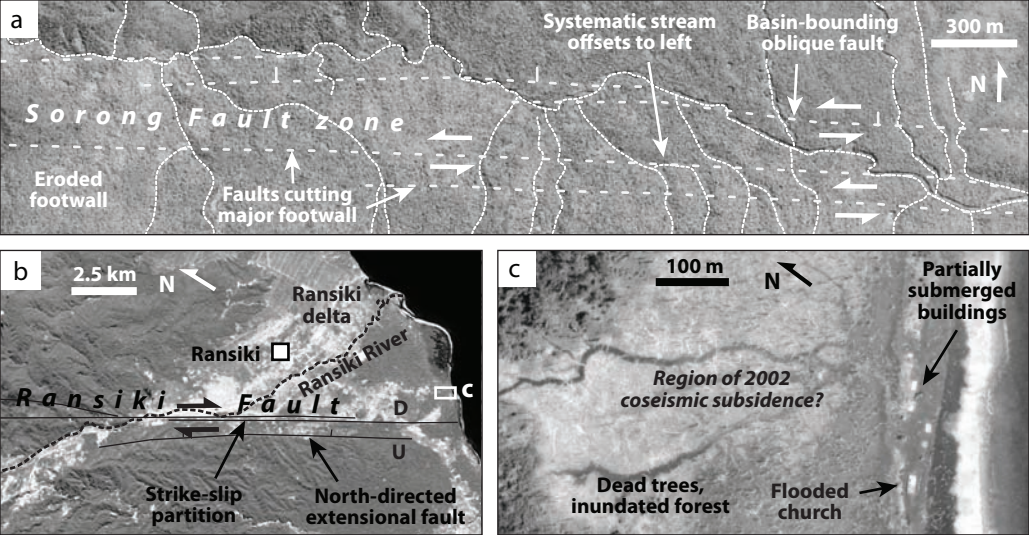


Fig. 20

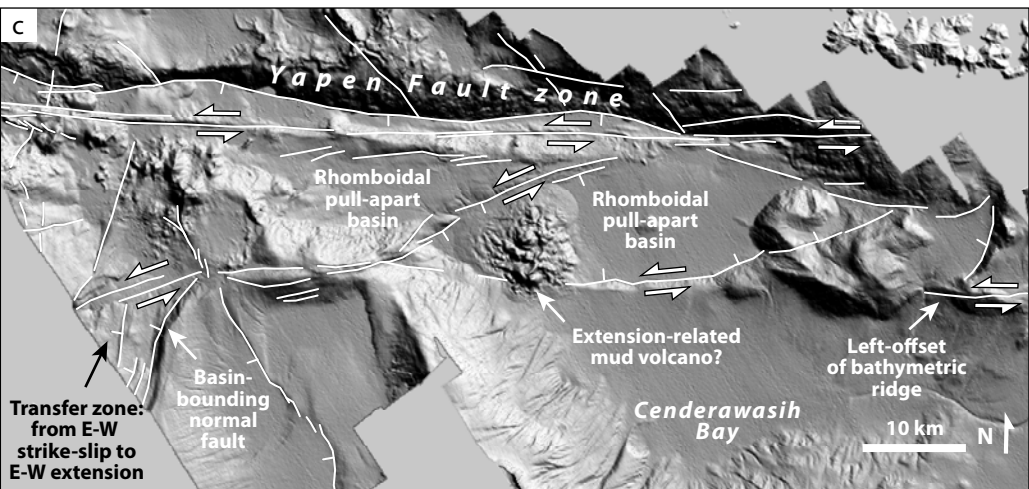
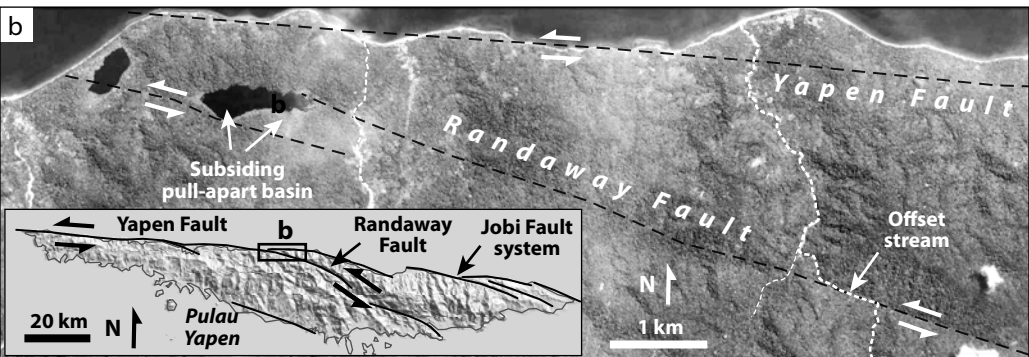
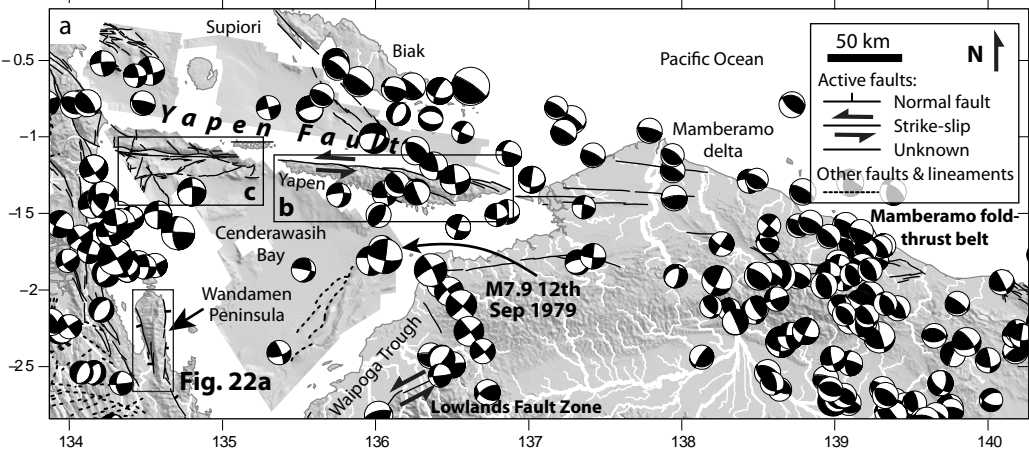


Fig. 21

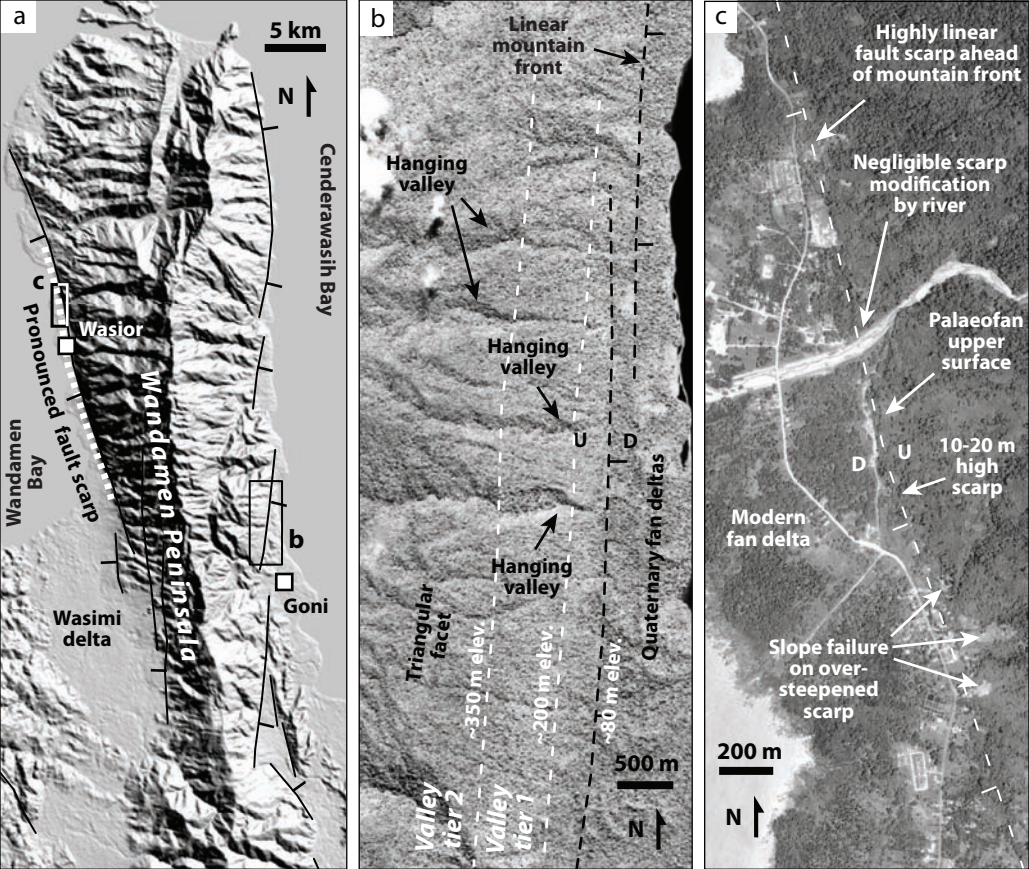


Fig. 22

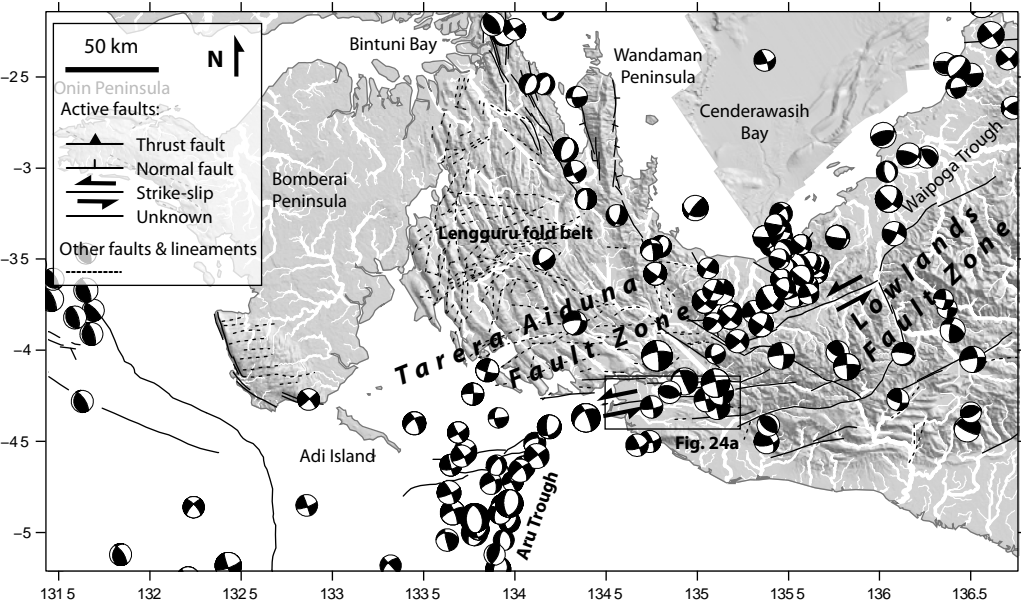


Fig. 23

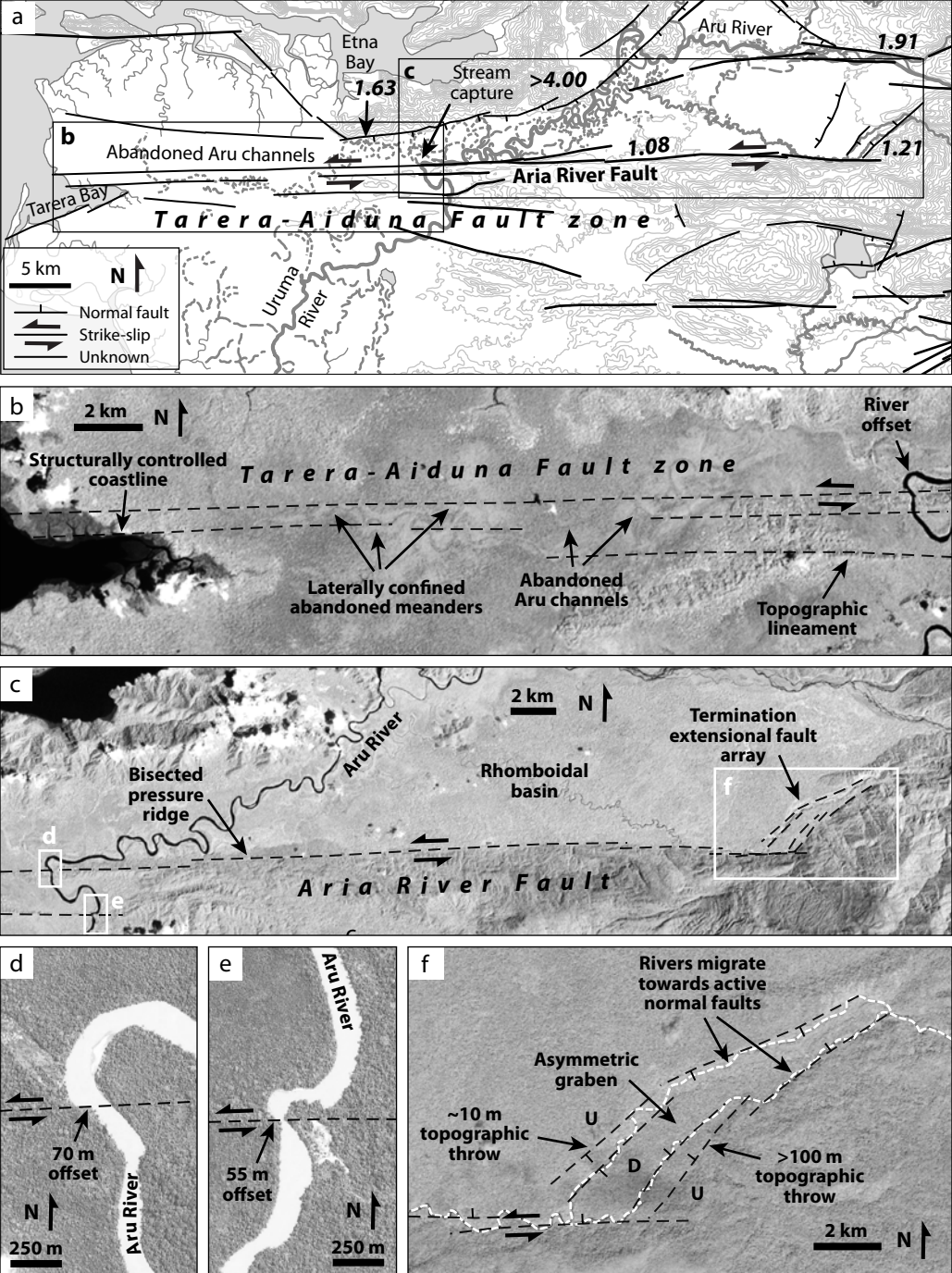


Fig. 24

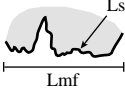
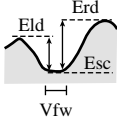
Parameter	Definition	Derivation	Measurement	Purpose	Potential difficulties
Smf	Sinuosity of topographic mountain fronts	Lmf / Ls		Define the degree of topographic modification of mountain front from the position of possible controlling structures	<ul style="list-style-type: none"> - Define actual topographic junction - Define discrete mountain front segments
Vf	Valley floor width to valley height index	$\frac{2Vfw}{(Eld - Esc) - (Erd - Esc)}$		Define the ratio of the valley floor width to the mean height of two adjacent divides, measured at given locations along a stream channel within the range block	<ul style="list-style-type: none"> - Resolution of satellite imagery in defining Vfw and divide elevations - Need to minimise variations in stream size (length area) - Effect of change in lithology

Table 1

Table 2. Summary of measurements of mountain front sinuosity and average valley width/height ratio for analysed fault segmen

Fault	Seg.	Lmf ¹	LS ²	Smf ³	Vf Av ⁴	Fig. X ⁵	Fault	Seg.	Lmf ¹	LS ²	Smf ³	Vf Av ⁴	Fig. X ⁵
Malino Boundary	ML1	45.16	27.17	1.66	1.01	a	Kolaka	KO1	8.79	8.38	1.05	1.25	h
Malino Boundary	ML2	52.00	49.60	1.05	0.33	a	Kolaka	KO2	52.12	33.80	1.54	1.12	h
Malino Boundary	ML3	28.79	27.53	1.05	0.64	a	Kolaka	KO3	10.07	8.24	1.22	1.68	h
Malino Boundary	ML4	22.99	16.08	1.43	0.29	a	Kolaka	KO4	10.25	7.91	1.30	0.23	h
Malino Boundary	ML5	38.22	33.86	1.13	0.22	a	Kolaka	KO5	49.44	30.21	1.64	1.19	h
Malino Boundary	ML6	27.41	17.27	1.59	0.29	a		Average:			1.35	1.09	
	Average:			1.32	0.46		Mangole	MN1	7.07	6.33	1.12	0.49	i
Gorontalo	GO1	33.24	16.37	2.03	0.88	b	Mangole	MN2	9.64	6.60	1.46	0.49	i
Gorontalo	GO2	39.29	16.64	2.36	1.27	b	Mangole	MN3	18.96	12.08	1.57	0.55	i
Gorontalo	GO3	12.03	6.58	1.83	1.69	b	Mangole	MN4	4.56	3.86	1.18	N/A	i
	Average:			2.07	1.28		Sanana	SN1	2.45	1.93	1.27	0.44	i
Palu-Koro	PK0	16.94	10.99	1.54	0.31	c		Average:			1.32	0.49	
Palu-Koro	PK1	8.94	6.60	1.35	0.22	c	Rana	RA1	2.86	2.83	1.01	0.35	j
Palu-Koro	PK2	10.48	9.64	1.09	0.29	c	Rana	RA2	3.68	3.12	1.18	0.23	j
Palu-Koro	PK3	7.24	6.69	1.08	0.21	c	Rana	RA3	8.19	7.73	1.06	0.18	j
Palu-Koro	PK4	4.33	3.99	1.09	0.19	c	Rana	RA4	20.19	10.31	1.96	1.53	j
Palu-Koro	PK5	9.43	7.90	1.19	0.99	c	Rana	RA5	24.35	18.31	1.33	0.28	j
Palu-Koro	PK6	11.02	6.91	1.59	0.35	c	Rana	RA6	15.49	10.40	1.49	0.68	j
Palu-Koro	PK7	7.15	6.44	1.11	0.56	c	Buru area	BU7	18.09	12.56	1.44	0.47	k
Palu-Koro	PK8	10.78	9.61	1.12	0.89	e	Buru area	BU8	18.61	15.08	1.23	0.50	k
Palu-Koro	PK9	9.72	6.22	1.56	0.20	c	Buru area	BU9	26.93	12.53	2.15	1.13	k
Palu-Koro	PK10	16.34	12.80	1.28	1.10	c	Buru area	BU10	25.16	12.62	1.99	0.75	k
Palu-Koro	PK11	27.15	19.02	1.43	0.32	c		Average:			1.48	0.61	
Palu-Koro	PK12	64.23	27.88	2.30	0.80	c	Southern Seram	TE1	42.32	23.05	1.84	1.88	l
	Average:			1.36	0.47		Southern Seram	TE2	49.68	23.89	2.08	1.36	l
Parigi boundary	PA1	69.67	21.44	3.25	0.90	d		Average:			1.96	1.62	
Parigi boundary	PA2	72.43	26.17	2.77	0.78	d	Kawa	KA1	27.55	20.75	1.33	0.28	l
Parigi boundary	PA3	62.33	19.92	3.13	1.45	d	Kawa	KA2	15.16	13.76	1.10	0.26	l
Parigi boundary	PA4	17.86	13.48	1.32	0.50	d		Average:			1.21	0.27	
	Average:			2.62	0.91		Bobol	ES1	14.59	11.61	1.26	1.57	m
Sapu Valley	PV1	6.17	5.67	1.09	0.40	d	Bobol	ES2	51.83	26.37	1.97	2.60	m
Sapu Valley	PV2	3.64	3.38	1.08	N/A	d	Bobol	ES3	35.56	17.84	1.99	1.44	m
Sapu Valley	PV3	4.99	3.90	1.28	N/A	d	Bobol	ES4	23.05	12.73	1.81	1.04	m
Sapu Valley	PV4	6.30	5.60	1.13	N/A	d		Average:			1.76	1.66	
Sapu Valley	PV5	6.89	4.74	1.45	N/A	d	Sorong	SG1	33.89	28.77	1.18	1.15	n
Sapu Valley	PV6	4.67	3.78	1.24	N/A	d	Sorong	SG2	13.90	11.94	1.16	1.54	n
Sapu Valley	PV7	5.27	3.84	1.37	N/A	d	Sorong	SG3	15.11	13.16	1.15	0.48	n
	Average:			1.23	0.40		Sorong	SG4	8.54	5.35	1.60	0.59	n
Bada Valley	BV1	5.97	5.73	1.04	0.57	e	Sorong	SG5	29.39	10.53	2.79	4.90	n
Bada Valley	BV2	10.09	9.47	1.07	0.36	e	Sorong	SG6	10.19	8.94	1.14	0.27	n
Bada Valley	BV3	13.27	9.30	1.43	0.73	e	Sorong	SG7	36.50	27.47	1.33	0.45	n
	Average:			1.18	0.55		Sorong	SG8	17.73	14.83	1.20	0.44	n
Poso area	PO1	18.15	13.74	1.32	0.29	e	Sorong	SG9	31.90	18.34	1.74	1.33	n
	Average:			1.32	0.29		Sorong	SG10	15.44	9.57	1.61	0.40	n
Balantak	BK1	13.02	11.80	1.10	0.25	f	Sorong	SG11	65.53	40.33	1.62	0.42	o
Balantak	BK2	6.85	6.59	1.04	0.47	f	Sorong	SG12	62.92	22.04	2.85	5.10	o
Balantak	BK3	5.16	4.24	1.22	N/A	f	Sorong	SG13	54.48	30.12	1.81	8.68	o
	Average:			1.12	0.36		Sorong	SG14	22.17	17.39	1.27	0.32	o

Pansu area	PU1	15.06	11.78	1.28	1.12	g
Pansu area	PU2	9.21	8.66	1.06	0.25	g
Matano	MA1	12.54	10.57	1.19	0.45	g
Matano	MA2	12.56	11.63	1.08	0.23	g
Matano	MA3	23.51	12.35	1.90	0.79	g
Matano	MA4	12.34	10.52	1.17	0.72	g
Matano	MA5	8.46	8.31	1.02	0.84	g
Average:				1.24	0.63	
Kendari	KD1	24.61	14.03	1.75	0.52	h
Kendari	KD2	24.62	20.42	1.21	0.58	h
Average:				1.48	0.55	
Lawanopo	LW1	43.13	28.29	1.52	0.83	g
Average:				1.52	0.83	
Towuti bounding	TO1	27.98	24.39	1.15	0.41	g
Towuti bounding	TO2	9.58	9.30	1.03	0.56	g
Towuti bounding	TO3	51.16	25.10	2.04	1.22	g
Average:				1.41	0.73	

Sorong	SG15	11.44	7.61	1.50	0.49	p
Average:				1.60	1.77	
Ransiki	RS1	18.83	17.71	1.06	N/A	p
Ransiki	RS2	31.31	11.87	2.64	N/A	p
Average:				1.85	N/A	
Wandaman bounc	WM1	17.22	13.76	1.25	N/A	q
Wandaman bounc	WM2	15.55	12.08	1.29	N/A	q
Wandaman bounc	WM3	23.73	18.57	1.28	N/A	q
Wandaman bounc	WM4	11.58	6.74	1.72	N/A	q
Wandaman bounc	WM5	19.75	13.83	1.43	N/A	q
Wandaman bounc	WM6	9.84	9.33	1.05	N/A	q
Wandaman bounc	WM7	9.99	7.80	1.28	N/A	q
Wandaman bounc	WM8	45.67	19.61	2.33	N/A	q
Average:				1.45	N/A	
Tarera-Aiduna	TA1	6.11	5.05	1.21	N/A	r
Tarera-Aiduna	TA2	20.74	19.19	1.08	N/A	r
Tarera-Aiduna	TA3	32.26	19.75	1.63	N/A	r
Tarera-Aiduna	TA4	38.83	8.48	4.58	N/A	r
Tarera-Aiduna	TA5	35.31	18.46	1.91	N/A	r
Average:				2.08	N/A	

¹ Straight line length of the mountain front.

² Sinuous length of the mountain front.

³ Mountain front sinuosity ($S_{mf} = L_{mf} / L_s$).

⁴ Average valley floor width to valley depth ratio ($V_f = 2V_{fw} / (E_{ld} - E_{sc}) - (E_{rd} - E_{sc})$), where V_{fw} is the valley floor width, E_{ld} and E_{rd} are the topographic elevations of the left and right valley watersheds and E_{sc} is the elevation of the valley floor).

⁵ Location of sinuosity segment on Figure X.

Table 1. Summary of observations made from active faults in eastern Indonesia, and hypothetical earthquake magnitudes, styles and tsunami risk.

Fault	Typical segment length (km)	Maximum observed total length (km)	Step-over / relay width (km)	Potential rupture length (km)	Attributable seismicity	Notable historical events	Smf range	Vf range	Tectonic activity class	Potential earthquake magnitude	Potential earthquake style	Associated tsunami?
Malino boundary	25-75	130	1.2	130	Y		1.05-1.66	0.22-1.01	Maximal to slow	7.6	Normal	Y
Gorontalo	30	95	7	35	N		1.83-2.36	0.88-1.69	Slow to minimal	6.9	Strike-slip	Y
Palu-Koro	10-35	220	<1	135	Y	Mw7.7, 1996	1.08-2.30	0.24-0.89	Maximal to slow	7.6	Strike-slip	Y
Parigi boundary	10-45	95	3	80	Y		1.32-3.25	0.50-1.45	Minimal	7.3	Normal	Y
Sapu Valley	5-20	75	? <2	75	N		1.08-1.45	0.40	Maximal to moderate	7.3	Strike-slip	N
Balantak	54	250	10 (offshore)	54	Y		1.04-1.22	0.25-0.47	Maximal to moderate	7.1	Strike-slip	Y
Matano	10-60	195	6	90	Y	Mw6.1, 2011	1.02-1.9	0.23-0.78	Maximal to slow	7.4	Strike-slip	Y (lake)
Lawanopo & Kendari	10-45	200	7	70	?		1.21-1.75	0.55-0.83	Moderate to slow	7.2	Strike-slip	N
Towuti bounding	25-55	55	<1	55	N		1.03-2.04	0.41-1.22	Maximal to slow	7.1	Normal	Y (lake)
Kolaka	5-45	175	10	50	Y		1.05-1.64	0.23-1.68	Maximal to slow	7.0	Strike-slip	Y
Mangole	20	135	2	135	Y		1.12-1.57	0.49-0.55	Rapid to slow	7.6	Normal/Strike	Y
Sanana	5-20	60	?	60	Y		1.27	0.44	Rapid	7.2	Normal/Strike	Y
Rana	10	65	3-4	>40	N	Sfc. Rupture?	1.01-1.96	0.23-1.53	Maximal to slow	>6.9	? Strike-slip	N
Namlea	10	48	<1	48	Y					7.0	Strike-slip	Y
Southern Seram	5-15	60	2	60	Y	? M7.6, 1950	1.84-2.08	1.36-1.88	Slow	7.2	Normal	Y
Kawa	15-40	120	2	120	Y		1.10-1.33	0.26-0.28	Rapid to moderate	7.5	Strike-slip	Y
Bobol	10-15	100	2.5	100	N		1.26-1.99	1.04-2.60	Moderate to minimal	7.4	Strike-slip	Y
Combined Kawa-Bobol	10-40	240	2.5	240	Y	? M7.8, 1899	1.10-1.99	0.26-2.66	Rapid to minimal	7.8	Strike-slip	Y
Seram FTB	5-15	135	>2	? 135	Y					7.6	Thrust	Y
Sorong (West Papua)	45-75	420	<1	420	Y	M7.4, 1944	1.14-2.85	0.27-8.68	Rapid to minimal	>8.0	Strike-slip	Y
Koor	15-35	100	6	75	Y					7.3	Strike-slip	Y
Ransiki	20-50	100	<1	100	Y	M7.6, 2002	1.06-2.64		Maximal to minimal	7.4	Strike-slip	Y
Yapen	30-50	420	2-3	420	Y	M7.9, 1979				>8.0	Strike-slip	Y
Mamberamo	10-20	180	<2	? 180	Y	Numerous				7.7	Thrust	Y
Wandamen boundary	6-20	55	2	55	Y		1.05-2.33		Maximal to slow	7.1	Normal	Y
Lowlands	30-70	220	?	?	Y					?	Normal/Strike	N
Paniai	?	150	?	?	Y					?	Normal/Strike	N
Tarera-Aiduna	30-60	130	7	90	Y		1.08-4.58		Maximal to minimal	7.4	Strike-slip	Y